THE DETERIORATION IN HEAT TRANSFER TO FLUIDS AT SUPERCRITICAL PRESSURES AND HIGH HEAT FLUXES

by

Bharat S. Shiralkar

Peter Griffith

Sponsored by American Electric Power Service Corp.

June 1968

Engineering Projects Laboratory

Department of Mechanical Engineering

Massachusetts Institute of Technology

Cambridge, Mass. 02139

DISCLAIMER

ABSTRACT

At slightly supercritical pressure and in the neighborhood of the pseudo-critical temperature (defined as the temperature corresponding to the peak in specific heat at the operating pressure), the heat transfer coefficient between fluid and tube wall is strongly dependent on the heat flux. For large heat fluxes, a marked deterioration takes place in the heat transfer coefficient in the region where the bulk fluid temperature is below and the wall temperature above the pseudo-critical temperature. An analysis has been developed, based on the integration of the transport equations, to predict the deterioration in heat transfer at high heat fluxes, and the results have been compared with the previously available experimental results for steam. Experiments have been performed with carbon dioxide for additional comparison.

Limits of safe operation in terms of the allowable heat flux for a particular flow rate have been determined both theoretically and experimentally. Experiments with twisted tape inserted in the test section to generate swirl have shown that the heat transfer rates can be improved by this method. Qualitative visual observations have been made of the flow under varying conditions of heat flux and flow rate.

ACKNOWLEDGMENTS

This study was supported at the Massachusetts Institute of Technology by the American Electric Service Corporation.

Professors Edward S. Taylor and Joseph L. Smith, Jr., gave generously of their time throughout the period of the investigation and made a number of valuable suggestions. The interest and recommendations of Professor Warren M. Rohsenow are also gratefully acknowledged.

Mr. Fred Johnson of the M.I.T. Heat Transfer Laboratory assisted ably with the construction of the entire high pressure loop set up for the experiments.

The I.B.M. 1130 computer in the Mechanical Engineering Department and the I.B.M. 360 at the M.I.T. Computation Center were used for machine computation.

TABLE OF CONTENTS

LIST OF FIGURES

LIST OF FIGURES
(Continued)

LIST OF FIGURES
(Continued)

NOMENCLATURE

Cp	local specific heat at constant pressure, (BTU/lb^{o}F)
Cp_o	reference value of specific heat, (BTU/lb^{o}F)
D	diameter of tube, (ft.)
g	acceleration due to gravity, (ft/hr.^{2})
G	mass flow rate, (lbs/ft^{-}-hr.)
Gr	Grashof Number = $(\rho_b - \rho_o)/\rho_o x(\rho_{o_2}/\mu_o)^2 R^e$
h'	heat transfer coefficient, (BTU/ft^{2}-^{o}F-hr)
h	local enthalpy, (BTU/lbs.)
H	bulk mean enthalpy at a cross section (BTU/lb)
k	local conductivity, (BTU/ft-hr-^{o}F)
k_o	reference value of thermal conductivity, (BTU/ft-hr-^{o}F)
K	constant = 0.36
L	length along tube, (ft.)
n	constant = 0.124
Nu	Nusselt Number = $h'D/k$
Nu_{mac}	MacAdams' Nusselt Number = $0.023(Re_b)^{0.8}(Pr_b)^{0.4}$
p	pressure, (lbs/ft.^{2})
Pr	Prandtl Number = $Cp\mu/k$
P_{ro}	$Cp_o \mu o/k_o$
q	local heat flux, (BTU/ft^{2}-hr)
Q_o/A(also q_o)	wall heat flux (BTU/ft^{2}-hr)
r	local radius (ft)
R	radius of tube, (ft)

NOMENCLATURE
(Continued)

Re	Reynolds Number = GD/μ
T	temperature (^{o}F)
U	local velocity, axial, (ft/hr)
U^{+}	$U/\sqrt{\tau_o/\rho_w}$
U^{++}	$\int_o^U dU/\sqrt{\tau_o/\rho}$
U^{*}	$\frac{GD}{\mu_o}$
V	local radial velocity, (ft/hr)
y	distance from wall, (ft)
Y	nondimensionalized distance = y/R
y^{+}	$y\sqrt{\tau_o/\rho_w}/\mu_w/\rho_w$
y^{++}	$\int_o^y \sqrt{\tau_o/\rho}/\mu/\rho \, dy$
Z	axial coordinate, (ft)
ε_h	eddy diffusivity of heat, (ft^2/hr)
ε_m	eddy diffusivity of momentum, (ft^2/hr)
μ	local viscosity, (lbs/ft-hr)
μ_o	reference value of viscosity, (lbs/ft-hr)
ρ	density, (lbs/ft^3)
ρ_o	reference value of density, (lbs/ft^3)
τ_o	wall shear stress ($lbs/ft\text{-}hr^2$)
τ	local shear stress ($lbs/ft\text{-}hr^2$)

Superscripts and Subscripts Used

b	refers to bulk mean quantity
w	refers to quantity at wall or wall temperature

NOMENCLATURE
(Continued)

o	refers to a reference value of quantity
+	nondimensionalized quantity

1. INTRODUCTION

1.1 The Problem

In recent years several high pressure steam generators have been designed to operate at supercritical pressure. This results in higher overall thermodynamic efficiency as for the same temperature limits, the working area on the T-S diagram is larger. A number of conventional steam power plants already operate under conditions of supercritical pressure, and the use of supercritical pressure water in water cooled reactors has been under consideration. A number of applications have also arisen for supercritical cryogens, particularly hydrogen in liquid fuel rockets, etc. These considerations have led to considerable interest in the problem of heat transfer to supercritical pressure fluids, and a number of investigations have been performed in the past decade to this end.

The main feature of heat transfer to fluids at supercritical pressure is the rapid variation of properties with both temperature and pressure in the critical region. Because of this, conventional heat transfer correlations are not applicable, and the correlations especially derived for heat transfer in the critical region are usually restricted to a small region of operating conditions. At slightly supercritical pressures and in the vicinity of the critical temperature, the heat transfer coefficient is known to increase due to a favorable increase in the specific heat of the fluid. However, the enhancement of heat transfer to supercritical fluids has been found to be limited to conditions of small heat fluxes. As the heat

flux is increased, unfavorable heat transfer characteristics are encountered. The problems of designing a supercritical pressure boiler are thus extended to determining the behaviour of the heat transfer coefficient when the heat flux is varied, so that adequate safety factors can be prescribed to avoid burnout at high heat fluxes.

Several supercritical steam generators in the recent past have shown evidence of tube overheat in the lower furnace at the point where the water bulk temperature is about 670 ^{o}F. The evidence is of two kinds. First, thermal fatigue has occurred and caused tube failures long before a failure of any kind was to be expected. Second, pairs of cordal thermocouples have shown very high wall temperatures and, extrapolating back to the inside of the tube, evidence reduced inside heat transfer coefficients. It was suspected that a possible cause of the high tube temperature was a supercritical "burnout." The primary purpose of this investigation is to determine the cause and conditions leading to a supercritical "burnout" such as might occur in a supercritical steam generator.

Before focusing on this aspect of the problem, it is worthwhile to mention several other possible causes for the high tube wall temperatures which have been observed. In this context high means higher than the design temperature. Let us just list these possibilities.

1. Scale inside the boiler tubes.
2. Hot spot factors in the design procedure which are too low.
3. Higher heat transfer from the combustion gases than expected.

Better design procedures or better control of the water purity might be sufficient to cause the problem of supercritical turnout to disappear without changing the water flow conditions inside the tube.

Because the three factors listed above are rather vague, the most promising approach to eliminate the excessive temperatures inside the tube at supercritical pressure is to eliminate the "burnout"; therefore, only the burnout aspect of the problem has been studied here.

A part of the difficulty in the design of boilers for high heat fluxes in the past has been the lack of adequate data under these conditions. Most investigations of heat transfer to supercritical pressure fluids in the past were at low heat fluxes, to explore the improved heat transfer region. Lately, however, there has appeared increasing evidence in the literature that a deterioration in heat transfer does take place as the heat flux is increased. The work of Styrikovich et al (1)* graphically shows the variation of the heat transfer coefficient to supercritical steam. Figure 1 is taken from this reference. The different curves show the variation of the heat transfer coefficient with increasing enthalpy of the fluid. The abcissa can be interpreted as length along a tube with uniform heat input. The mass velocity is held constant at 550,000 lbs/ft^{2}hr, and the heat flux is varied from 120,000 - 300,000 BTU/ft^2-hr. At the lowest heat flux, the heat transfer coefficient has a maximum in the critical region. As the heat flux is increased,

---

*Numbers in parentheses refer to the References on page

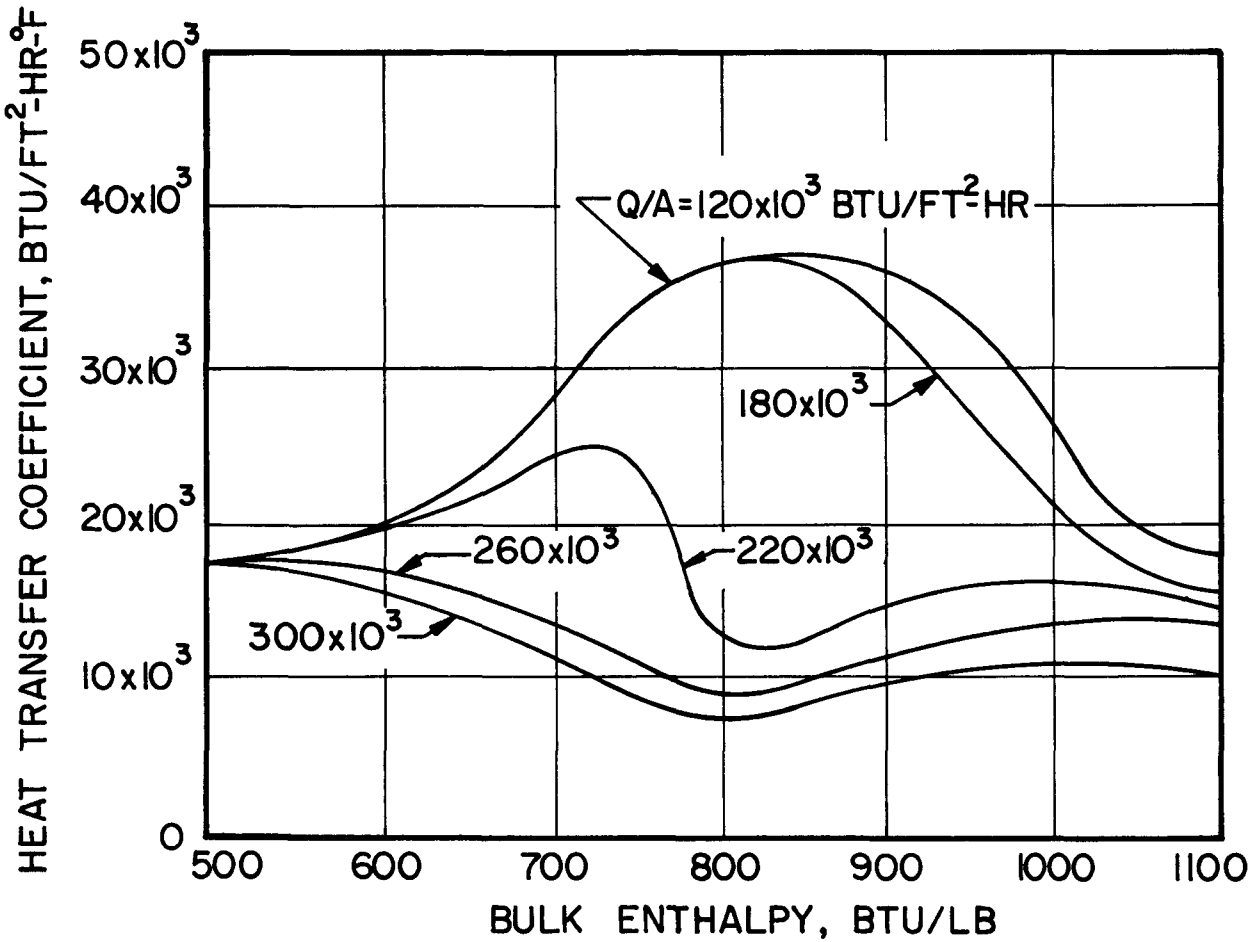

FIG. 1 : VARIATION OF THE HEAT TRANSFER COEFFICIENT WITH HEAT FLUX IN THE CRITICAL REGION (REF. 1)

there is a progressive decrease in the heat transfer coefficient until it shows a distinct minimum at 300,000 BTU/ft^2-hr. This corresponds to a drop in the heat transfer coefficient by a factor of four as compared to that for the smaller heat fluxes, and the heat transfer is lower than would be predicted by the usual correlations. This region, referred to as the deteriorated heat transfer region in this report, is the object of the present investigation. The aims of this work are to predict when and by what amount this deterioration takes place.

1.2 Scope and Objectives

A theoretical and experimental investigation of the problem was made at the Heat Transfer Laboratory, with the objectives of determining the heat transfer characteristics to supercritical fluids at high heat fluxes and mapping out safe regions of operation for supercritical pressure boilers in terms of the relevant parameters.

In general, the methods available for analysis of turbulent flows are either based on the integration of the transport equations with engineering assumptions for the eddy diffusivities of momentum and heat or on integral methods. Often, a Reynolds analogy is useful for correlating the friction factor to the Stanton number.

Another method, frequently used, is to attempt to modify the normal correlations for constant properties by evaluating the dimensionless groups at some reference temperature usually somewhere between the wall and bulk temperatures. In the present instance, it is doubtful whether a reference temperature taken as a fixed linear combination of the wall temperature and bulk temperature

will prove useful, because of the strong variation of the heat transfer coefficient with heat flux.

The method most extensively used in this report is based on the integration of the radial transport differential equations.

The experimental part of the program was carried out with carbon dioxide as the working fluid because of its convenient critical range. The experiments were performed with relatively high mass velocities so that free convection was not a governing parameter. The limits of safe operation in terms of the allowable heat flux for a particular flow rate were mapped for supercritical carbon dioxide with pressure, diameter of the test section and the orientation of the flow as the main variables. A test section with artificially generated swirl was also studied as a possible means of reducing or eliminating the deterioration in heat transfer. A visual test section was also studied, but did not prove very useful in terms of additional information.

2. WORK OF PREVIOUS INVESTIGATORS

A number of investigators have examined the heat transfer to fluids at supercritical pressure. A large number of these have been concerned with the improvement in heat transfer at low heat fluxes or large mass velocities and in free convection, e.g., the work of Dickinson and Welch (2), Dubrovina and Skripov (3), Knapp and Sabersky (4), Larson and Schoenhals (5), Petukov et al. (6), etc. Some investigators have been concerned with the existence of instabilities in the critical region. (7,8)

The phenomenon of deteriorated heat transfer at high heat fluxes when transferring heat to a fluid at supercritical pressure has also been observed with several fluids by various investigators. The most detailed work is probably that of Shitsman (9) for water. Deterioration has also been reported by Styrikovich et al. (1), Schmidt (10), Picus, Miropolskiy and Shitsman (11), and Vikrev and Lokshin (12) in water under various conditions. Swenson et al. (13) observed a decrease in the heat transfer coefficient to water at high heat fluxes, while sharp deterioration has been observed by Powell (14) in oxygen, Szetela (15) and Hendricks et al. (16) for hydrogen,and McCarthy (17) in nitrogen tetroxide.

The conditions under which the deterioration has been observed to occur are:

1. The wall temperature must be above and the bulk temperature below the pseudocritical temperature. (The pseudocritical temperature is the temperature corresponding to the peak in the specific heat at the operating pressure.)

2. The heat flux must be above a certain value, dependent on the flow rate and the pressure.

The experiments of these investigators encompass a wide range of flow rates, heat fluxes, test section sizes and pressure, and the deterioration in heat transfer varies in magnitude and sharpness. A comparison of the operating conditions for different investigators and the nature of the deterioration obtained are shown in Table 1.

Shitsman (9) made a detailed study of the deteriorated region for water. He used a tube 0.4 inch in diameter and 60 inches in length, which was heated electrically. Figure 2 shows a typically deteriorated region from his data. It is seen that a sharp deterioration takes place in the heat transfer coefficient, corresponding to the peak in the wall temperature, when the heat flux is increased from 80,000 to 100,000 BTU/ft^2-hr. The dotted line shows the wall temperature profile for a heat flux of 135,000 BTU/ft^2-hr. as predicted using the MacAdams correlation ($Nu = .023 \times Pr^{.4} \times Re^{.8}$) in which the bulk temperature is used to evaluate the properties. This serves as a reference to indicate the amount of deterioration. The minimum in the MacAdams wall temperature profile is due to the increase in the Prandtl number at the cross-section where the bulk enthalpy is equal to the critical enthalpy, which leads to a corresponding increase in the Nusselt number predicted by the equation.

Shitsman's results show that the deteriorated region is confined to a rather small range of enthalpies, between 750 - 780 BTU/ft^2-hr., depending on the ratio of heat flux to the mass flow rate. As the

TABLE 1

Comparison of Previous Experimental Evidence

No.	Source	Reference	Fluid	Pressure psi	P/P_c	Tube Dia. Inches	G lb/ft^2-hr	Q/A BTU/ft^2-hr	Orientation	Temp. Perc.
1	Styrikovich et al	1	Steam	3500	1.09	0.87	4×10^5 -2.4×10^6	80×10^3 -400×10^3	Vertical	Broad
2	Shitsman	9	Steam	3300 - 3650	1.03 to 1.14	0.4	3.4×10^5 -7×10^5	100×10^3 - 300×10^3	Vertical	Sharp
3	Schmidt	10	Steam	3250	1.01	025, 0.32	5.5×10^5 $- 13.4 \times 10^5$	160×10^3 - 320×10^3	Vertical Horizontal	Broad
4	Miropolsky et al	11	Steam	3550	1.11	0.63	4.5×10^5	165×10^3	Vertical	Very Sharp
5	Vikrev et al	12	Steam	3300 - 4400	1.03 - 1.37	0.4	3.4×10^5 $- 8.5 \times 10^5$	120×10^3 $- 250 \times 10^3$	Horizontal	Broad
6	Swenson et al	13	Steam	3300 6000	1.03 - 1.88	0.37	4×10^5 - 16×10^5	65×10^3 $- 580 \times 10^3$	?	Broad Small
7	Powell	14	Oxygen	780 - 1100	1.07 - 1.51	0.194	15×10^5 - 100×10^5	465×10^3 $- 1.4 \times 10^6$	?	Sharp
8	Szetela	15	Hydrogen	?	?	0.259 0.448	?	?	?	Sharp
9	Hendricks et al	16	Hydrogen	80 - 800	0.43 - 4.3	0.188 0.507	3.6×10^5 - 36×10^5	10^6	Vertical	Sharp

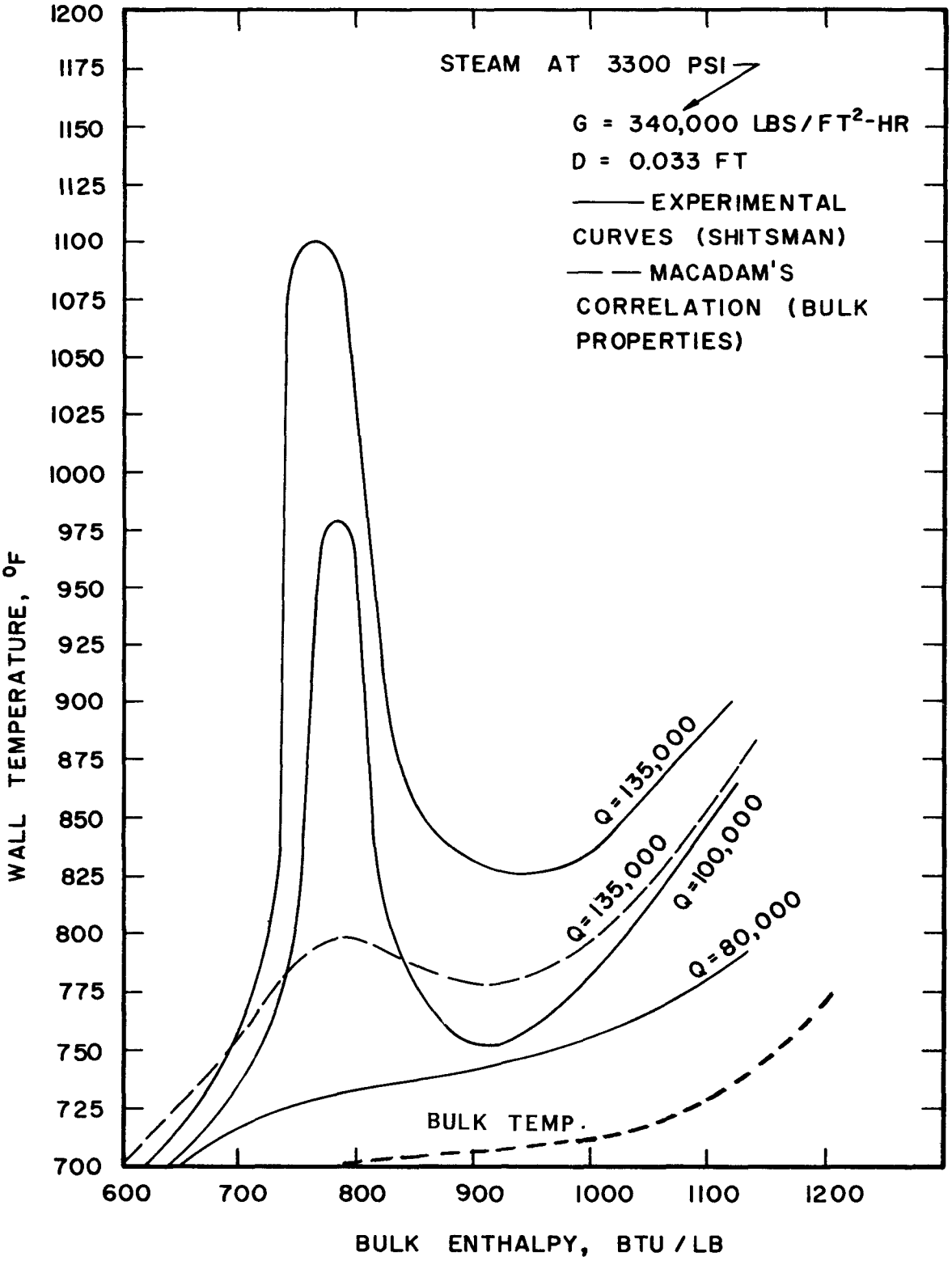

FIG. 2: DETERIORATED HEAT TRANSFER REGION (SHITSMAN)

ratio is increased, the temperature peak becomes higher and occurs sooner. He found that inlet effects can be important. The inlet enthalpy was also found to have an effect on the temperature peak. For inlet enthalpies larger than 845 BTU/lb, no peaks were observed. If the peak occurred either in the entrance or exit regions, it was suppressed to some extent. As the pressure was increased, the temperature peak became broader and was not as large. No impairment of the wall temperature was observed with high mass velocities, probably because of the lack of sufficiently high heat fluxes.

The importance of inlet effects is also evident in the results of Hsu and Zoschak (18), who worked with a very short test section. They report deterioration in heat transfer to some extent, but not as sharp as that observed by Shitsman. They also experienced difficulty in getting reproducible results, and the wall temperature was found to vary with time.

Vikrev and Lokshin (12) used a horizontal section of 0.4 inch and 300 ft long arranged in horizontal turns. They have shown that deterioration in heat transfer can take place in a horizontal section. The orientation of the test section does, however, have an effect on the results. The results of Vikrev and Lokshin show that the deterioration in horizontal tubes is less than and not as sharp as that occurring in vertical tubes for a comparable heat flux and flow rate. They present an empirical formula for the minimum coefficient of heat transfer in the critical region

$$h_{min} = (.38 - .40 \times 10^{-6} \times Q) x G^{1.7} (1 + 0.6[p - p_{crit}]/p_{crit}) \text{ Watts/m}^2\text{-degree C}$$

where Q = heat flux in watts/m^2

G = mass flow rate in kg/m^2-sec.

The effects of natural convection have been illustrated by Shitsman (19) for 16 mm. (0.63") tubes, who showed that significant temperature differences can exist between the top and bottom surfaces of a horizontal tube. Hall (20), working at low mass velocities and a large diameter tube, has observed significant differences in the heat transfer characteristics between upflow and downflow. There is also evidence to suggest that there is larger deterioration in larger diameter tubes (21). However, no quantitative results are available at present to indicate the relative importance of natural convection on the forced convection in terms of the usual parameters of Grashof or Graetz numbers. Some free convection data (3,4,5) is available at supercritical pressure and low heat fluxes, but this is of little use in determining the effects of natural convection when superposed on the main flow and at high heat fluxes.

Styrikovich et al. (1) have explored a wide range of conditions under which deterioration takes place in the heat transfer to supercritical steam. Based on their experiments, they present a plot of allowable heat fluxes for 0.87-inch tubes in terms of the mass flow rates. The heat flux is deemed "allowable" if the outside tube wall temperature does not exceed 1080 ^{o}F. In their experiments at 3500 psi., they found that an approximate condition for the allowable heat flux was given by

G/(Q/A) = 4 lbs/BTU.

Recirculation of the working fluid as a means of increasing the mass velocity and improving the allowable heat flux is suggested for supercritical pressure boilers by the authors.

Schmidt (10) conducted a large number of experiments at high subcritical and supercritical pressures with both vertical and horizontal test sections. The mass velocities used in his experiments were generally higher than used by Shitsman (9) and Vikrev and Lokshin. Deterioration in heat transfer was observed in both the vertical and horizontal test sections, though the temperature peaks were broader than in the Russian work and also occur at a larger value of the bulk enthalpy (810 - 830 BTU/lb).

Miropolskiy et al. (11) have observed similar deterioration patterns in curved tubes at supercritical pressure. The high temperatures were found along the inner wall in the curved sections.

Deterioration in heat transfer has been observed by Powell (14) in supercritical oxygen. The temperature rise for cryogens has been observed to be of even larger magnitude than in water. The ratio of the absolute wall to bulk temperatures has been found to be as high as eight. This corresponds to a drop in the heat transfer coefficient by a factor of more than ten.

Similar temperature peaks have been observed in the wall temperature when heating supercritical pressure hydrogen by Szetelz (15) and Hendricks et al. (17). For hydrogen also, the ratio of the wall to bulk temperature at the peaks has been found to be as high as eight.

Though several investigators have used carbon dioxide as the working fluid, deterioration has not been observed with carbon

dioxide. The investigations include those of Bringer and Smith (22), Wood and Smith (23), Tanaka et al. (24), Hall, Jackson, and Khan (25), Sabersky and Hauptmann (26), Koppel and Smith (27), etc. However, most of these investigations were at relatively small heat fluxes and without sufficient subcooling necessary to observe the deterioration. Only Koppel and Smith use large heat fluxes, which are necessary for the deterioration to occur. In some recent experiments by Hall (20) at low mass velocities, sharp peaks in wall temperature were observed in upflow but not in downflow. It is suspected that this phenomenon is somewhat different from the deterioration observed by other investigators in other fluids because of the different operating conditions in Hall's experiments. This is discussed in greater detail in a later section, and the results of the various investigators are compared with the results obtained in the present work.

Several explanations have been advanced by various researchers for the mechanism of the deterioration phenomenon. An analogy has been made with film boiling in two phase flow. Another theory proposes that a "relaminarization" of the flow takes place due to the thickening of the fluid layer near the wall. Hall has emphasized the importance of natural convection effects in the mechanism of deterioration.

A number of correlations have been proposed for supercritical pressure heat transfer. Most of these are applicable only at low heat fluxes or for bulk temperatures above the critical temperature. Among these are the correlations due to Shitsman (29), Humble and

Lowdermilk (14), etc., which use the conventional type of correlation for the Nusselt number in terms of the Reynolds and Prandtl numbers, with different exponents and with the properties evaluated at various reference temperatures.

Deissler (28) has proposed a more general relation between the Nusselt number and the Reynolds number for various combinations of the bulk and wall temperatures, on an analytical basis. The Nusselt and Reynolds numbers are based on a reference temperature t_x given by the relation

$$t_x = x(t_w - t_b) + t_b.$$

The values of x are plotted graphically as a function of t_w/t_b, the ratio of the wall temperature to the bulk temperature, and t_w the wall temperature. The analytical method used by Deissler is discussed in a later section. Szetela (15) has compared his data for hydrogen with Deissler's predictions and found discrepancies of up to 50 percent, with the greatest differences at high heat fluxes.

Hess and Kunz (30) have suggested a correlation based on analytical considerations. In order to obtain agreement between their calculations and data, they postulated that the viscous damping parameter A^+ was a function of the kinematic viscosity ratio at the wall and bulk temperatures. They suggested an empirical relation for heat transfer to hydrogen

$$Nu_f = 0.0208 \left(\frac{\rho_f U_b D}{\mu_f}\right)^{0.8} Pr_f^{0.4} (1 + .01457\ \nu_w/\nu_b)$$

where f denotes the film temperature which is the average of the bulk and wall temperatures.

Swenson et al (13) correlated a wide range of their data for supercritical pressure steam by the relation

$$\frac{hD}{k_w} = 0.00459\left[\frac{GD}{\mu_w}\right]^{.923}\left[\left(\frac{H_w - H_b}{T_w - T_b}\right)\frac{\mu_w}{k_w}\right]^{0.613}\left(\frac{\rho_w}{\rho_b}\right)^{0.231}$$

which uses an average value of the specific heat given by the ratio of the enthalpy drop to the temperature drop. This correlation also fits the carbon dioxide data of Bringer and Smith (22), Wood and Smith (22), and Koppel and Smith (27).

Hendricks et al (16) treat the problem as an extension of the problem at subcritical pressures. A pseudo-quality is defined, and the ratio of the experimental Nusselt number to the calculated Nusselt number is plotted as a function of a modified Martinelli parameter χ_{tt}

where $\chi_{tt} = \left(\frac{1 - x_2}{x_2}\right)^{0.9}\left(\frac{\rho_f}{\rho_\ell}\right)^{0.5}\left(\frac{\mu_\ell}{\mu_f}\right)^{0.1}$

and x_2 = pseudo-quality = $\left(\frac{\rho_{p.g.}}{\rho_b}\right)\left(\frac{\rho_\ell - \rho_b}{\rho_\ell - \rho_{p.g.}}\right)$

(Here f refers to the film temperature and ℓ refers to the heavy density conditions, and p.g. refers to "perfect gas" conditions.)

The calculated Nusselt number is based on

$$Nu = .021\left(\frac{\rho_{fm} U_b D}{\mu_f}\right) Pr_f^{0.4}\left\{1 + 15\left(\frac{P_b}{P_{crit}}\right)^{0.4}\left[1 + \left(\frac{\rho_f}{\rho_b}\right)^{2/3}\right]\frac{Q_o/A}{\rho_f U_b (H_f - H_b)}\right\}\left(\frac{U_b^2}{gD}\right)^{-.1}.$$

Where $\frac{1}{\rho_{fm}} = \frac{x_2}{\rho_f} + \frac{(1 - x_2)}{\rho_\ell}$.

This new correlation was proposed to fit the extensive supercritical hydrogen data of Hendricks et al. This correlated the data within 40 percent.

Another correlation for supercritical pressure heat transfer has been proposed by Petukov et al (6) in the form of a Reynolds analogy:

$$Nu = \frac{\xi/8 \cdot Re\ Pr}{12.7\ \sqrt{\xi/8}\ (Pr^{2/3} - 1) + 1.07}$$

where ξ = friction factor = $(1.82 \log Re - 1.64)^{-2}$.

This has been found to be unsuccessful in predicting the heat transfer rates at high heat fluxes.

3. PROPERTIES NEAR THE CRITICAL POINT

The reason for the variation of the heat transfer coefficient with the heat flux is the strong dependence of the properties of the fluid on the temperature and the pressure in the neighborhood of the critical point.

Figure 3 shows the state diagram for fluids like carbon dioxide and water in a temperature-entropy plane. A constant pressure line at subcritical pressure is represented by 1-1, while 2-2 represents a constant pressure line at supercritical pressure. Assuming thermodynamic equilibrium to exist, an equation for an isotherm in the two-phase region may be derived by satisfying the conditions for the liquid and vapor to co-exist in stable equilibrium with a plane interface. In the limiting case this yields the critical isotherm. Thus, above the critical pressure though the fluid undergoes a rapid change in its physical properties in the vicinity of the pseudocritical temperature, it does not undergo a phase transition; i.e., the fluid can exist as a homogeneous medium at any temperature.

At the critical temperature, the transport properties, viscosity, and thermal conductivity, as well as the density, fall sharply while the specific heat peaks to a high value. At supercritical pressures, the temperature corresponding to the peak in specific heat is referred to as the pseudocritical temperature. Properties of various fluids in the critical region have been investigated and are fairly well known. The properties of water in the critical region have been determined by Novak et al, (31), Novak and Grosh (32), etc., and the properties of carbon

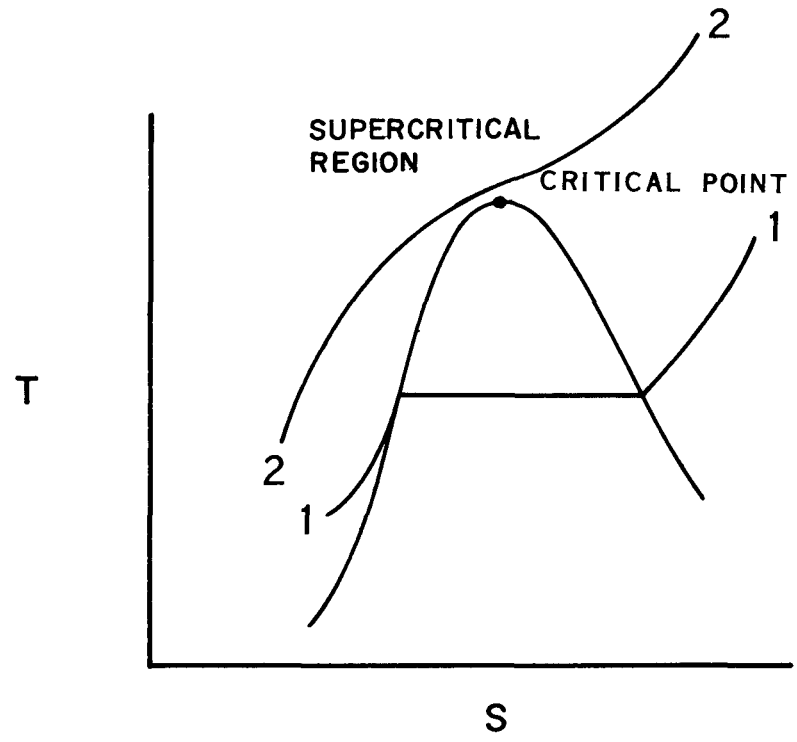

FIG. 3 : STATE DIAGRAM FOR STEAM

dioxide were determined by Michels et al (33, 34, 35, 36, 37), Clark (38), Keesom (39), Tzederberg and Morosova (40), etc. Figure 4 shows the variation of properties for water at 3300 psi., taken from reference 13. The viscosity, thermal conductivity and density (inverse of specific volume in the figure) are seen seen to fall by factors of four to eight.

The most reliable property data is the p-v-T data for various fluids in the critical region. There has been some controversy regarding the measurement of the viscosity and thermal conductivity. The methods used to measure viscosity were the transpiration of fluid through a capillary tube and the use of an oscillating disc. While Michels et al (35) found a peak in the viscosity near the critical temperature, others, for example, Starling et al (41) did not find peaks for the same fluid (carbon dioxide). There is therefore some doubt about the existence of peaks in the critical region data.

The data of Sengers and Michels (42) for thermal conductivity also shows a peak in the vicinity of the critical temperature, while that of Tzederberg and Morosova (40) does not. These peaks have usually been discounted as due to effects of free convection present in the test cell in the critical region in the presence of large density gradients.

A detailed review of the properties of carbon dioxide in the critical region has been made by Khan (43), in which he compares the results and methods of measurement used by various investigators. In this report, the transport properties have been assumed to decrease monotonically in the critical region. This has been assumed by the majority of the workers in the field, though Tanaka et al (24) incorporated the peak in thermal

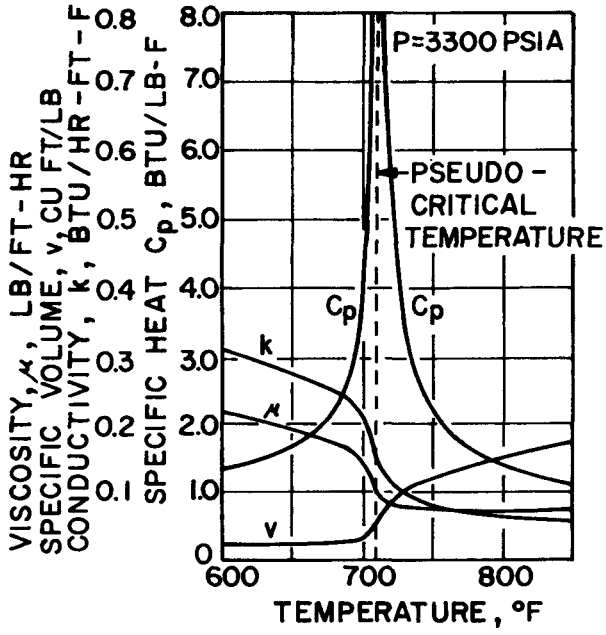

FIG. 4: PROPERTIES OF WATER IN CRITICAL REGION (FROM SWENSON ET AL)

conductivity into their analysis so as to get a better fit with their low heat flux data for the heat transfer coefficient.

4. THEORETICAL APPROACH

4.1. Introduction

Some of the previous analytical methods of prediction of supercritical pressure heat transfer were discussed in Section 3. These include the various correlations for the Nusselt number in terms of the Reynolds number and various property parameters based on both empirical and analytical considerations.

Kutateladze (44) has developed an integral method for calculations for turbulent flow. This consists in relating the Stanton numbers and friction factors under conditions of variable, temperature dependent properties, to the well-known values for constant property flows. The ratios of the corresponding Stanton numbers and friction factors are evaluated as limits for very large Reynolds numbers and essentially involve the density ratio at wall and bulk temperatures. For supercritical pressure heat transfer, Kutateladze suggests the relation:

$$\frac{S}{S_o} = \left(\int_o^1 \left(\frac{\rho}{\rho_b}\right)^{1/2} d\theta\right)^2$$

where S = Stanton number = $Q_o/A/\rho_b U_b (h_w - h_b)$

S_0 = Stanton number for constant property fluid at the bulk temperature,

$\theta = (h - h_w)/(h_b - h_w)$,

h = enthalpy.

This relation appears to be inadequate in the critical region, since it completely ignores the large variations in conductivity and viscosity.

However, the present calculations have shown that at high heat fluxes, the change in density is the most important property change.

4.2. Present Approach

The main approach in this work has been based on the integration of the differential equations governing the flow. The problem has been treated as that of heat transfer to a single phase, turbulent flow with variable properties, and the simultaneous differential equations governing the momentum and energy balance in the fluid have been solved after making numerous simplifications. Due to the nature of the eddy diffusivity expressions and the property variations, an analytical integration was not possible, and a numerical procedure was used in conjunction with the IBM 360 computer at the M.I.T. Computation Center.

4.3. Basic Equations

The equations governing the mean flow of a turbulent fluid through a constant area pipe, (Fig. 5) in the steady state, and assuming axial symmetry are:

Continuity

$$\frac{\partial(\rho U)}{\partial Z} + \frac{1}{r}\frac{\partial}{\partial r}(\rho r V) = 0 \tag{4.1}$$

Momentum

$$\frac{\partial \tau}{\partial r} + \frac{\tau}{r} + \frac{dp}{dZ} = 0 \tag{4.2}$$

Energy

$$\rho Cp\left(U\frac{\partial T}{\partial Z} + V\frac{\partial T}{\partial r}\right) = \frac{1}{r}\frac{\partial}{\partial r}(rq) \tag{4.3}$$

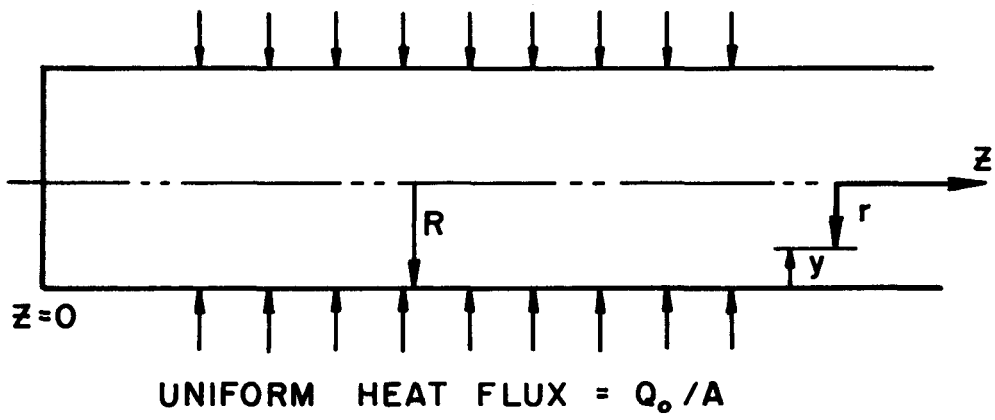

FIG. 5 : COORDINATE SYSTEM FOR FLOW OF FLUID

where

r = local radius

Z = axial coordinate (Fig. 5)

U = local axial velocity

V = local radial velocity

T = local temperature

τ = local wall shear stress

dp/dZ = pressure gradient in the axial direction

q = local heat flux

ρ = local density

Cp = local specific heat at constant pressure

The assumptions made in this formulation are:

1. The momentum terms are small compared to the shear stress terms.
2. The radial velocities are small enough, so that the radial pressure drop can be neglected.
3. Axial conduction is considered to be negligible.
4. The momentum equation does not take the gravitational terms into account.

Of these assumptions, only the last one may lead to significant errors. In the critical region, the density differences are so large that an appraisal of this assumption is necessary. The errors due to neglecting the buoyancy terms will depend on the Grashof number, which in turn depends on the test section diameter, and the Reynolds number, which depends on the mass flow rate. The effect of the distortion of of the shear stress profile due to buoyancy forces is treated in Section 4.5.

In two dimensional turbulent flow, the transport equations can be expressed as

$$q_r = -(k + \rho C_p \varepsilon_h) \frac{\partial T}{\partial r}$$

$$\tau_r = (\mu + \rho \varepsilon_m) \frac{\partial U}{\partial r}$$

where k = thermal conductivity

μ = viscosity

ε_m = eddy diffusivity of momentum

ε_h = eddy diffusivity of heat.

The additional terms $\rho\varepsilon_m$ and $\rho C_p \varepsilon_h$ in the transport equations are the Reynolds stress and heat transport terms. These arise when the local properties, velocities, and temperatures are expressed as the sum of a mean component and a fluctuating component, and the results are substituted in the equations of continuity, momentum, and energy. Here $\overline{(\rho V)'u'}$ is defined by $\rho\varepsilon_m \frac{\partial U}{\partial r}$, and $\overline{(\rho V)'h'}$ is defined as $\rho C_p \varepsilon_h \frac{\partial T}{\partial r}$.

This system of two dimensional equations can be solved with specified initial velocity and temperature profiles at the beginning of a long section and the boundary conditions U = 0, V = 0 at the wall of the tube.

Two-dimensional solutions for turbulent flow have been obtained by Buleev et al (58) and Deissler (59), both for entrance regions. Buleev et al followed a method similar to the one outlined, performing a rigorous two-dimensional integration of the differential equations, and they also included the axial conduction terms both in the fluid and

in the tube wall in their equations. The solution was obtained for constant property flow, though a variation in the thermal conductivity of the metal wall was considered. Unfortunately, the expressions used for the eddy diffusivities are not given in the paper.

Deissler followed a different line of attack. Solving for the thermal entrance region, he used an integral energy balance procedure to obtain the variation of the thickness of the thermal boundary layer with axial distance in which he used the one-dimensional transport equations for each cross section for the radial variation in the fluid temperature within the thermal boundary layer. The radial shear stress and heat flux distributions were assumed to be constant for the integration of the transport equations, and the same form of the eddy diffusivity as used by him for one-dimensional solutions (described in the next section) was employed.

A two-dimensional solution was first attempted with some degree of success, but was given up in favor of a simpler solution which required less time on the computer. The main disadvantages of a two-dimensional solution are:

1. It is time consuming and involved.
2. It is restricted to a particular set of initial conditions.
3. The conventional expressions for the eddy diffusivities are based on local conditions in the flow, and objections may be raised as to the validity of this formulation in a two-dimensional solution where the history effects are presumably important.

Great simplification is achieved by treating the problem as one of "fully developed" flow and using only the overall continuity condition over the cross section.

The simplified system of equations becomes:

Continuity

$$G = \frac{1}{\pi R^2} \int_0^R 2\pi r \rho U dr \tag{4.6}$$

Momentum

$$\frac{\tau}{\tau_o} = \frac{r}{R} \tag{4.7}$$

Energy

$$r\rho Cp \frac{U\partial T}{\partial Z} = Ur\rho\ Cp \frac{\partial T}{\partial Z}_{bulk}$$

$$= \rho U r \frac{\partial h}{\partial Z}_{bulk} = \frac{\partial}{\partial r}(rq) \tag{4.8}$$

where

G = mass flow rate/area

τ_o = wall shear stress

R = radius of tube.

Introducing

$$\frac{\partial h}{\partial Z}_{bulk} = \frac{\frac{2Q_o}{A}}{GR}$$

where

Q_o/A = wall heat flux/area, the energy equation becomes

$$\frac{\partial}{\partial r}(rq) = \frac{2r\rho U \frac{Q_o}{A}}{GR} \tag{4.9}$$

which gives the variation of q along the radius. A still simpler form can be used for the variation of q by noticing that near the wall $q = (Q_o/A)$, and at the center $q = 0$. In the central turbulent core, the variation of q does not influence the results by much. Thus a linear variation in q may be prescribed

$$\frac{q}{Q_o/A} = \frac{r}{R} . \tag{4.10}$$

Both forms of Equations (4.9) and (4.10) were tried, and the results were found to differ very slightly, hence the simpler form of Equation (4.10) was later adopted.

The final simplified equations now become

$$\frac{\tau}{\tau_o} = \frac{r}{R} = \frac{R - y}{R}$$

$$\frac{\frac{q}{Q_o}}{\frac{A}{}} = \frac{r}{R} = \frac{R - y}{R}$$

$$G = \frac{1}{R^2} \int_0^R 2\rho U(R - y)\, dy$$

where y = distance from the wall = R - r, together with the transport equations

$$\tau = (\mu + \rho\varepsilon_m) \frac{dU}{dy}$$

$$q = - (k + \rho C_p \varepsilon_h) \frac{dT}{dy}$$

which yield

$$\tau = \frac{\tau_o(R - y)}{R} = (\mu + \rho\varepsilon_m)\frac{dU}{dy} \tag{4.11}$$

$$q = \frac{\frac{Q_o}{A}(R - y)}{R} = -(k + \rho Cp\varepsilon_h)\frac{dT}{dy} \tag{4.12}$$

which can be solved simultaneously for U, T with the boundary conditions.

$$y = 0,\ U = 0,\ T = T_{wall}$$

with prescribed wall shear stress τ_o, and heat flux Q_o/A, and when the eddy diffusivities are known.

The mass flow rate and bulk enthalpy at a section are then obtained as

$$G = \frac{1}{R^2}\int_0^R 2(R - y)\ U\rho dy \tag{4.13}$$

$$H = \frac{1}{R^2 G}\int_0^R 2(R - y)\ U\rho h dy\ . \tag{4.14}$$

A rudimentary nondimensionalization may be achieved by using reference values of the properties and reference temperature and a reference enthalpy.

$$(1 - Y) = (\mu^+ + \rho^+ \frac{\varepsilon_m}{\nu_o})\frac{dU^*}{dY} \tag{4.15}$$

$$Q_o^+(1 - Y) = -\left(k^+ + \rho^+ Cp^+ Pr_o \frac{\varepsilon_h}{\nu_o}\right)\frac{dT^+}{dY} \tag{4.16}$$

$$G^+ = 2 \int_0^1 (1 - Y)\, \rho^+ U^* \tau_o^+ \, dY \tag{4.17}$$

$$H^+ = \frac{2}{G^+} \int_0^1 (1 - Y)\, \rho^+ U^* \tau_o^+ h^+ \, dY \tag{4.18}$$

where + indicates nondimensionalized values, o indicates reference values

$Y = y/R$

$\mu^+ = \mu/\mu_o$

$\rho^+ = \rho/\rho_o$

$\nu_o = \mu_o/\rho_o$ = reference kinematic viscosity

$U^* = U\mu_o/R\tau_o$

$Q_o^+ = RQ_o/A/T_o k_o$

$k^+ = k/k_o$

$Cp^+ = Cp/Cp_o$

$Pr_o = Cp_o\mu_o/k_o$ = reference Prandtl number

$T^+ = T/T_o$

$G^+ = GR/\mu_o$

$\tau_o^+ = \tau_o R^2 \rho_o/\mu_o^2$

$H^+ = H/h_o$

$h^+ = h/h_o$

with the boundary conditions

$y = 0,\ U^* = 0,\ T^+ = T^+_{wall}$.

This formulation has the advantage of eliminating the radius of the tube R as a separate variable and reduces the input variables to T_{wall}, Q_0, τ_o, and the output variables to G, H, T, U for a particular pressure.

However, in line with the previously made comments, this is subject to the limitations that the gravity terms are not significant, so that for large diameter tubes the validity of this formulation is in doubt.

Theoretical solutions using the method of radial integration of this sort have been performed in the past by several investigators, notably by Deissler (28) and Hsu and Smith (45), which generally lead to relations between the Nusselt number and the shear stress. The main difference between their methods and the present one is the form of non-dimensionalization and presentation of the results. The variables were chosen so as to allow direct computation of heat transfer results for given conditions of flow rate and heat flux. Deissler et al have utilized the method of non-dimensionalization with respect to the wall shear stress, and their results involve a parameter β defined as $\frac{Q_o/A\sqrt{\tau_o/\rho_w}}{Cpg\tau_o T_w}$ (where T_w is the absolute wall temperature in degrees Rankine), which also involves the shear stress. In this form, the plot cannot be used to calculate the Nusselt number or the heat transfer coefficient, unless the wall shear stress is assumed. This is presumably obtained from the friction factor for the turbulent flow, evaluated at the bulk temperature and properties. The present method relates the wall shear stress to the mass flow rate through the continuity condition, and the form of the results does not involve the wall shear stress. The wall shear stress can differ substantially from that obtained by a conventional friction factor estimate based on bulk properties. A conventional Reynolds number versus Nusselt number plot as used by Deissler cannot be used to show this shear stress variation. All the governing parameters

cannot be represented in one two-dimensional plot. While Deissler's results involve a separate plot for each wall temperature, the present format for the results requires a separate plot for each heat flux.

4.4 Expressions for the Eddy Diffusivity

In order to solve for the velocity and temperature profiles from the preceding equations, expressions are required for the eddy diffusivities of momentum and heat transfer.

Boussinesq was the first to introduce the concept of eddy viscosity as a turbulent exchange coefficient in order to obtain some practical results from the Reynolds equations. However, the most successful semi-empirical theory of turbulence is Prandtl's mixing length theory in which he introduced the similarity of turbulence with the kinetic theory of gases. By introducing the theory that certain turbulent fluctuations in a particular quantity may be assumed to be proportional to the gradient of the mean value of the quantity in the flow, Prandtl was able to express the eddy viscosity as $\ell^2 \frac{du}{dy}$ where ℓ is the mixing length over which the eddies are assumed to retain their properties.

Even though the mixing length theory has successfully predicted the mean velocity distributions in many practical problems, it is known to have serious limitations and inconsistencies. The more fundamental objections to the general validity of the mixing length approximations concern not so much the crudity of the assumed mixing process as the dependence of mixing length and eddy transport on local conditions in the flow, and they are supported by the observations that the turbulent kinetic energy at a point may depend as much on transport processes from remote parts of the flow as on the local conditions of production and

dissipation (46). A history effect would seem indicated for a more satisfactory description of the flow. However, in the absence of any reliable formulations of this kind, it is advisable to use one of the empirically available forms which have proved useful in the past under various circumstances. A brief survey of these is now presented.

In the past ten years, a number of analytical and empirical expressions have been proposed for the velocity or eddy diffusivity distributions near a wall. Of these, Deissler's (47) is probably the easiest to use while van Driest's (48) the most accurate (49). All except the complex expressions of Reichardt (50) and van Driest, however, are composed of two expressions valid for different ranges of the dimensionless distance from the wall, y^+. Spalding (51) has proposed a new single formula which expresses y^+ as a function of U^+ (dimensionless velocity).

Additional difficulties arise when the flow involves variable properties. Moreover, the eddy diffusivity for heat transfer has not been as widely investigated as the eddy diffusivity for momentum. It is customary to assume that they are equal for most cases. There is some evidence to show (52) that this is a good assumption when the Prandtl number is not significantly different from unity and that in this range the ratio of the two diffusivities is at most a weak function of the Prandtl number.

For constant property flow, Deissler's expression is

$$\varepsilon = n^2 U y \qquad y^+ < 26$$

$$= \frac{K^2 \left(\frac{du}{dy}\right)^3}{\left(\frac{d^2u}{dy^2}\right)^2} \quad .$$

(The expression for the core is based on von Karman's similarity hypothesis.)

where

$$y^+ = \frac{\frac{\tau_o}{\rho_w}}{\frac{\mu_w}{\rho_w}} y, \quad n = 0.109, \quad K = 0.36 .$$

The velocity profiles generated with this expression match experimental profiles closely.

For variable property flow, in order to take into account the effect of the local kinematic viscosity, Deissler (47) has suggested the use of the following expression:

$$\varepsilon = n^2 U y (1 - e^{-n^2 U y \rho/\mu}) \qquad y^+ < 26$$

$$= K^2 (dU/dy)^3 / (d^2U/dy^2)^2 \qquad y^+ > 26$$

where ρ, μ are the local properties and ρ_w/μ_w are the properties evaluated at the wall temperature.

In the central region $y^+ > 26$, it is easier to use Prandtl's expression for diffusivity

$$\varepsilon = K^2 y^2 \, dU/dy$$

$$K = 0.36 .$$

This form has the advantage that it can predict peaks in the velocity profile at points other than in the center, which might exist in the presence of large free convection effects. Karman's formulation cannot

be used for this purpose. Thus, Deissler's formulation for the eddy diffusivity becomes (as used by Hsu (45))

$$\varepsilon = n^2 U^+ y^+ \frac{\mu_o}{\rho_o} [1 - e^{-n^2 U^+ y^+ \rho\mu_o/\rho_o\mu}] \qquad y^+ < 26$$

$$= K^2 \frac{\mu_o}{\rho_o} y^{+2} \frac{dU^+}{dy^+} \qquad y^+ > 26$$

Since this formulation involves the use of y^+, U^+ based on the properties at the wall temperature, an improvement has been suggested by Goldmann (53) in which y^+, U^+ are replaced by y^{++}, U^{++} where

$$y^{++} = \int_o^y \frac{\frac{\tau_o}{\rho}}{\frac{\mu}{\rho}} dy, \quad U^{++} = \int_o^U \frac{dU}{\frac{\tau_o}{\rho}}$$

so that the expressions for the diffusivity become Goldmann:

$$\varepsilon = n^2 U^{++} y^{++} \frac{\mu}{\rho} [1 - \exp(-n^2 U^{++} y^{++})] \qquad y^{++} < 26$$

$$= K^2 \frac{\mu}{\rho} y^{++2} \frac{dU^{++}}{dy^{++}} \qquad y^{++} > 26$$

This procedure involves the integrated values of the parameter U^+ and y^+ and appears more suitable for the case of variable property flow.

Van Driest (48) has proposed a single "law of the wall" in which the mixing length is modified to the form $Ky(1 - \exp(- y/A))$ in order

to introduce the viscous damping of eddies near the wall. Thus, the expressions for the eddy diffusivity becomes

$$\varepsilon = K^2 y^2 [1 - \exp(- y/A)]^2 \frac{du}{dy} \quad .$$

A fourth well-known form for the eddy diffusivity has been suggested by Spalding (50) on an empirical basis to fit the velocity distribution for constant property flow. This differs from the others in that y^+ and the diffusivity are given as functions of U^+.

The dimensionless eddy viscosity is given by

$$\varepsilon^+ = \frac{\mu_{total}}{\mu_{molecular}} = 1 + .04432 \{0.4\ U^+ + \frac{(0.4U^+)^2}{2!} + \quad \} \ .$$

The diffusivities suggested by Deissler, Goldmann, and van Driest were tried and found to yield the same type of results with differences in the wall to center line temperature drops of less than 10 percent. Goldmann's scheme has been employed for the bulk of the work since it is more appealing on a physical basis for the reason that it uses an integrated value of the Reynolds number y^+ to determine the transition from the viscous to the turbulent region, rather than y^+ based on the properties at the wall temperature and because it uses averaged values of U^+ and y^+ in the calculations.

Several modifications have been proposed in the form of the eddy diffusivity to take into account the presence of the large density gradients that exist in the flow in the critical region, which may tend to promote greater mixing. Hsu and Smith (45) and Hall et al (25) have suggested multiplying the conventional diffusivity by an amplification

factor to take this into account. Hsu and Smith make the following argument.

The Reynolds shear stress in turbulent flow can be written as

$$\tau = vL \frac{d(\rho U)}{dy} .$$

For constant density,

$$\tau_l = vL \rho \frac{dU}{dy} = \varepsilon_{mi} \rho \frac{dU}{dy} .$$

For variable density

$$\tau = vL \rho \frac{dU}{dy} \left[1 + \frac{U \frac{d\rho}{dy}}{\rho \frac{dU}{dy}}\right] ,$$

or

$$\varepsilon_m = \varepsilon_{mi}[1 + F_m]$$

where

$$F_m = \frac{U \, d\rho/dy}{\rho \, dU/dy} = \frac{d(\ln\rho)}{dy} \Big/ \frac{d(\ln U)}{dy} .$$

F_m is then calculated in terms of the density and the rate of change of density with temperature.

Deissler (45) has raised some objections to this form of diffusivity. Hall et al used an enchancement factor given by

$$A \left[\frac{\frac{1}{\rho} \left(\frac{\partial \rho}{\partial T}\right)_p}{\left[\frac{1}{\rho} \left(\frac{\partial \rho}{\partial T}\right)_p\right] T = 87.8 \, ^oF} \right]$$ for carbon dioxide.

A was chosen to be 0.4 for their setup to obtain a quantitative agreement between experiment and theory.

These enhanced diffusivity models suffer from the defect that they lead to enormous diffusivities very close to the wall when the critical temperature is in the vicinity of the wall and yield very large heat transfer rates, irrespective of the magnitude of the heat flux, which is clearly contrary to experiment. Modifications are possible for this in two directions: history effects and viscous damping near wall. In a recent paper, Melik-Pashaev (60) has suggested two modifications in the previous models for the diffusivity. He evaluated the effect of density variations on the diffusivity in the following manner:

The Reynolds shear stress and heat flux terms are

$$\tau = -\overline{\rho}\,\overline{u'v'} - \overline{\rho'u'v'} \quad , \quad q = \overline{\rho}\,\overline{h'v'} + \overline{\rho'h'v'}$$

which can be written in the usual manner as

$$\tau = \rho\left(\frac{du}{dy}\right)^2 \ell^2\left[1 + \frac{\ell_\rho}{\rho}\frac{d\rho}{dy}\right]$$

$$q = -\rho\ell\,\ell_h\frac{du}{dy}\frac{dh}{dy}\left[1 + \frac{\ell_\rho}{\rho}\frac{d\rho}{dy}\right] .$$

If the mixing lengths of enthalpy and density (ℓ_ρ) are assumed to be of the order C.ℓ compared to the mixing length ℓ for the velocities,

$$\tau = \rho\left(\frac{du}{dy}\right)^2 \ell^2\left[1 + \frac{c\ell}{\rho}\left(\frac{d\rho}{dh}\right)\frac{dh}{dy}\right]$$

$$= \rho\left(\frac{du}{dy}\right)^2 \ell^2\left[1 + c\ell\,\frac{dh}{dy}\cdot x\right] ,$$

and

$$q = -\rho \ell^2 c \frac{du}{dy} \cdot \frac{dh}{dy} \left[1 + c\ell \frac{dh}{dy} \cdot x\right]$$

where

$$x = \frac{1}{\rho} \frac{d\rho}{dh} .$$

To a first approximation, the shear stress equation yields

$$= \sqrt{\tau/\rho} \frac{du}{dy} ,$$

and division of the heat flux equation by the shear stress equation yields

$$\frac{dh}{dy} = - \frac{q}{\tau} \cdot \frac{du}{dy} \cdot \frac{\ell}{c} .$$

This can be combined with the expression for ℓ to give

$$cx\ell \frac{dh}{dy} = - \frac{qx}{\sqrt{\tau\rho}} .$$

This is the addition to the diffusivity due to the density gradients.

The other difference in Melik-Pashaev's solution is the different boundary used for determining the transition from the wall layer to the turbulent core. The criterion used for this purpose is that the ratio of the molecular and turbulent viscosities is a constant. This leads to the criterion of the form $U^+y^+ = 335$ for transition. The amplification term in the diffusivity is used only in the turbulent core unlike Hsu and Smith, who have some amplification very close to the wall. A comparison using this form of diffusivity has led Melik-Pashaev to conclude that the heat transfer coefficient is about 7-10 percent higher than that computed without the density gradient amplification in diffusivity.

However, for most of the work in this report, Goldmann's form for the diffusivity has been employed where

$$y^{++} = \int_o^y \sqrt{\frac{\tau_o}{\rho}} \frac{\rho}{\mu} dy = \sqrt{\tau_o^+} \int_o^Y \frac{\rho^+}{\mu^+} dY$$

$$U^{++} = \int_o^U \frac{dU}{\sqrt{\frac{\tau_o}{\rho}}} = \sqrt{\tau_o^+} \int_o^{U^+} \sqrt{\rho^+}\, dU$$

in terms of previously nondimensionalized quantities where

$$\tau_o^+ = \frac{\tau_o R^2 \rho_o}{\mu_\tau^2}, \quad U^+ = \frac{U\mu_o}{R\tau_o} .$$

The use of Melik-Pashaev's expression for the diffusivity might lead to slightly better agreement with experiments; however, there is no experimental evidence to support it, and some of the assumptions in its derivation may be open to question.

4.5 Method of Solution

The solution consists in numerically solving the Equations (4.11) and (4.12) (using the expressions for eddy diffusivity in the previous section) for a prescribed heat flux Q_o/A, shear stress, and wall temperature and then evaluating the mass flow rate and bulk enthalpy from the integrals in Equations (4.13) and (4.14). The method used was an explicit finite forward difference procedure, starting at the wall and proceeding inwards to the center of the tube. Because of the large

amount of calculation involved in computing the profiles for various wall temperatures and wall shear stresses, this method was preferred as being the quickest over a formal relaxation procedure, though it is less accurate. The grid intervals were fixed by trying several sets for constant properties until the propagated truncation error was less than 2 percent. By comparing the results of a first-order difference solution, which yields a positive propagated error in the temperature drop and a second-order procedure which yields a negative propagated error, bounds were placed on the solution. Properties of steam at 3300 psi and carbon dioxide at 1075, 1100, and 1150 psi. were obtained from References 13 and 43. A computer subroutine was written to interpolate properties from this data.

The essentials of the solution can be tabulated as in Table 2 below, which shows the inputs and outputs for the solution.

TABLE 2

Inputs				Outputs			
D	Q_o/A	T_{wall}	τ_o	T	U	G	H
	50,000	800	2×10^7	800	0	4×10^5	685
				798	200		
			3×10^7	800	0	4.5×10^5	705

4.6 Effect of Buoyancy Terms

In the preceding sections a calculation procedure has been outlined, which does not take the buoyancy terms into account. However, omission of the buoyancy forces may not be permissible under certain conditions.

Obviously, the gravitational terms are the most significant at low mass velocities and for large diameter tubes (large Grashof numbers and small Reynolds numbers). Two investigators have considered the gravitational forces in their analyses. Hsu and Smith (45) came to the conclusion that when the parameter Gr/R^{+3} is of the order of 0.1, natural convection terms are important, as far as the effects on the velocity and temperature profiles are concerned.

$$\text{Gr} = \text{Grashof No} = \frac{(\rho_b - \rho_w)}{\rho_w} \left(\frac{\rho_w}{\mu_w}\right)^2 R^3 g$$

$$R^+ = R\left(\frac{\tau_o}{\rho_w}\right)^{1/2} \left(\frac{\rho_w}{\mu_w}\right) .$$

They indicate that the result for heating in upflow is to flatten the velocity and dimensionless temperature profiles and increase the heat transfer coefficient at a given Reynolds number. The objections to this analysis have been mainly the form of the eddy diffusivity employed (enhanced diffusivity model). Also, this approach is based on the assumed values of the shear stress appearing in the parameter β in their results.

On the other hand, Hall (54) has proposed a qualitative model to explain the sharp deterioration in heat transfer that he observed in upflow but not in downflow. He assumed a discontinuous change in properties between a "wall layer" and the core of the flow. He attributes the decrease in the heat transfer to a suppression of turbulence caused by a sharp drop in the shear stress near the wall due to the

buoyancy forces. The improvement in heat transfer beyond the temperature peak is attributed to the wall layer becoming turbulent.

An extension of the theory proposed in the previous section can be made to cover this case by modifying the shear stress distribution across the cross section of the fluid due to the buoyancy forces.

If a ring-shaped differential volume is considered, of radius (R-y) and height Δz, a force balance on a unit area perpendicular to the direction of flow yields:

$$\frac{\partial \tau}{\partial y} - \frac{\tau}{R - y} - (\rho g + \frac{\Delta p}{\Delta z}) = 0. \tag{4.19}$$

where y = distance from the wall. Integrating this equation with the boundary condition

$$\tau = \tau_o \text{ at } y = 0 ,$$

$$\tau = \frac{R}{R - y} \tau_o + \frac{1}{R - y} \int_o^y (\rho g + \frac{\Delta p}{\Delta z}) (R - y) \, dy . \tag{4.20}$$

Using an overall force balance condition

$$\frac{2\tau_o}{R} + \rho_b g + \frac{\Delta p}{\Delta z} = 0 . \tag{4.21}$$

Here the bulk density ρ_b is defined by

$$\rho_b = \frac{1}{\pi R^2} \int_o^R 2\pi\rho(R - y) \, dy . \tag{4.22}$$

Combining equations (4.21) and (4.20)

$$\tau = \frac{(R - y)}{R}\,\tau_o + \frac{1}{R - y}\int_o^y (\rho - \rho_b)\, g(R - y)\, dy \qquad (4.23)$$

$$\text{or} \quad \tau/\tau_o = (1 - Y) + \frac{Rg(\rho_b - \rho_w)}{\tau_o(1 - Y)}\int_o^Y \frac{(\rho - \rho_b)}{(\rho_b - \rho_w)}\,(1 - Y)\, dY$$

$$\text{or} \quad \tau/\tau_o = (1 - Y) + \frac{Gr}{\tau_o^{+}(1 - Y)} \cdot \frac{\rho_o\,\mu_w^{\,2}}{\rho_b\mu_o^{\,2}}\int_o^Y \frac{(\rho - \rho_b)}{(\rho_b - \rho_w)}\,(1 - Y)\, dY \qquad (4.24)$$

where $\tau_o^{+} = \dfrac{\tau_o R^2 \rho_o}{\mu_o^{\,2}}$.

Thus, the governing equations become in this case

$$(1 - Y) + \frac{Gr}{\tau_o^{+}(1-Y)} \cdot \frac{\mu_w^{+2}}{\rho_b^{+}}\int_o^Y \frac{(\rho - \rho_b)}{(\rho_b - \rho_w)}\,(1-Y)dY = (\mu^{+} + \rho^{+}\frac{\varepsilon_m}{\nu_o})\,\frac{dU^*}{dY} \qquad (4.25)$$

$$Q_o^{+}(1 - Y) = -\,(k^{+} + \rho^{+}\, Cp^{+}\, Pr_o\,\frac{\varepsilon_h}{\nu_o})\,\frac{dT^{+}}{dY} \qquad (4.16)$$

$$G^{+} = 2\int_o^1 (1 - Y)\,\rho^{+}\,U^*\,\tau_o^{+}\, dY \qquad (4.17)$$

$$H^{+} = \frac{2}{G^{+}}\int_o^1 (1 - Y)\,\rho^{+}\,U^*\,\tau_o^{+}\,h^{+}\, dY \qquad (4.18)$$

$$\rho_b^{+} = 2\int_o^1 \rho^{+}\,(1 - Y)\, dY\ . \qquad (4.26)$$

One additional complication is introduced since the value of the bulk density ρ_b is not known to start with. Hence the process of solution involves the choice of an initial value for the bulk density and

iteration to satisfy equation (4.26) after solving for the temperature and, therefore, the density distribution.

A much more serious difficulty arises in the formulation of the eddy diffusivity due to the following reasons:

1. When the shear stress profile is sufficiently distorted so that the value of the shear stress falls to a small value near the wall, the applicability of the Goldmann or Deissler expressions near the wall is in question because they are based on an almost constant shear stress near the wall. The results obtained from the van Driest formulation, which relates the diffusivity to the shear stress near the wall as well as in the core, are significantly different from those obtained with other formulations. The van Driest expression appears to be a better one to use in these circumstances.
2. If the effect of buoyancy forces is sufficiently large so that the shear stress passes through zero near the wall and becomes negative, other questions are raised. It is doubtful that the eddy diffusivity goes through zero when the shear stress does. There is evidence to show that even the center line value of the eddy viscosity is not zero. (55)

Also, the fact that the shear stress goes through zero implies that a velocity maximum exists at a radial distance from the wall away from the center line. This means that the velocity and temperature profiles are basically different in shape and that the eddy diffusivities for heat and momentum can be quite different in certain regions of theflow. Bourne (56) has investigated the free convection problem

on a vertical plate, where a similar situation exists. By substituting empirical formulas for experimental velocity and temperature profiles, he integrated the mean momentum and temperature equations to determine ε_m and ε_h. The results showed that the value of $\varepsilon_h/\varepsilon_m$ varied from zero to a maximum of 5.5 in the inner 50 percent of the boundary layer. He concludes that the assumption of the equality of the diffusivities of heat and momentum is valid only when the boundary conditions for the temperature and the downstream component of the velocity are similar.

The theoretical approach has therefore been restricted to the case where the shear stress distribution was not sufficiently distorted to create these difficulties. The results are thus only a qualitative measure of the trends in the heat transfer coefficient as the buoyancy forces are introduced. More data, either of an empirical or analytical nature, are required regarding the turbulence production and the variation of the eddy diffusivities under conditions of this kind before the theory can be used to predict quantitatively the effects of large buoyancy forces in the critical region.

A simpler approach can be used to relate the effects of the gravity forces to certain experimental parameters. On examining equation (4.24), it appears that the effect of the buoyancy terms on the radial shear stress variation is given by the right-hand term in the equation. This indicates the extent of the distortion of the shear stress profile from its initial linear profile. Since this is the only difference in the basic equations governing the flow when buoyancy terms are introduced, the extent of this distortion is presumably a criterion that determines

the importance of the superposed gravitational terms. The parameter that determines the distortion is

$$\frac{Gr\mu_w^{+2}}{\tau_o^{+}\rho_b^{+}} \quad \text{or} \quad \frac{Gr\mu_w^{2}}{\tau_o R^2 \rho_b} \ .$$

If τ_o is expressed as

$$\tau_o = f\rho_b U_b^{2}$$

where f is the friction factor, which is a weak function of the Reynolds number in turbulent flow

$$\frac{Gr\mu_w^{2}}{\tau_o R^2 \rho_b} \sim \frac{Gr\mu_w^{2}}{f\rho_b^{2} R^2 U_b^{2}} \sim \frac{Gr}{Re^2} \ .$$

Thus, Gr/Re^2 represents a criterion for evaluating the influence of free convection on the main flow. It is evident that this criterion has the right form in that buoyancy effects increase with the Grashof number and decrease at high Reynolds numbers. A more general expression might be Gr/Re^x, where x might be different from 2 if the friction factor cannot be assumed to be constant. Comparison with experimental results with large convection effects would be useful in determining the applicability of this criterion and in attaching critical values to it.

Some of the results obtained by using the methods described in this chapter are presented in the next chapter.

5. ANALYTICAL RESULTS FOR STEAM

5.1 Introduction

The computed results based on the method described in Section 4 are presented in this section. The computed output consists of the dimensionless mass velocity parameter G^+, dimensionless bulk enthalpy H^+, and the temperature and velocity profiles for each set of input variables, consisting of the wall temperature, dimensionless heat flux Q_0^+, and the dimensionless shear stress at the wall, τ_o^+. The results presented here are based on Goldmann's formulation for the eddy diffusivity. In order to use the properties of steam without dividing by standard values of the respective properties, it was found convenient to assign the value of unity to all reference values. Then $\rho = f(T)$ can be represented numerically by $\rho/\rho_o = f(T/T_0)$, etc., and GR has the same numerical value as $GR/\mu_o = G^+$.

RQ_0/A has the same numerical value as $RQ_0/A/T_0k_0 = Q_o^+$.

$\tau_o R^2$ has the same numerical value as $\rho_o R^2\ \tau_o/p_o^2 = \tau_o^+$.

5.2 Mass Velocity Parameter vs. Bulk Enthalpy Plots

The GD vs. H plots constitute the bulk of the computed results. Every value of the heat flux parameter QD requires a separate plot of this kind. The figures 6, 7, 8, 9 are GD vs. H plots for four different values of the heat flux parameter QD = 3300, 5000, 15000, and 25000 BTU/ft-hr, respectively. The curves on the plots are constant wall temperature lines. Each plot shows the GD range in the region of interest where hot spots are likely to occur. There is a continuous variation in wall shear stress along the constant temperature

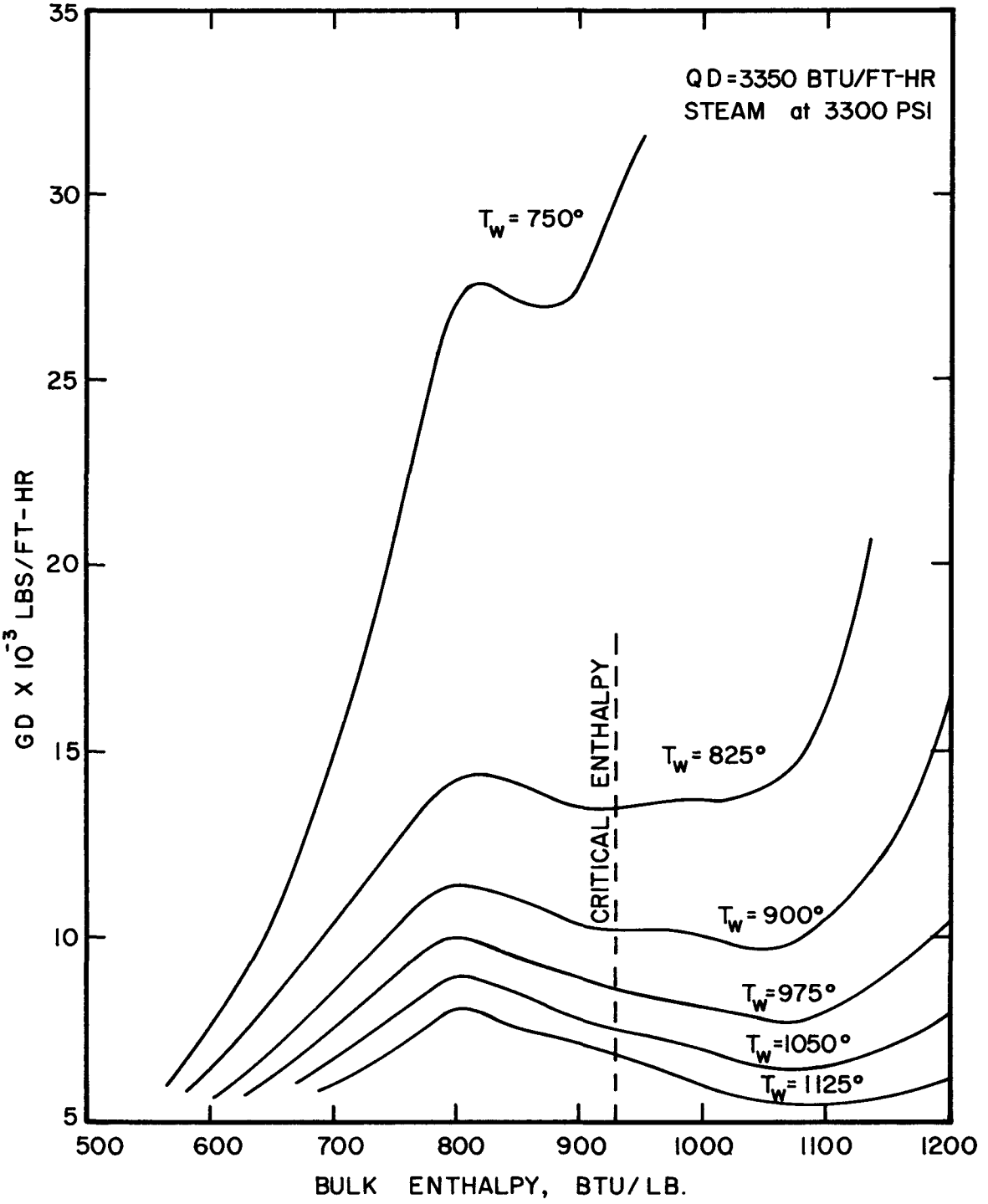

FIG. 6 : COMPUTED RESULTS : MASS FLOW RATE VS. BULK ENTHALPY FOR SYSTEM

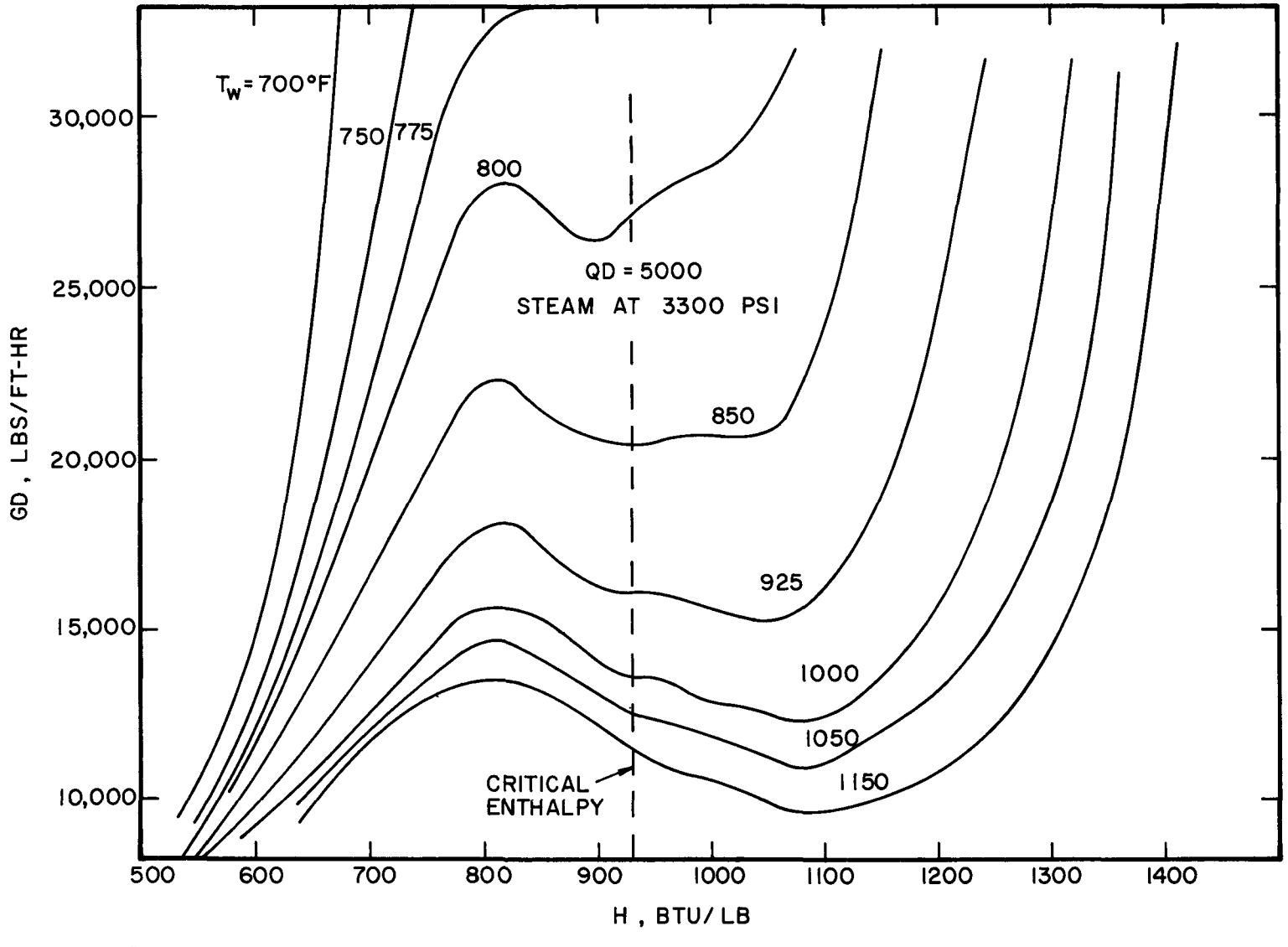

FIG. 7 : COMPUTED RESULTS : MASS FLOW RATE VS. BULK ENTHALPY FOR SYSTEM

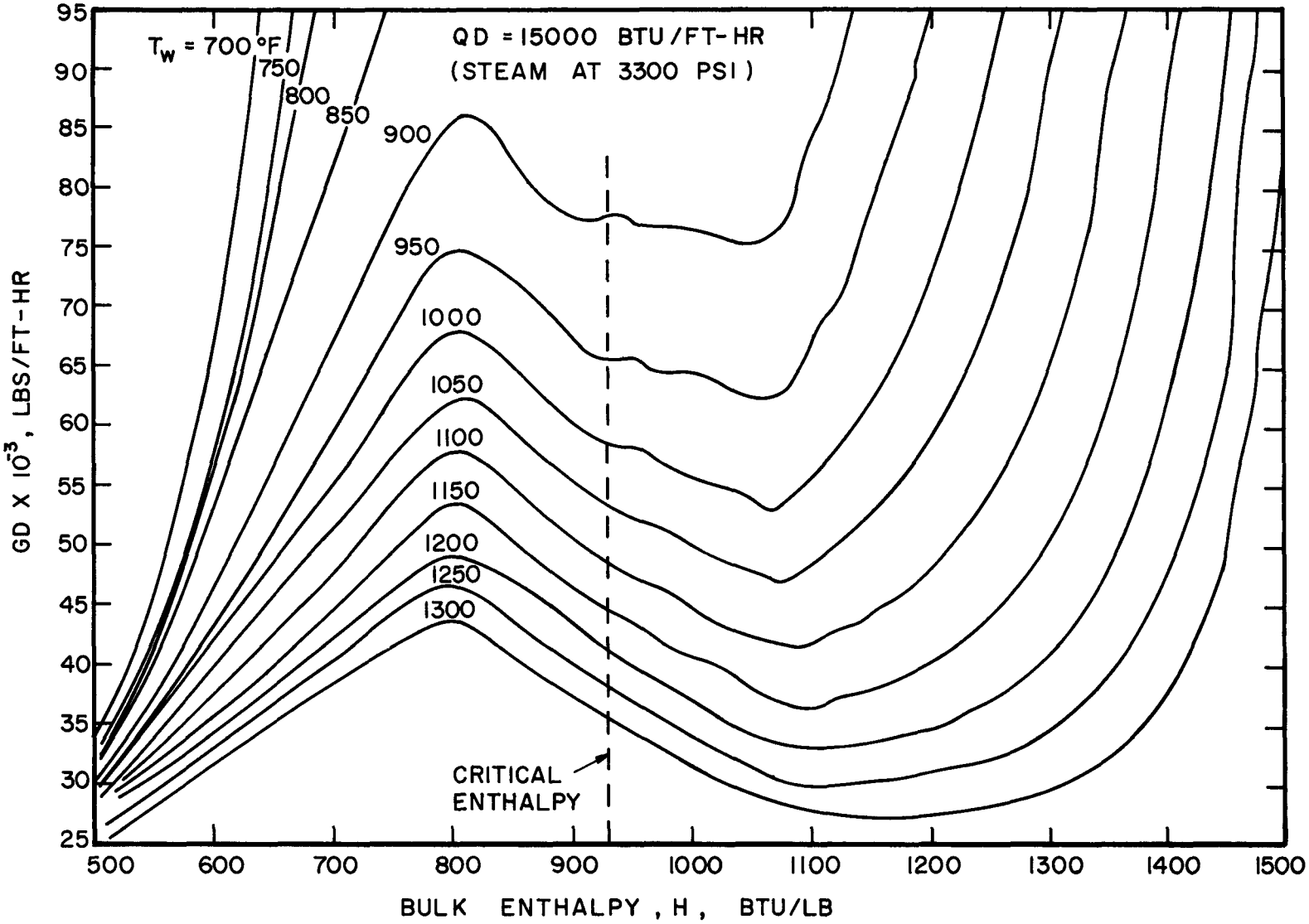

FIG. 8 : COMPUTED RESULTS : MASS FLOW RATE VS. BULK ENTHALPY FOR SYSTEM

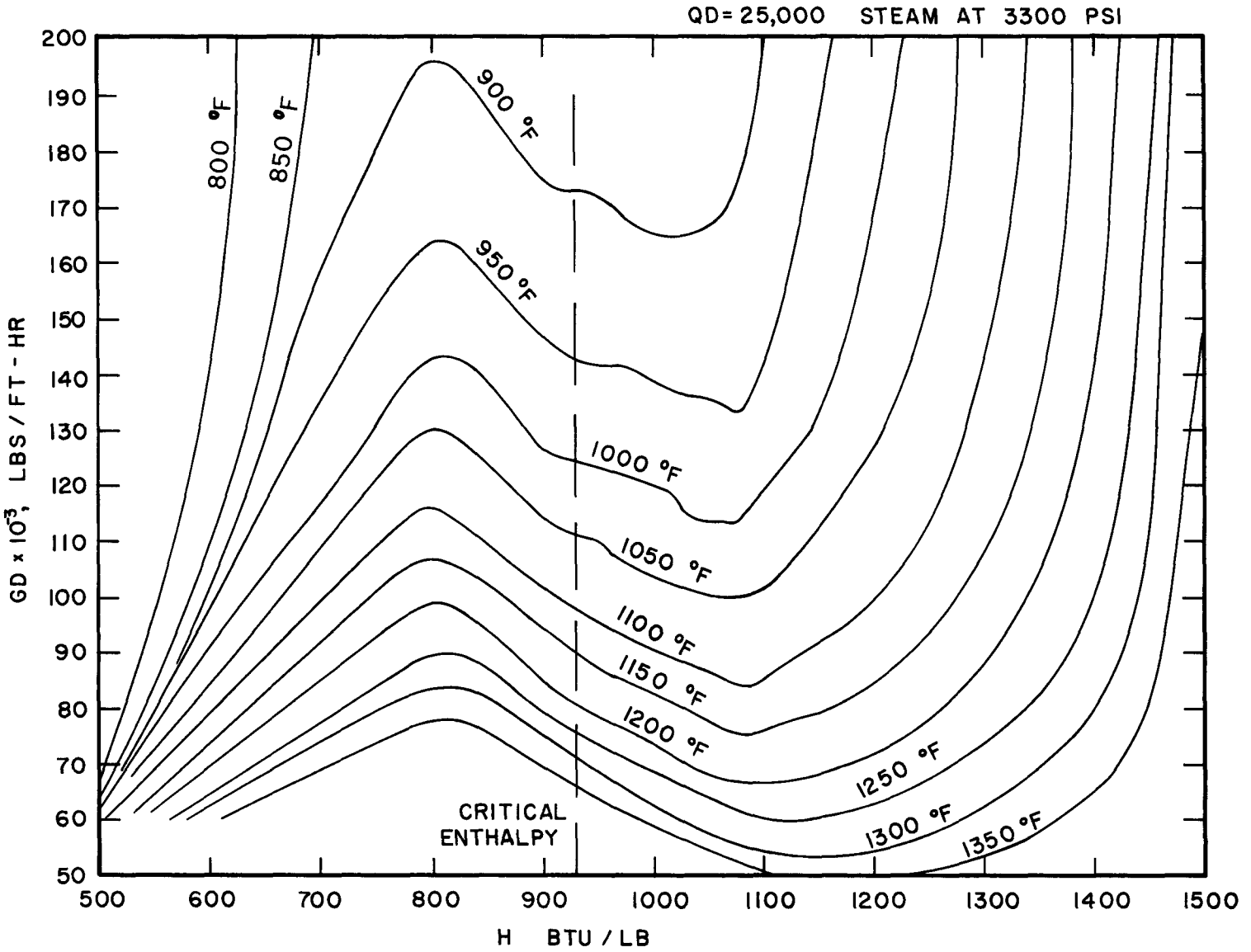

FIG. 9 COMPUTED RESULTS: MASS FLOW RATE VS. BULK ENTHALPY FOR STEAM

lines. The S-shaped isotherms indicate the peculiar behaviour of the heat transfer coefficient which is a feature of the critical region. In a constant property region, the isotherms would go up monotonically. The maximum in the isotherm represents the maximum flow rate which would yield that temperature. This point corresponds to the peak wall temperature at that flow rate. The minimum in the isotherm represents the minimum flow rate for which that wall temperature is reached. This point corresponds to the minimum temperature in the post critical enthalpy region that occurs at the wall for the flow rate in question. In the limiting case of very large mass velocities, the isotherms are asymptotic to the vertical lines corresponding to the enthalpy at the wall temperature.

A plot of this kind is obtained much more easily by the use of equation (4.10)rather than equation (4.9) for the radial heat flux distribution. If equation (4.9) is used, the coupling between the heat flux distribution and the mass flow rate G requires iteration to obtain agreement between the assumed and computed values of the mass flow rate.

5.3 Comparison with the Experimental Results of Shitsman (9)

In order to use the GD vs. H plots for a particular problem, it is necessary to make a crossplot of the wall temperature versus bulk enthalpy for a constant flow rate. This entails marking the intersections of a horizontal line parallel to the H axis, at the required value of the mass flow rate parameter, with the constant temperature curves and noting the enthalpy at these intersections. Figure 10 shows the crossplots made for G = 340,000 lbs/ft^2-hr for a tube of

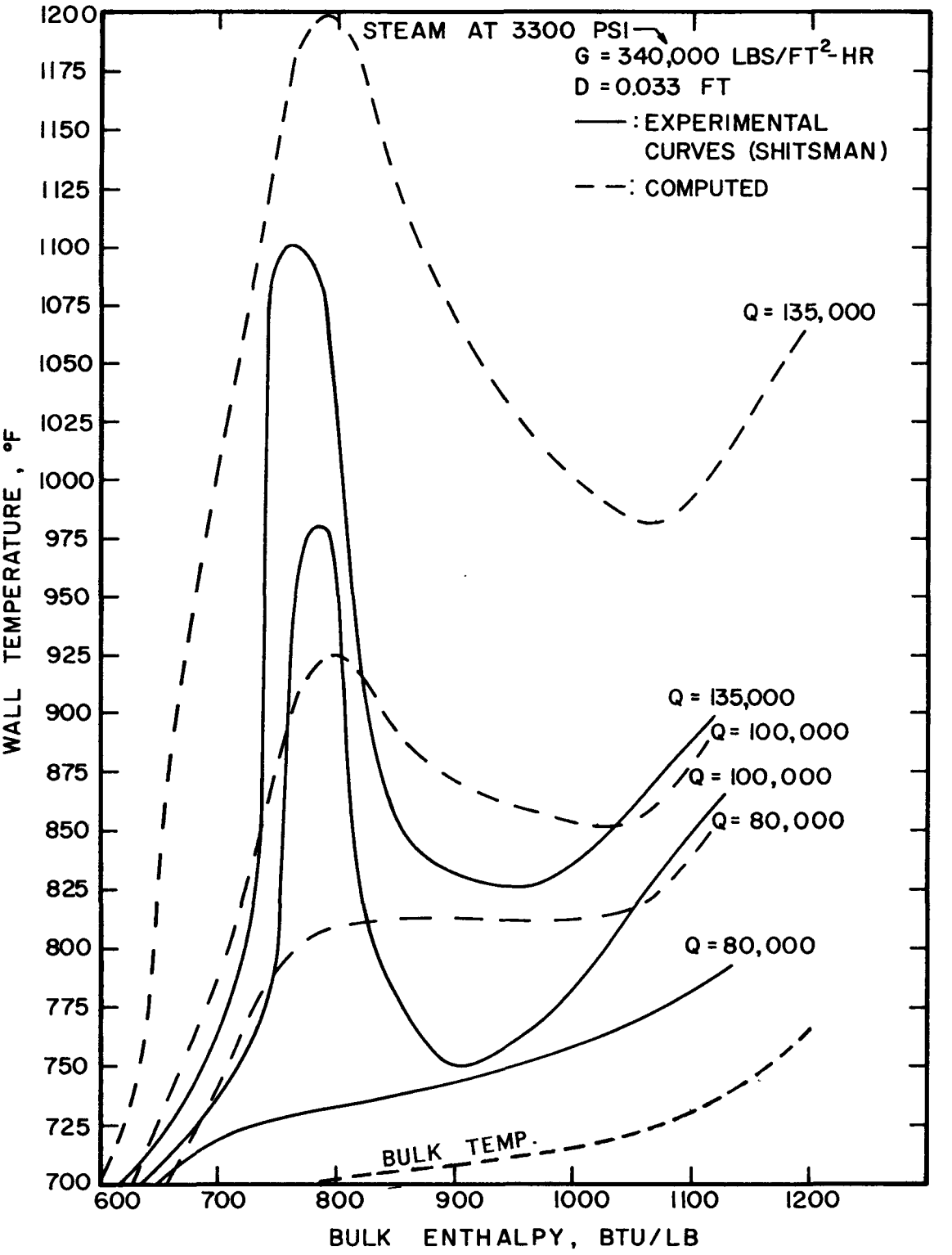

FIG. 10 : COMPARISON OF THEORETICAL AND EXPERIMENTAL RESULTS

diamter 0.033 ft., and for three heat fluxes Q = 80,000, 100,000, and 132,000 BTU/ft^2-hr in order to correspond to the conditions used by Shitsman in his experiments. A plot of this type corresponds to the variation of wall temperature along the length of a tube with uniform heat input. It is seen that the calculations predict a marked deterioration in heat transfer at about the same heat flux observed experimentally. Three features of comparison are noteworthy:

1. The calculations do not predict a sudden deterioration in the heat transfer but a progressive one.
2. Comparison with Shitsman's results shows that while at the inception of the experimental peak, the calculated peak in wall temperature is lower than the experimental peak, at higher values of the heat flux the situation reverses, and the predicted peak is higher. At the higher heat fluxes, therefore, the predictions are on the conservative side from the designer's point of view.
3. It is evident that the predictions are somewhat high in the enthalpy region beyond the peak in wall temperature. This is probably due to the fact there is additional mixing in the core of the flow in this region of large density gradients in the core, which has not been accounted for in the calculations. Also, this is the region where the fully developed profile assumptions are least valid.

A comparison with the earlier two-dimensional model has shown that due to axial derivatives, the peak occurs a little earlier, i.e., at a smaller value of the bulk enthalpy and would lead to slightly better agreement with the experimental results.

5.4 Wall Shear Stress Variation Along the Tube

The variation of wall shear stress plays an important role in the solution. Figure 11 shows a sample plot of GD vs. bulk enthalpy with constant shear stress lines instead of constant temperature lines as in Figures 6-9. The peak in the shear stress lines corresponds to the maximum flow rate that yields that shear stress at the wall. If a crossplot of shear stress vs. bulk enthalpy is made from this data, the peak represents the minimum value of the shear stress at that flow rate. A shear stress calculated from the friction factor based on bulk properties would not show this minimum. This is an important aspect in which this solution differs from other solutions.

A crossplot of the wall shear stress vs. bulk enthalpy is shown in Figure 12. This shows more clearly that the shear stress dips to a low value before rising again to a higher value corresponding to the "gaseous" (more correctly--low density) state. An examination of the effect of heat flux shows that the dip gets more pronounced as the heat flux is increased. The decrease in shear stress can be related to the drop in the density near the wall before there is an increase in the core velocity.

5.5 Computed Velocity and Temperature Profiles

Figures 13 and 14 show typical velocity and temperature profiles at different values of the bulk enthalpy, corresponding to different sections along a heated tube. The profiles shown represent sections in the deteriorated region of heat transfer and sections in the enthalpy regions corresponding to the heavy and light states far removed from

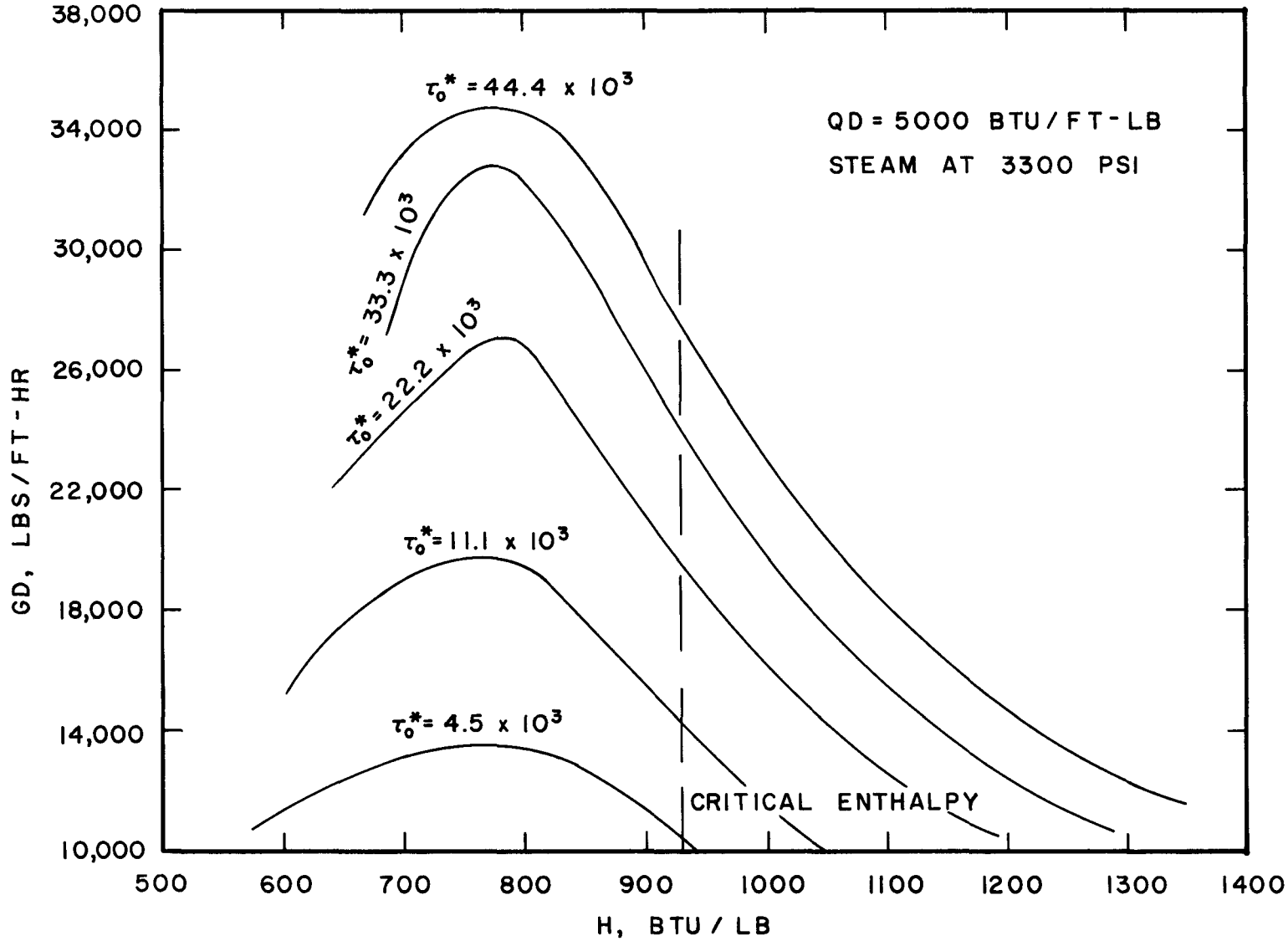

FIG. 11 COMPUTED RESULTS : CONSTANT SHEAR STRESS LINES

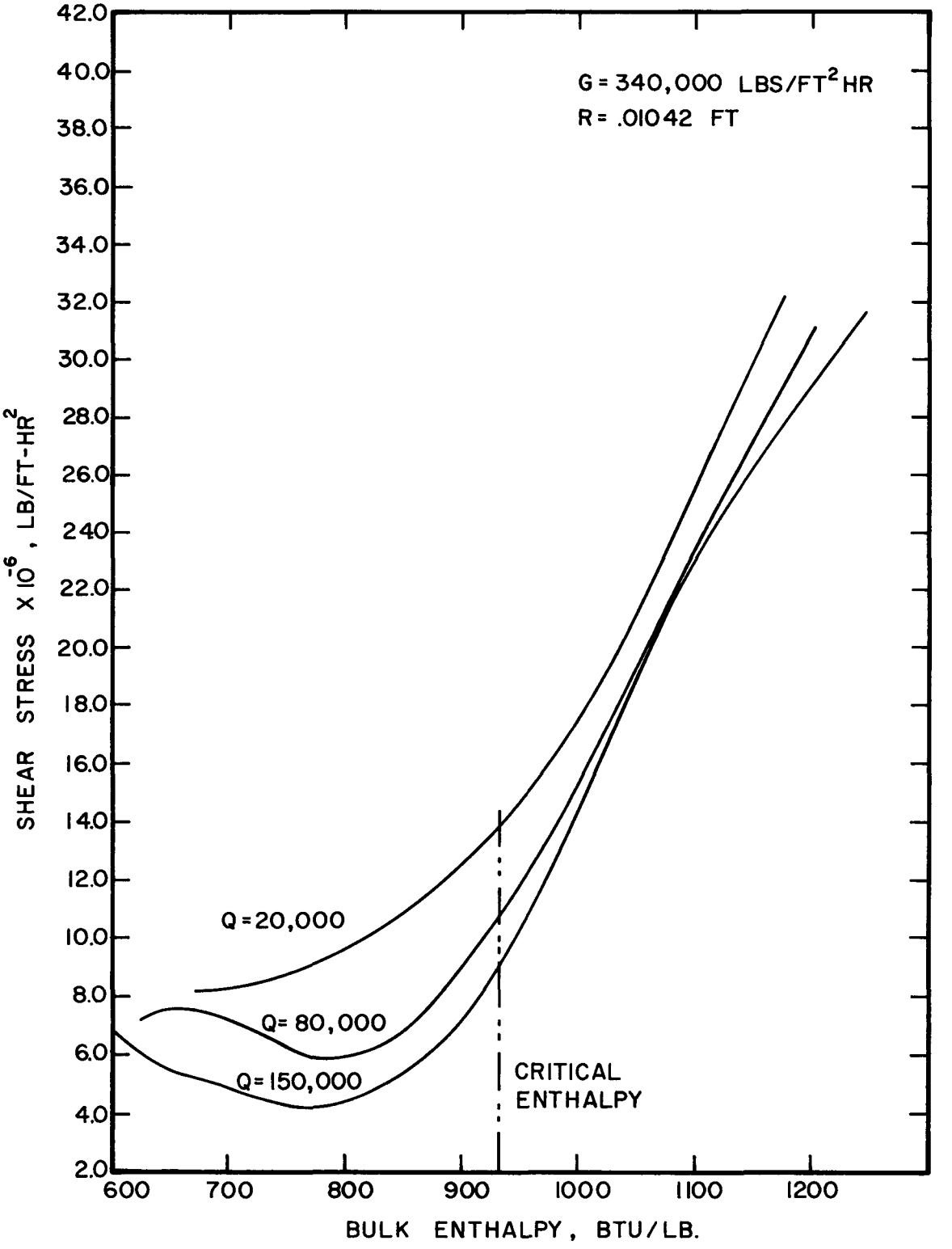

FIG. 12 : VARIATION OF SHEAR STRESS WITH HEAT FLUX

the critical enthalpy. The velocity profiles away from the critical region are very similar. This is to be expected when the flow is highly turbulent and the Reynolds numbers are fairly high. An explanation sometimes suggested for the deterioration phenomenon is that "re-laminarization" of the flow takes place. Though this is confirmed by this investigation to the extent that there is a drop in the shear stress in the deteriorated region, the velocity profiles do not tend to the parabolic laminar profiles. On the contrary, the velocity profile is "fuller" in the deteriorated region.

The temperature profiles show that the temperature drop in the region close to the wall is larger in the region associated with the peak in the wall temperature. The reason for the difference between the temperature profiles in the high and low density regions is because of the much lower conductivity in the low density region which accounts for the proportionately larger temperature drop near the wall.

The radial locus of the critical temperature in the fluid is of some interest, for example, in the formulation of integral methods of solution. Figure 15 shows that the locus is "flatter" than for a constant property flow; i.e., the critical temperature persists longer near the wall. This is not surprising since the region around the point in the flow at the critical temperature behaves like a "heat sink."

Calculations have shown that the deterioration in heat transfer occurs when the critical temperature is in the so-called "buffer" region, i.e., where $5 < y^{++} < 26$, and the turbulent and laminar transport properties are of the same order of magnitude.

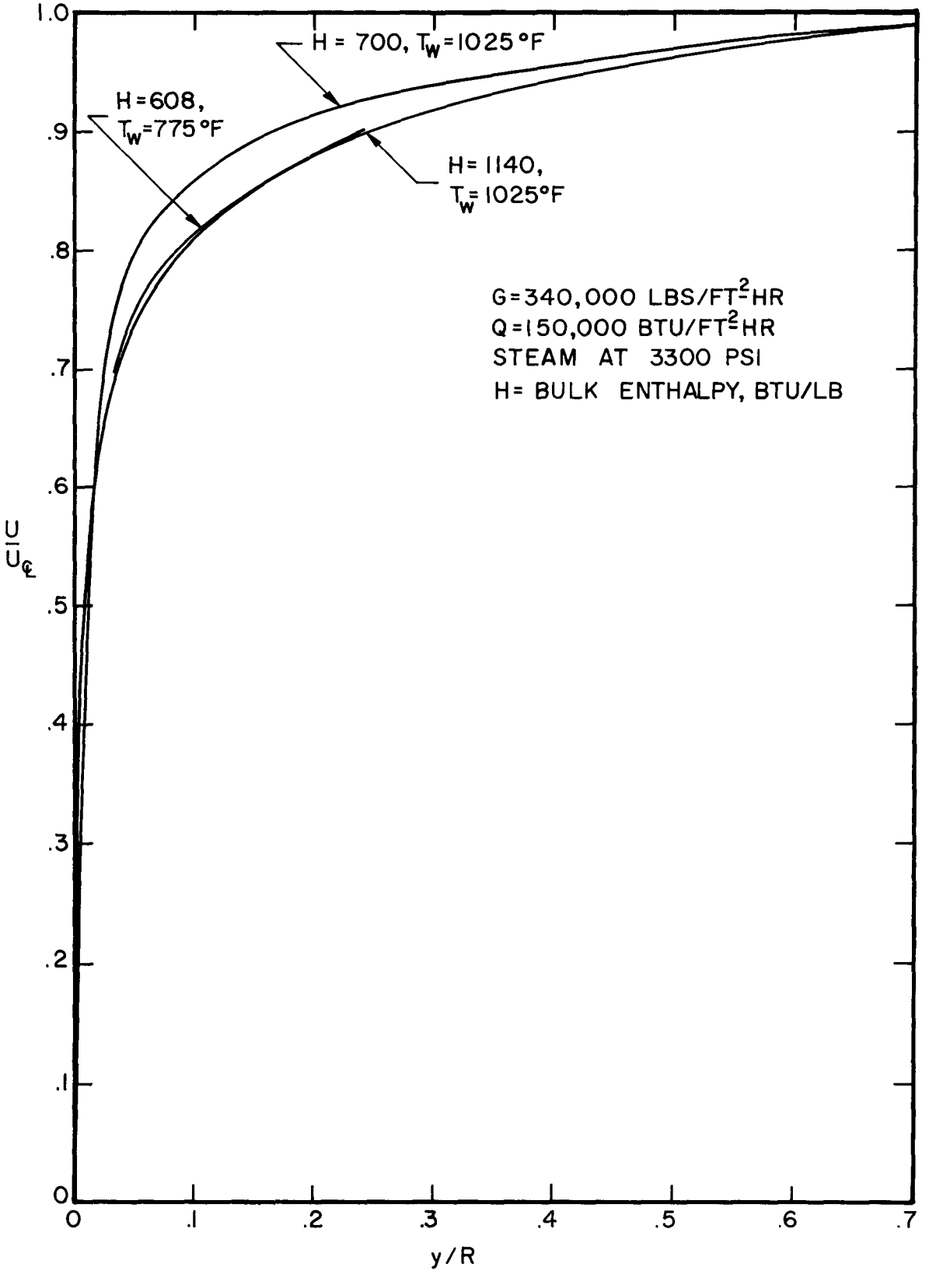

FIG. 13: COMPUTED VELOCITY PROFILES

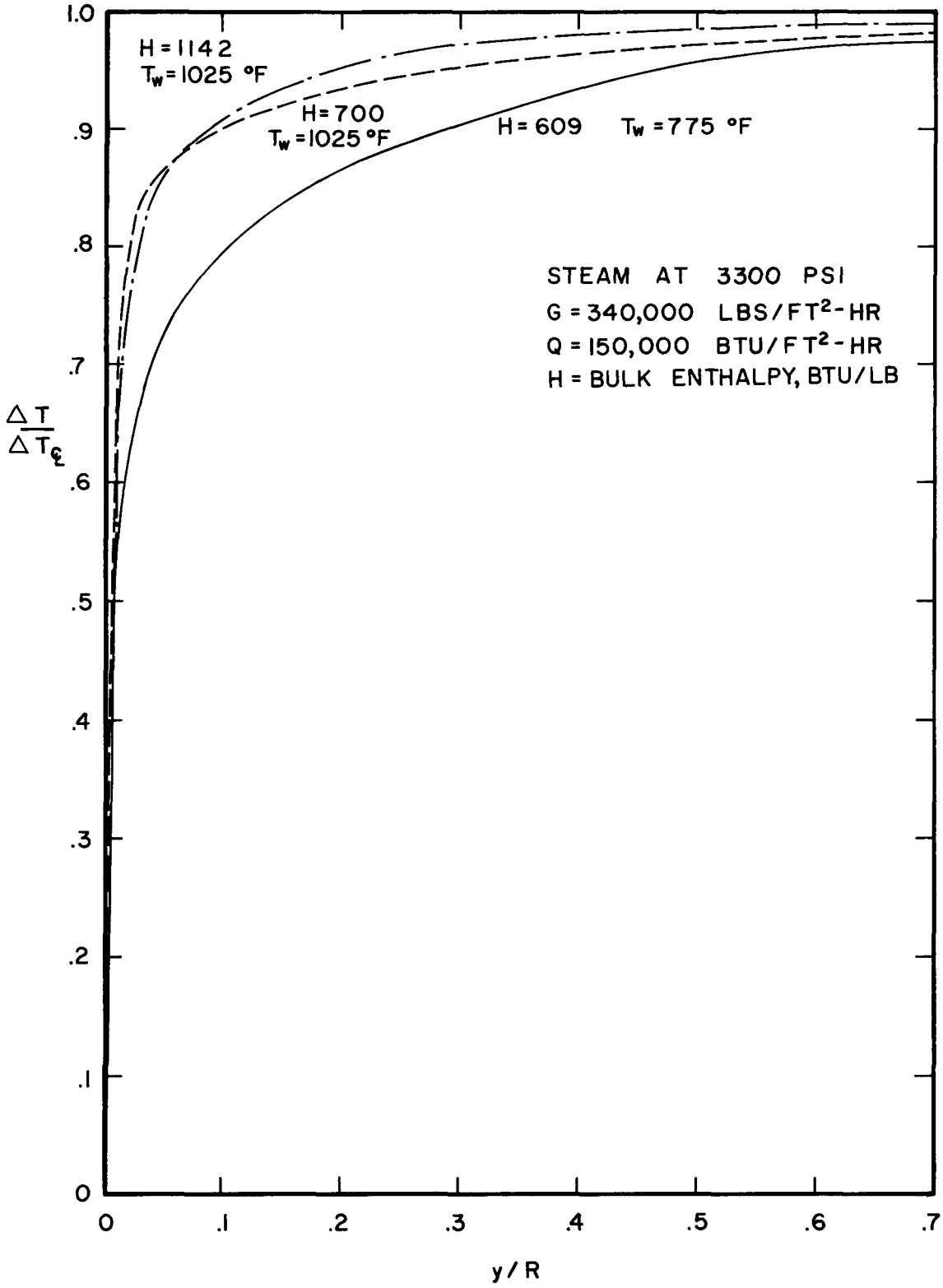

FIG. 14 COMPUTED TEMPERATURE PROFILES

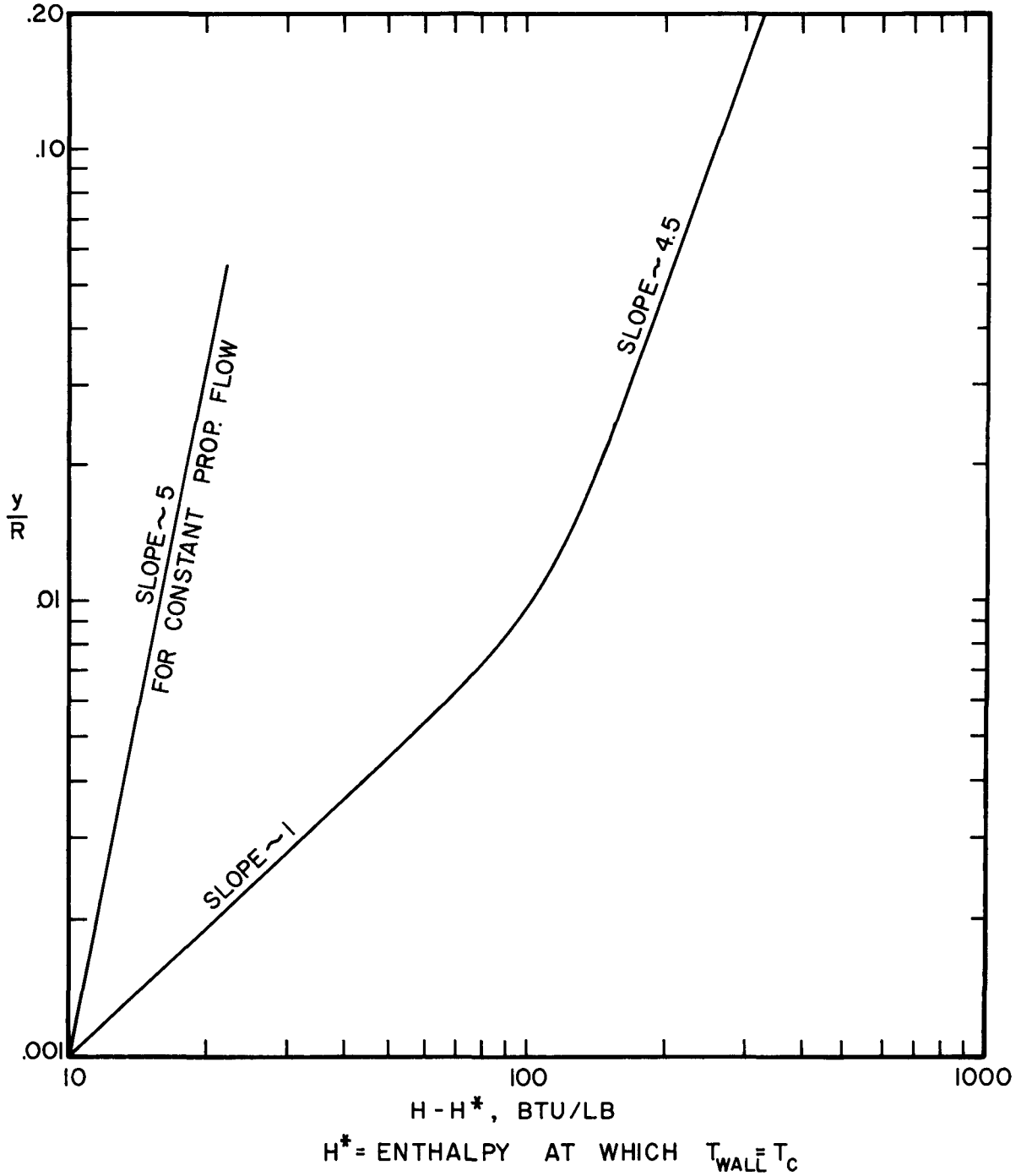

H^* = ENTHALPY AT WHICH $T_{WALL} = T_c$

FIG. 15 : RADIAL LOCUS OF T_c IN A TYPICALLY DETERIORATED REGION

5.6 Simplified Physical Model

It is possible to postulate a simple physical model to explain the deterioration phenomenon based on the evidence of the computed results.

If the equations governing the flow are examined,

$$(1 - Y)q_o = \rho(\alpha + \varepsilon_h) \frac{dh}{dy} \tag{5.1}$$

$$(1 - Y)\tau_o = \rho(\nu + \varepsilon_m) \frac{du}{dy} \tag{5.2}$$

where $\alpha = k/\rho Cp$, $\nu = \mu/\rho$,

it is evident that the velocity profiles and the enthalpy profiles will be identical if the molecular $Pr = C_p\mu/k$, and the turbulent Prandtl number $\varepsilon_h/\varepsilon_m$ are both unity.

Since the assumption $\varepsilon_h = \varepsilon_m$ has been made and the molecular Prandtl number does not differ significantly from unity except in small regions in the pre-critical enthalpy region, it should be expected that the relation

$$\frac{q_o}{\tau_o} = \frac{\Delta h}{\Delta U} \tag{5.3}$$

will hold in the pre-critical enthalpy region,

$$\text{or} \quad \frac{q_o}{\Delta h\, \rho_b\, U_b} = \frac{\tau_o}{\rho_b U_b^{\,2}} \tag{5.4}$$

which is Reynolds analogy with the enthalpy drop Δh used instead of $C_p.\Delta T$. Thus there is a correlation between the friction factor and the heat transfer rate, and the deterioration corresponds to the drop in the shear stress.

Actually, the molecular Prandtl number is substantially greater than one near the wall in the deteriorated region, due to the critical temperature being in the buffer region. Because of this, the deterioration in heat transfer coefficient is greater than the drop in the shear stress. Typical calculations have shown that the ratio of $\frac{\tau_o/\rho_b U_b^2}{q_o/\Delta h \rho_b U_b}$ peaks to a high value of about 2.5 to 3 when the wall temperature is close to the critical temperature and is substantially greater than one (1.5 to 2) in the region of the wall temperature peak. The drop in shear stress is basically governed by the radial temperature drop in the fluid stream as it approaches the critical region. When there is sufficiently large temperature difference between the wall and the bulk of the fluid, with the wall temperature being above and the bulk temperature below the pseudo-critical temperature, the bulk velocity is essentially that of the high density fluid whereas the fluid near the wall is of low density. This causes the shear stress, governed by $\rho\ \overline{u'v'}$ to drop by a substantial amount.

Furthermore, along the tube as the bulk enthalpy reaches a value close to the critical enthalpy, there is an improvement in heat transfer due to increased shear stress and turbulence, a high value of the bulk Prandtl number, and enhanced mixing.

Thus the phenomena of deterioration and improvement in heat transfer always exist side by side. At low heat fluxes, the deterioration is wiped out due to the nearness of the bulk temperature to the wall temperature, since the reduced viscosity and density in the film is almost simultaneously accompanied by increasing velocities and an increase

in ρC_p in the core of the flow. At high heat fluxes the improvement in heat transfer is smaller because the high Pr region occupies a correspondingly smaller part of the cross section.

The situations in the case of low and high mass heat fluxes are illustrated in Figure 16.

The variation in density is necessary to the physical model for the occurrence of the temperature peak. This is verified in Figures 17 and 18. Figure 17 is a GD vs. bulk enthalpy plot in which the density and the specific heat are those of steam at 3300 psi., but the viscosity and conductivity are assigned constant values corresponding to the low density region. The S-shaped isotherms indicate that this situation will yield a maximum in the wall temperature-length along tube curve. Because of the low values of the conductivity and viscosity chosen, the wall temperatures are seen to be higher than those in Figure 7 (for QD = 5000 BTU/ft-hr, and all the properties of steam at 3300 psi) for corresponding enthalpy and flow rate, which is to be expected.

Figure 18 shows the GD vs. bulk enthalpy plot when the specific heat, conductivity, and viscosity correspond to steam at 3300 psi., but the density is assigned a constant value of 18 lbs/ft^3, which is in between the high density and low density regions. The isotherms in this case are seen to rise monotonically. Though there is a variation in the heat transfer coefficient as the enthalpy increases, there is no temperature peak corresponding to a minimum in the heat transfer coefficient.

This enables us to put maximum and minimum bounds on the heat transfer coefficient in the critical region. The worst case, obviously,

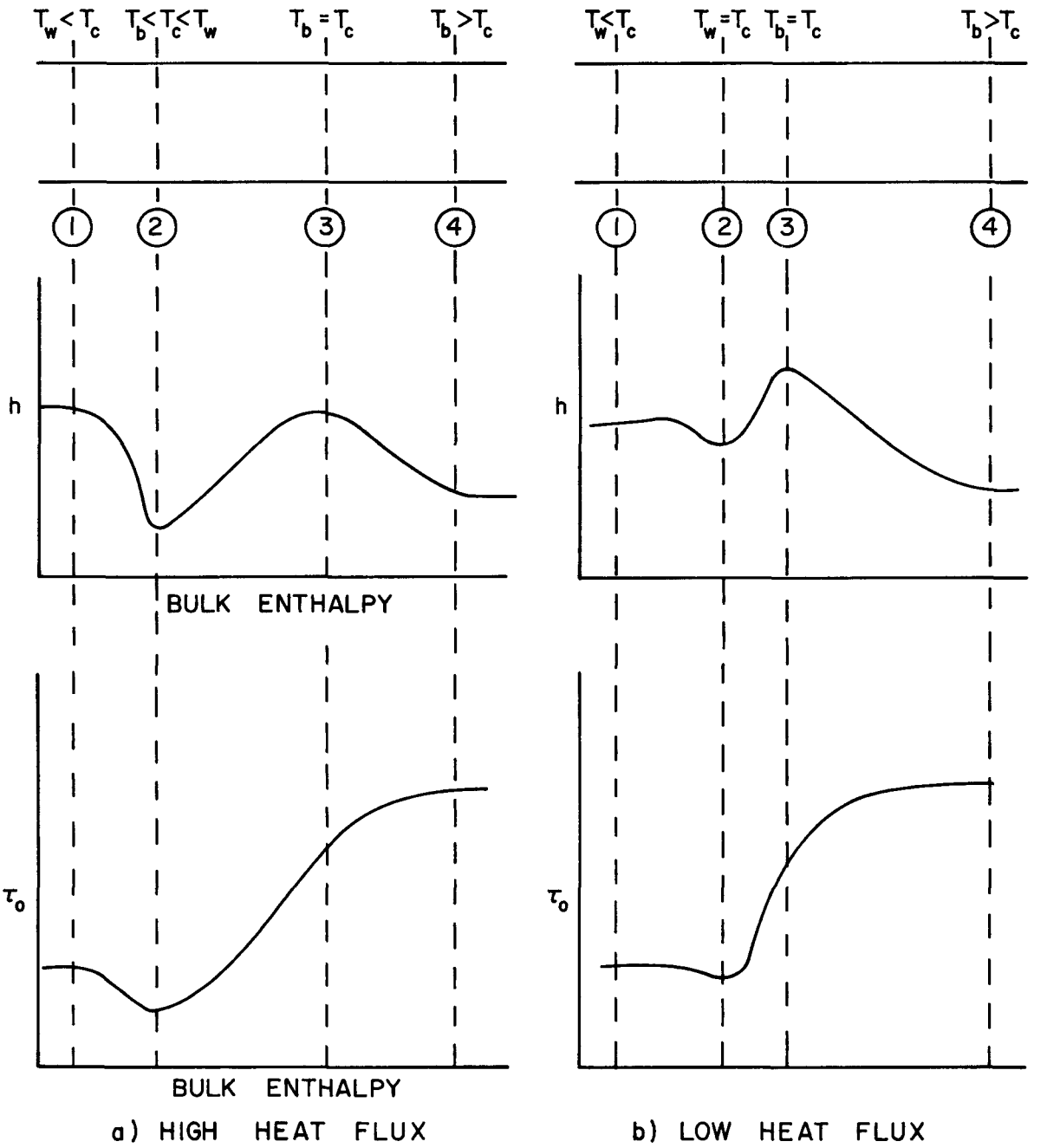

FIG. 16 : PHYSICAL EXPLANATION OF HEAT TRANSFER VARIATION

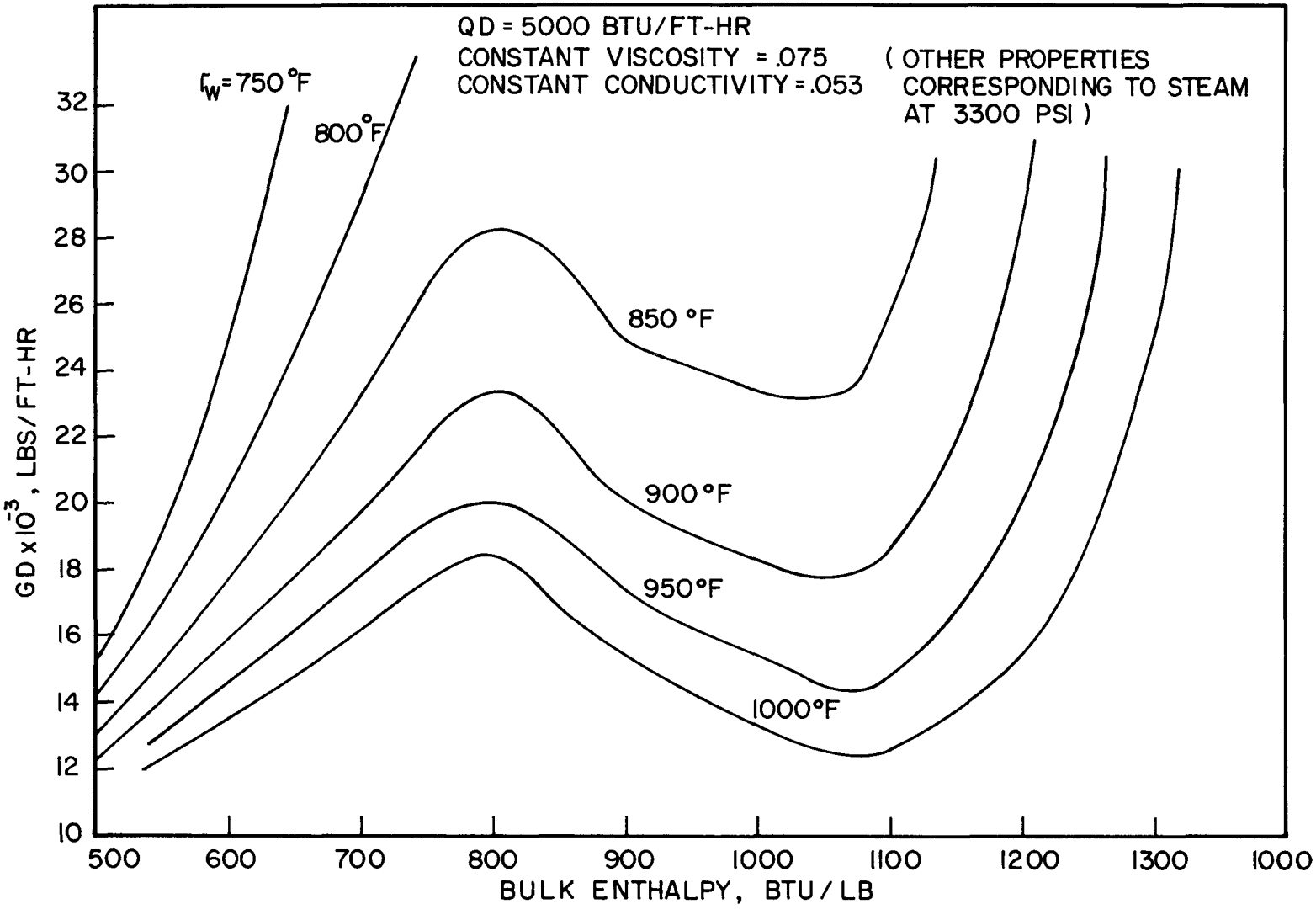

FIG. 17: COMPUTED GD VS. BULK ENTHALPY PLOT FOR CONSTANT VISCOSITY AND THERMAL CONDUCTIVITY FLUID

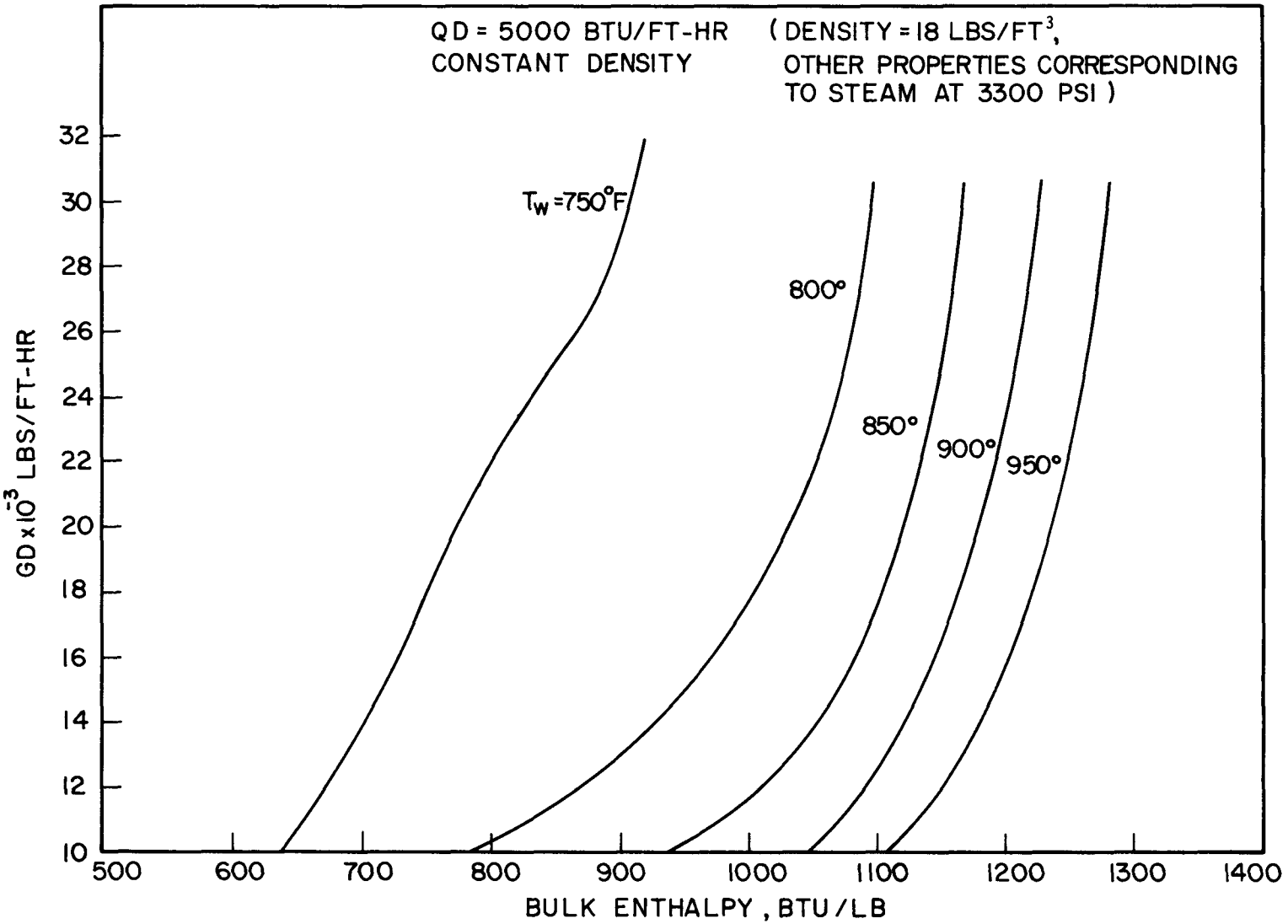

FIG. 18 : COMPUTED GD VS. BULK ENTHALPY PLOT FOR CONSTANT DENSITY FLUID

is when the temperature difference is so large that the density in the buffer layer corresponds to the wall temperature while the bulk velocity corresponds to the bulk density. The most favorable case is when the temperature drop is so small that all properties correspond to the bulk temperature. Thus

$$h_{max} = .023 \frac{k_b}{D} \left(\frac{GD}{\mu_b}\right)^{0.8} \left(\frac{C_{pb}\mu_b}{k_b}\right)^{0.4}$$

$$h_{min} = .023 \frac{k_w}{D} \left(\frac{GD\rho_w}{\rho_b\mu_w}\right)^{0.8} \left(\frac{C_{pb}\mu_w}{k_w}\right)^{0.4} .$$

Unfortunately, these bounds are much too conservative to be of much use in most cases.

5.7 Safe vs. Unsafe Plot for Steam

It is desirable for the designer to know when deterioration in heat transfer may be expected. For a fluid at a specific pressure, the design parameters are the diameter of the heated tube and the mass velocities for which the system is designed. In terms of these parameters, the designer would like to know the "allowable" heat flux beyond which operation becomes unsafe. In some situations as, for example, in nucleate boiling at subcritical pressures, there is a sharp "burnout" point when the heater temperature can increase by a large factor. In the present problem, the computed results do not yield a sharp demarcation in heat flux where the heat transfer gets poor. It is rather a progressive deterioration that occurs in the heat transfer rate as the heat flux is increased. This raises a problem in defining an allowable heat flux.

It, therefore, becomes necessary to make a somewhat arbitrary decision as to when the deterioration is "unsafe."

This may be done in a number of ways. One way is to fix the maximum allowable temperature for the heater wall. For steam this may be fixed, for instance, at 1100 degrees F., or 1200 degrees F. based on the material capabilities. This would probably be the appropriate criterion for a designer concerned with steam generators. Perhaps a more general method is to define the heat flux as "unsafe" when the computed heat transfer coefficient is a certain fraction of that calculated by using one of the conventional heat transfer correlations. This provides a means of judging the amount of deterioration for different fluids whose critical temperatures may be widely different. The easiest correlation to use for this purpose is the MacAdams correlation with the bulk properties used to evaluate the dimensionless parameters. This has two advantages:

a. It removes the need for iteration, which becomes necessary when one of the other correlations involving the properties at the wall temperature is used, because the wall temperature is not known a priori.
b. It is convenient since for most cases, it represents an upper bound on the heat transfer coefficient, and the computed heat transfer coefficient is always a fraction of it.

The fraction of the MacAdams bulk property correlation that is deemed unsafe is again arbitrary. This may be fixed at 0.5 or 0.33, or some other convenient fraction. In this report, the fraction used

is 1/2; i.e., the heat flux is unsafe if in the bulk temperature range

$T_{bulk} < T_c < T_{wall}$

$$Nu/Nu_{Mac} < 0.5$$

where $Nu_{Mac} = 0.023\ (Re)^{.8}(Pr)^{.4}$,

and the Reynolds and Prandtl numbers are evaluated for bulk properties, and Nu = computed Nusselt number = hD/k_b.

The bulk conductivity is used in calculating the Nusselt number so that the ratio of the two Nusselt numbers is equivalent to the ratio of the heat transfer coefficients.

The virtues of making an arbitrary decision like this in determining the allowable heat flux lie not so much in its applicability as an absolute safety guide line, but as a means of comparison for different fluids and for measuring the effects of various factors on the allowable heat flux. It is also a very convenient means of comparison between computed and experimental results.

With this definition, it is possible to make a "safe vs. unsafe" plot for steam in terms of the heat flux and the mass flow rate. By using the parameters QD(= Q_0^+) and GD(= U^*), the effect of diameter is taken into account. Care must be taken, however, to restrict the use of this plot to relatively small diameter tubes, or high velocity (i.e., small Gr/Re^2) so that the free convection effects do not become dominant. A plot of this kind is shown in Figure 19. The curve labeled 1 is based on computed results with the above mentioned criterion of allowable heat flux. The regions above and below this curve are labeled

"unsafe" and "safe," respectively. This means that if the conditions of heat flux and mass flow rate are such that they correspond to a point above the curve, the heat transfer coefficient in the pre-critical enthalpy region is less than half of the heat transfer coefficient as calculated using the MacAdams correlation using bulk properties. Similar curves could be drawn to represent the conditions where the heat transfer coefficient is 2/3 or 1/3 or some other desirable fraction of the heat transfer coefficient calculated from MacAdams' correlation. In the former event, the curve would lie above the drawn curve, and in the latter case, below it.

In a recent paper by Styrikovich et al (1), design considerations for supercritical boilers have been presented based on experimental data. The authors suggest that the deterioration in heat transfer for steam corresponds to the condition $G/(Q_0/A) < 4$ $(lbs/ft^2\text{-}hr)/(BTU/ft^2\text{-}hr)$ and give "allowable heat fluxes" for tubes 22 mm (.87 inch) in diameter. The criterion used for allowable heat flux appears to be that the outside tube surface should not exceed 580 ^oC (1080 ^oF). Curve 2 in Figure 19 shows this plot for the allowable heat flux in terms of the mass velocities. A comparison between curves 1 and 2 shows that the computed curve is conservative compared to the experimental curve. Part of the reason for this is that the criteria used for defining the allowable heat flux are different. Curve 3 in Figure 19 shows the computed curve which employs the criterion of a maximum wall temperature of 1050 ^oF as interpolated from Figures 6-9, allowing for a 30-degree temperature drop through the wall. The agreement between curves 2 and 3 is seen to be extremely good.

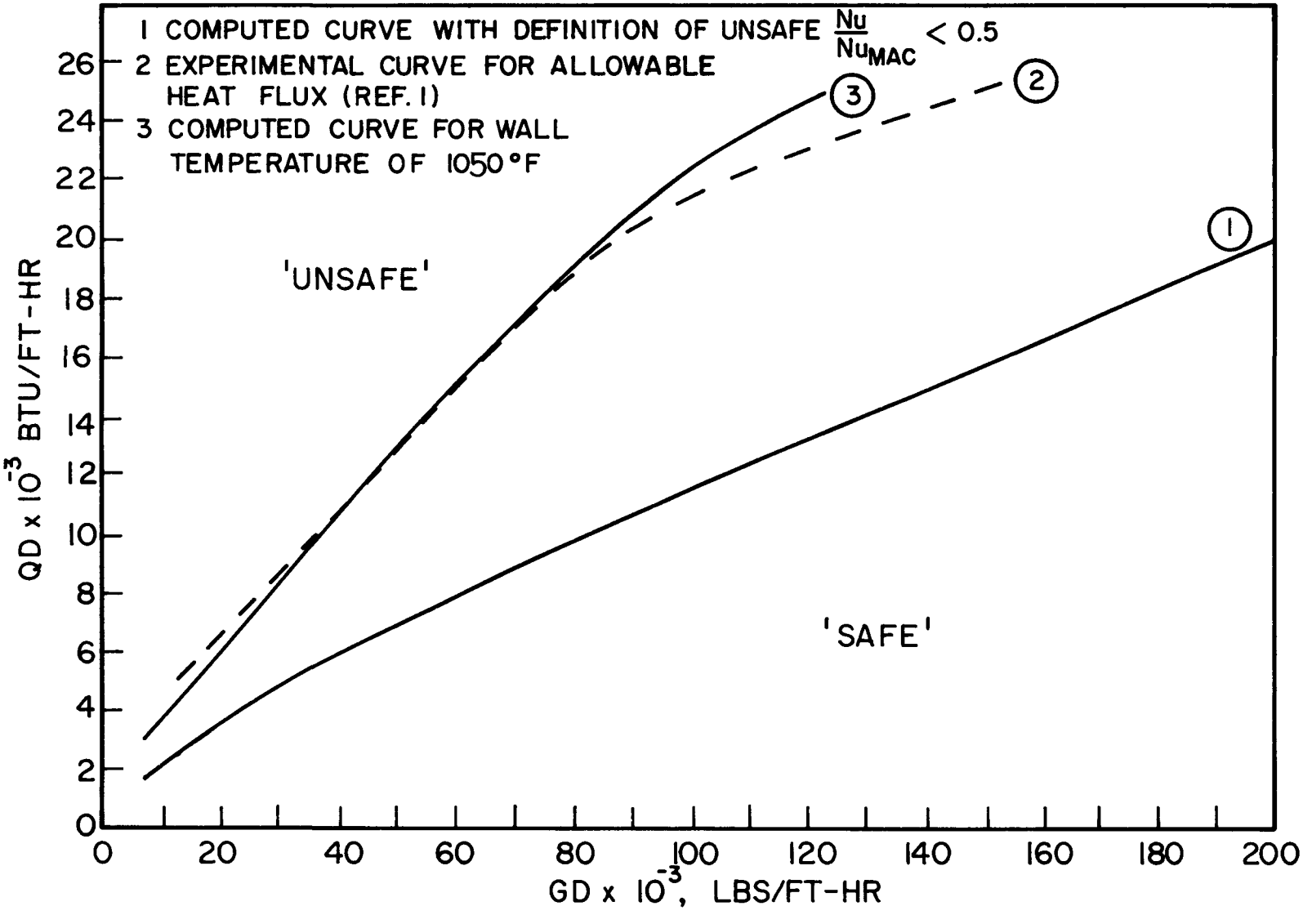

FIG. 19 COMPUTED SAFE VS. UNSAFE PLOT FOR STEAM

5.8 Effect of Buoyancy Terms

As mentioned in Section 4.6, difficulties arise in the estimation of the eddy diffusivity under conditions of large buoyancy effects which make the quantitative evaluation of the superposition of buoyancy forces difficult.

An examination of the corresponding GD vs. bulk enthalpy plots computed with van Driest's formulation for the eddy diffusivity for upflow, downflow, and without gravitational terms leads to the following conclusions:

1. At fairly high values, which covers most of the results in the present work, there is very little effect due to the buoyancy terms.
2. At low mass velocities, the heat transfer coefficient seems to be worse in upflow than in downflow or without gravitational terms. The downflow results differ less from the no-gravity results than the upflow results.

   The reason for this unexpected result can be qualitatively seen in Figure 20 which shows the radial shear stress variation for upflow, downflow, and without gravity terms at similar conditions of flow rate and enthalpy. The poor heat transfer in upflow is tied in with the drop in the eddy diffusivity of momentum because of a sharp drop in the shear stress near the wall. Under corresponding conditions in downflow, the shear stress distribution is not such that it is likely to affect the diffusivity drastically. As to how much this will affect the eddy diffusivity of heat is not clear at this time. Also, significant changes in the flow

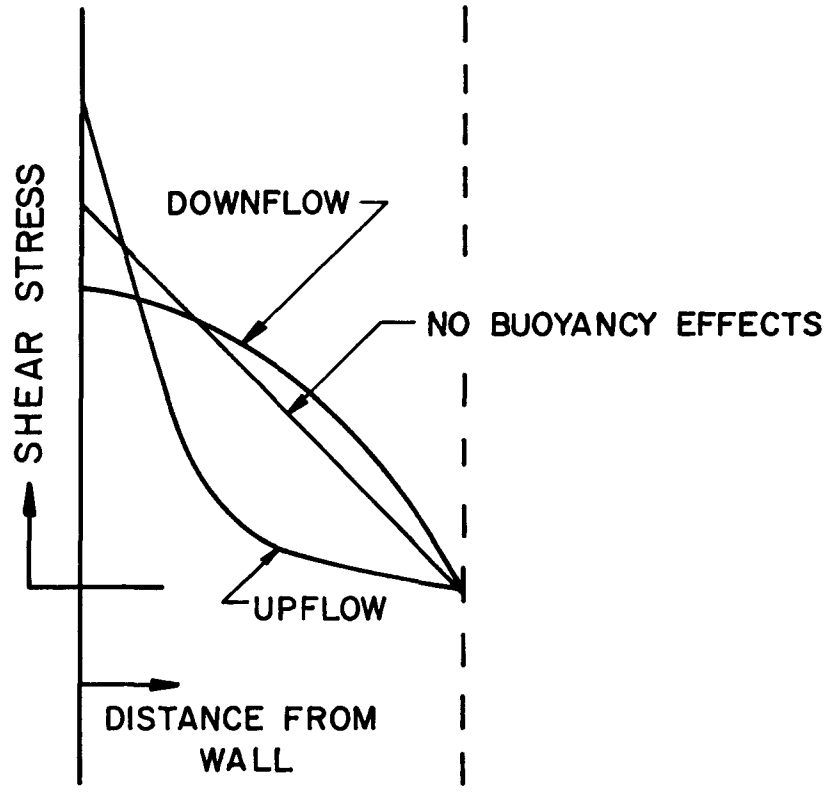

FIG. 20 : EFFECT OF BUOYANCY ON THE RADIAL SHEAR STRESS VARIATION

pattern such as flow reversal are possible and are not accounted for in the theory.

3. An order of magnitude value of 2×10^{-3}, within a factor of two, can be attached to the parameter Gr/Re^2 at the place where the buoyancy effects significantly change the heat transfer results by a comparison of the GD vs. H plots.

5.9 Discussion of Computed Results

An analytical procedure has been developed which is successful in predicting the progressive deterioration in the heat transfer coefficient at supercritical pressure as the heat flux is increased. The results yield a value of the temperature peak which agrees well with experimental evidence, though it usually yields a peak temperature that is somewhat higher than the experimental temperature. In the post peak region, due to shortcomings in the expressions used for the diffusivity, the predicted temperature is too high, and an enhanced diffusivity model is probably necessary in this region. A safe vs. unsafe plot has been drawn which can be of direct use to the designer, while somewhat conservative.

An important qualification on the use of the analytical procedure is that it cannot be extended to include large free convection effects. The parameter of GR/Re^2 has been suggested to determine when the free convection effects become important.

It is useful at this stage to compare the computed results with the experimental results of various investigators for steam. This is done in Table 3. The table shows the operating conditions used by various investigators as well as the important findings. The parameter

TABLE 3

Comparison of Experimental and Theoretical Results for Steam

Source	Pressure psi.	Tube Dia. Inches	G lbs/ft^2hr	Q/A BTU/ft^2hr	Orientation	Enthalpy at Peak BTU/lb	Nature of Peak	$Re = \frac{GD}{\mu_w}$	$Gr = \frac{\Delta\rho}{\rho_b}(\frac{\rho_b}{\mu_w})^2 R^3 g$	Gr/Re^2
Miropolskiy	3300	0.63	450,000	165,000	Upflow	710	Very Sharp	295,000	3.1×10^8	3.56×10^{-3}
Shitsman	3400	0.4	340,000	100,000 - 735,000	Upflow	760 - 780	Sharp	142,000	8.1×10^7	3.95×10^{-3}
Shitsman	3650	0.4	550,000	300,000	Upflow	790	Small	230,000	8.1×10^7	1.53×10^{-3}
Schmidt	3250	0.32	550,000	160,000 - 320,000	Vertical Horizontal	810 - 840	Broad	184,000	4.1×10^7	1.21×10^{-3}
Schmidt	3250	0.25	1,340,000	160,000 - 320,000	Vertical Horizontal	-	No Peak	450,000	1.9×10^7	0.86×10^{-4}
Styrikovich	3500	0.87	400,000 - 2,400,000	80,000 - 400,000	Vertical (?)	790-820	Broad	362,000 - 2.17×10^6	66×10^7	0.14×10^{-3} to 5.05×10^{-3}
Swenson et al	3300 - 6000	0.371	400,000 - 1,600,000	65,000 - 580,000	(?)	-	No Peak Decrease in Heat Transfer	27,000 - 880,000	6.3×10^7	0.13×10^{-3} and above
Calculations	3300	0.4	340,000	100,000 - 135,000	No Gravity Terms	810-820	Broad	142,000	-	-
Foster-Wheeler*	3540	0.982	200,000 - 540,000	100,000 - 260,000	Vertical	790-820	Small	204,000 - 550,000	1.18×10^9	28.2×10^{-3}

*Small L/D = 50

Gr/Re^2 is also calculated to evaluate its significance. The Grashof number is calculated as $\frac{\rho_b - \rho_w}{\rho_b} \times (\frac{\rho_b}{\mu_w})^2 R^3 g$ and the Reynolds number as GD/μ_w.

The following observations can be made from the table:

1. The nature of the deterioration varies from a sharp peak in the wall temperature to a broad temperature rise spread over a larger part of the test section. The computed peak lies in between the two extremes.
2. There seems to be some correlation between the free convection effect as measured by the GR/Re^2 parameter and the sharpness of the peak. A sharp peak in wall temperature is probably influenced by additional deterioration due to free convection effects.
3. The region of enthalpies where the deterioration in heat transfer takes place is also seen to vary in a manner similar to the nature of the deterioration; i.e., the sharpest peak occurs at a smaller value of the bulk enthalpy. Here too the calculated peak occurs in between the two extreme values of the bulk enthalpy. It should be noted that the use of a two-dimensional model yields a temperature peak that occurs at a slightly smaller bulk enthalpy.
4. The order of magnitude value of 2×10^{-3} for the free convection parameter is in line with the experimental findings. Only the results of Shitsman and Miropolskiy lie above this value, and the temperature peak in Miropolskiy's experiments does appear to be of a different character than the other experiments. The temperature peaks in his experiments are much sharper and occur at substantially smaller values of the bulk enthalpy.

5. In general, the computed results agree well with the results of Schmidt and Shitsman and Vikrev et al but not with those of Miropolskiy. Satisfactory agreement is obtained even when the distortion in the shear stress profile is considerable as in the experiments of Shitsman. The Foster Wheeler data does not tie in with either the computed results or those of the other experimenters. This is probably because of dominant entrance effects in their experiments.

6. EXPERIMENTAL PROGRAM

6.1 Introduction

A detailed experimental program was undertaken to verify the computed results and to study the effects of various parameters such as the pressure, orientation, inlet effects, geometry, etc. on the deterioration phenomenon. Carbon dioxide was chosen as the working fluid because of its convenient critical range (T_c = 88 ^{o}F, p_c = 1071 psia) as compared to those of water (T_c = 705 ^{o}F, p_c = 3206 psia). Carbon dioxide has been used by various investigators for supercritical pressure studies for the same reason. The previous experimental work in this field with carbon dioxide includes the work of Hall, Jackson et al (25), Knapp and Sabersky (4), Koppel and Smith (27), Tanaka et al (24), Bringer and Smith (22), etc. None of these investigators report a sharp deterioration in heat transfer to carbon dioxide as in other fluids. The reasons may be that Hall et al did not use high enough heat fluxes while Koppel and Smith, though using a wide range of heat fluxes, did not have low enough inlet temperatures to observe deterioration effects. A recent Russian investigation (61) reports very low heat transfer coefficients at high heat fluxes. A temperature peak as seen in other fluids is not reported because here again the inlet temperatures were not low enough.

Another reason for using carbon dioxide is that its properties in the critical region have been the subject of much investigation and are fairly well known as a result. Figure 21 shows the properties of carbon dioxide at 1075, 1100, 1150, and 1200 psia. taken from

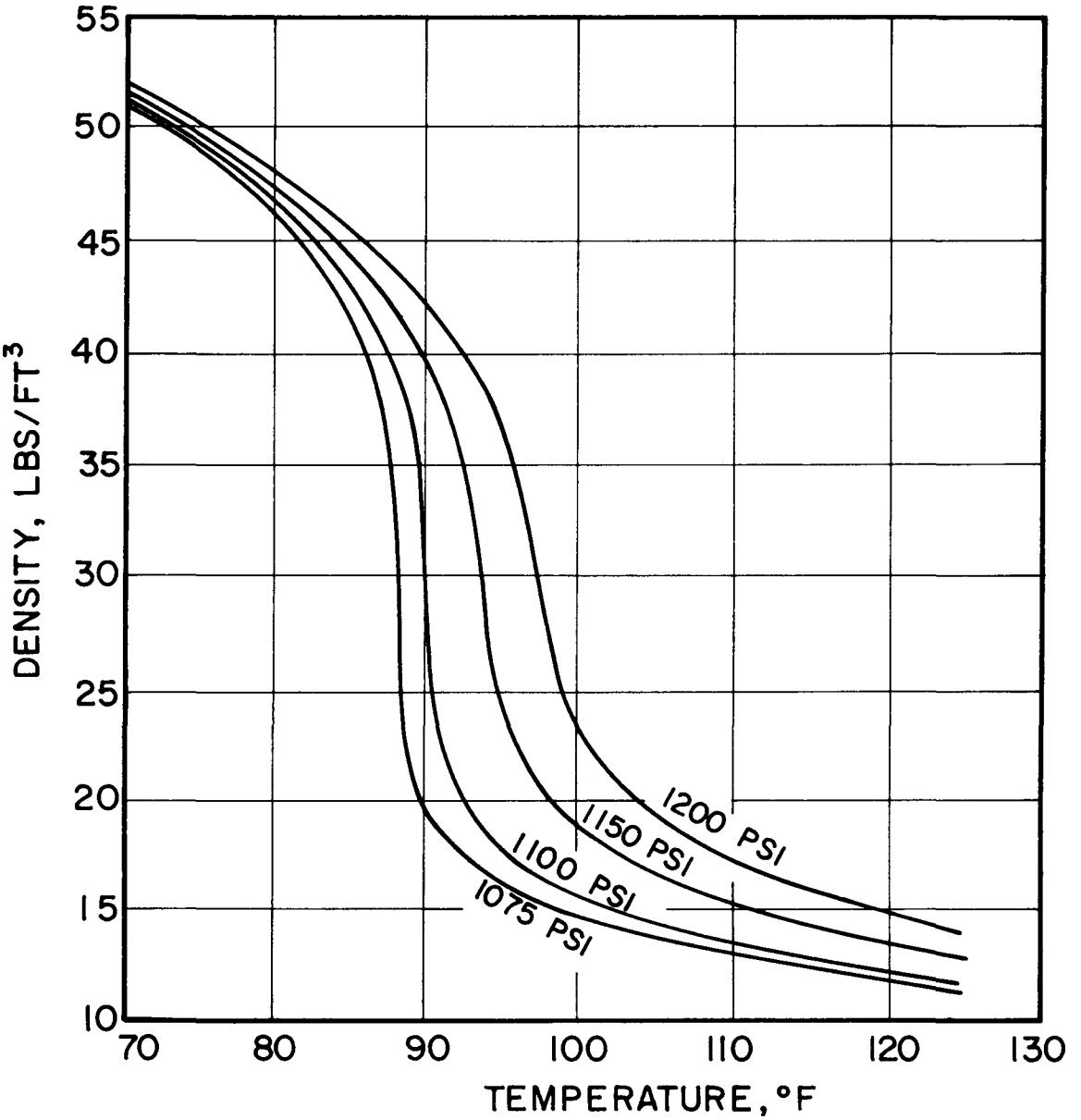

FIG. 21(a) : DENSITY OF CARBON DIOXIDE

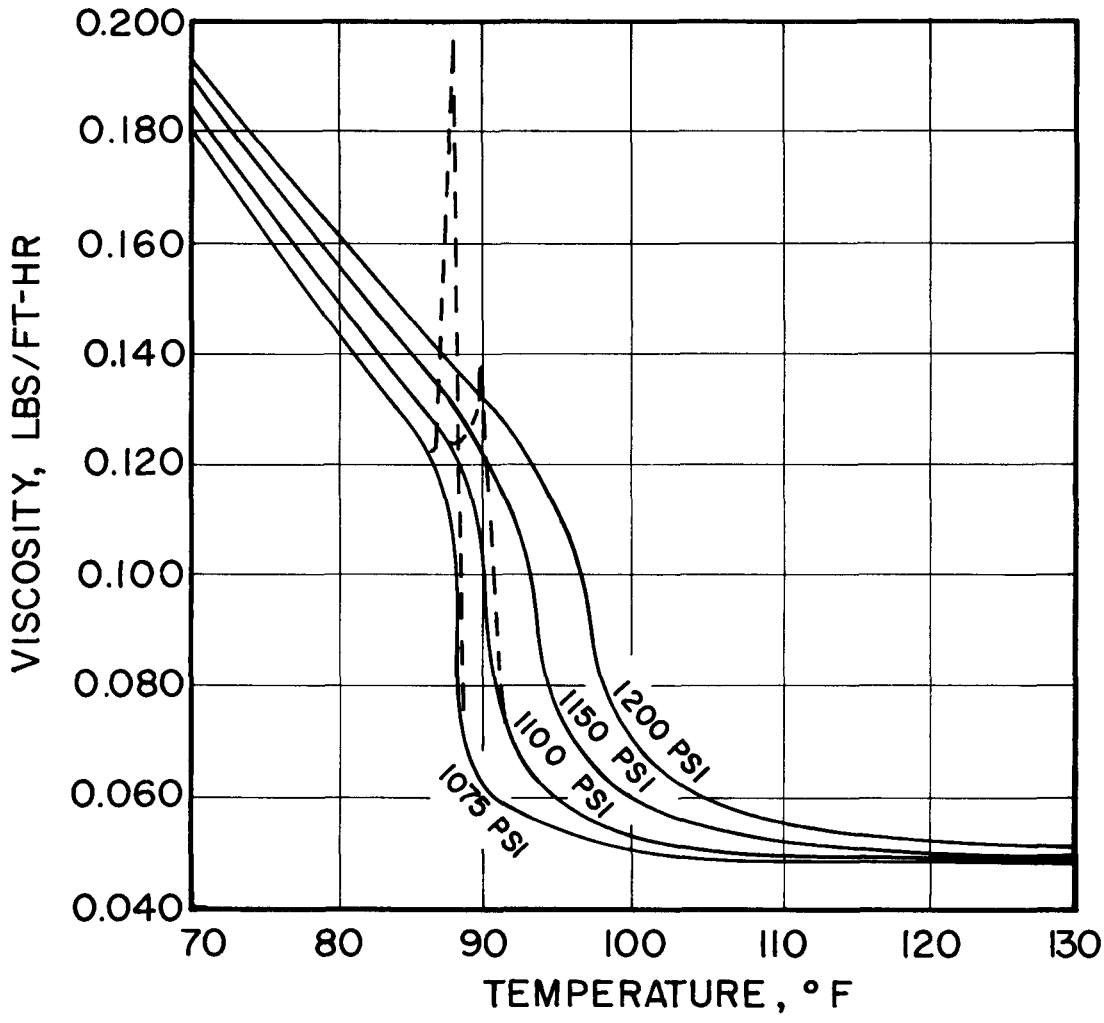

FIG. 21(b) : VISCOSITY OF CARBON DIOXIDE

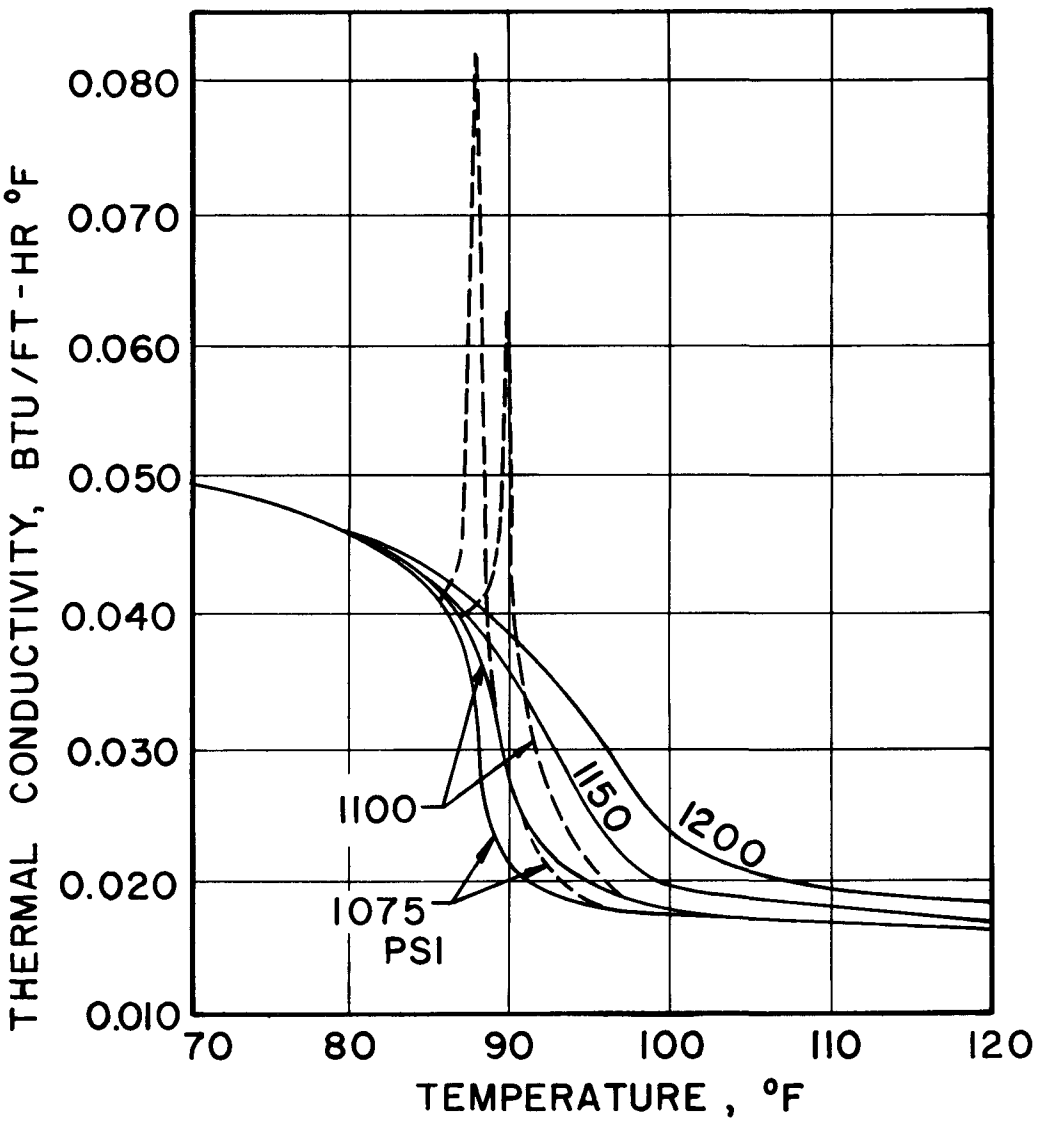

FIG. 21(c): THERMAL CONDUCTIVITY OF CARBON DIOXIDE

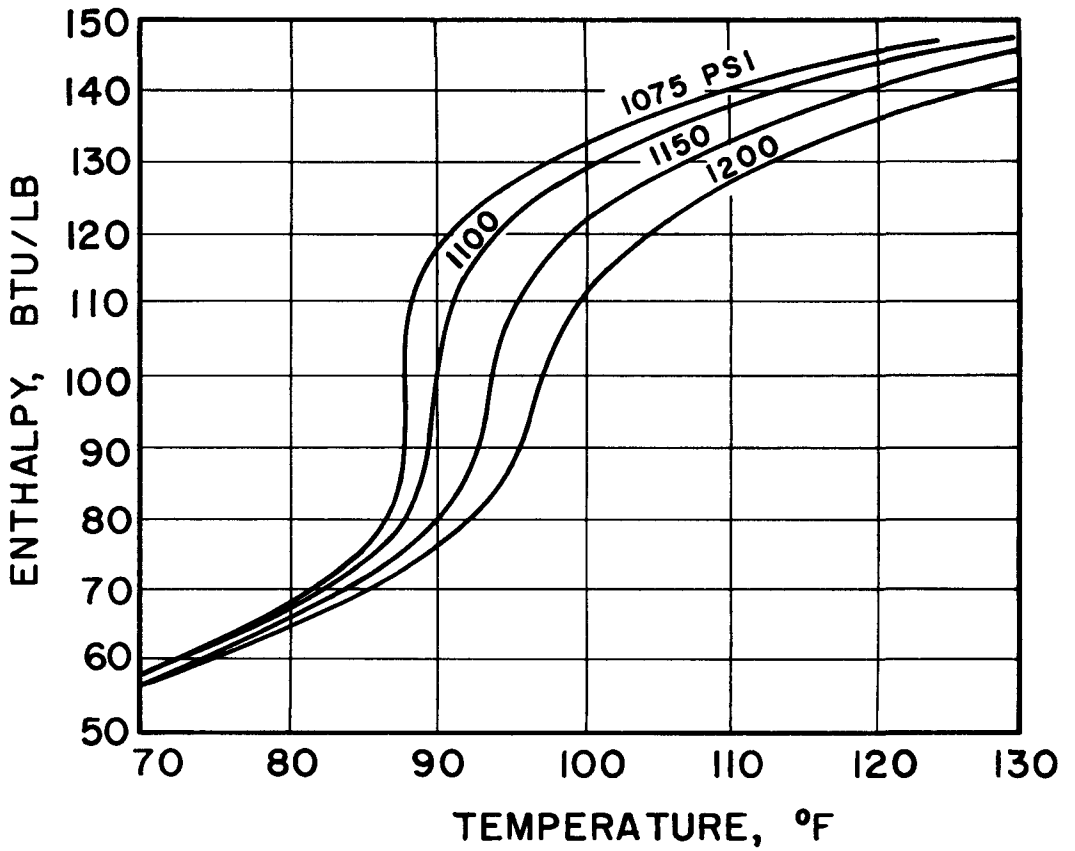

FIG. 21 (d): ENTHALPY OF CARBON DIOXIDE

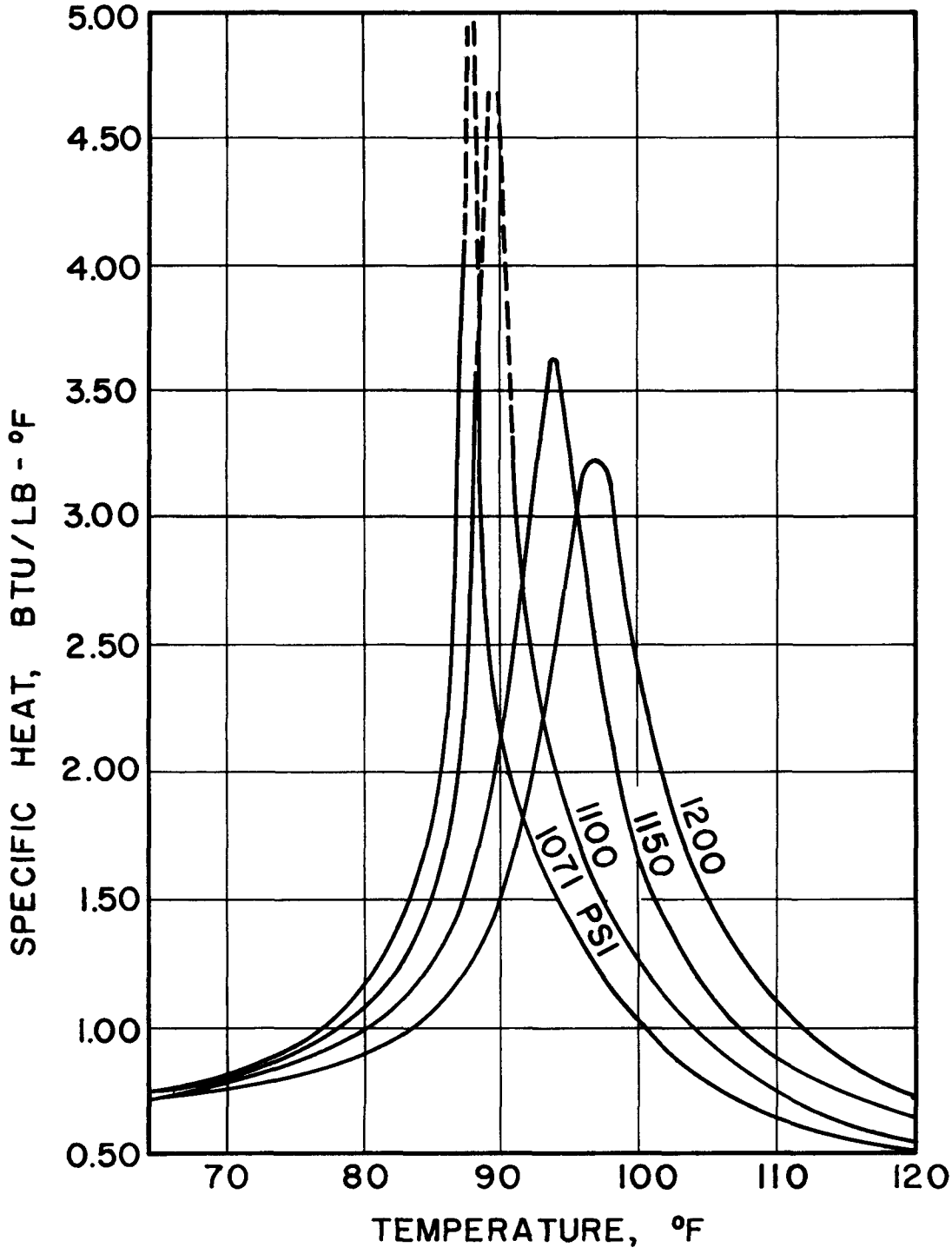

FIG. 21 (e): SPECIFIC HEAT OF CARBON DIOXIDE

reference 43. The viscosity and thermal conductivity graphs at 1075 and 1100 psia are shown with peaks at the critical temperature in dotted lines. As was mentioned in Section 3, some investigators have reported measuring these peaks and others have not. The properties used in this report were assumed to decrease in the critical region rather than peak at the critical temperature.

Another reason for choosing carbon dioxide as the working fluid is that it is quite stable near its critical point. Investigations with freons, which also have a convenient critical range, have shown in the past that severe problems can arise due to chemical disassociation in the critical region.

In this investigation, deterioration in heat transfer was found to exist in carbon dioxide and to be sensitive to a number of factors such as the inlet enthalpy, swirl, etc.

6.2 Description of Test Loop

The high pressure loop used in this study was designed and built for the purpose at the Heat Transfer Laboratory at M.I.T. An overall view of the experimental setup is shown in Figure 22. The test loop was enclosed in a framework of wood and dexion. In order to increase the corrosion resistance and prevent rusting, the fittings and piping were made of stainless steel. The piping consists mainly of 1/2-inch seamless tubing, with sections of 1-inch pipe in the pump bypass loop and 2-inch pipe in the main heat exchanger. The entire loop was designed for a pressure of 2000 psi. Figure 23 shows a schematic diagram of the loop. The system pressure was maintained with a Liquidonics gas accumulator,

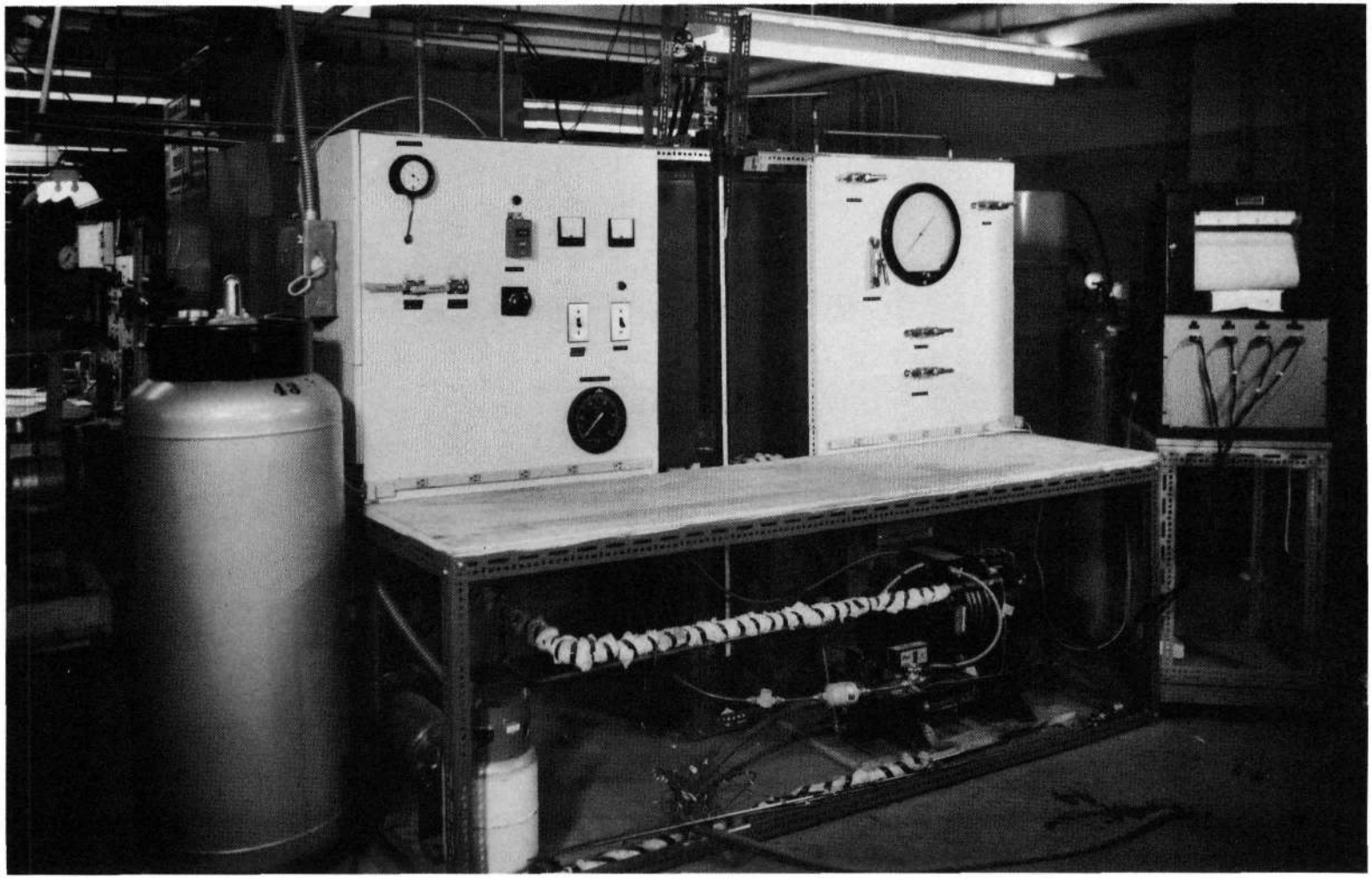

FIG. 22: OVERALL VIEW OF EXPERIMENTAL SETUP

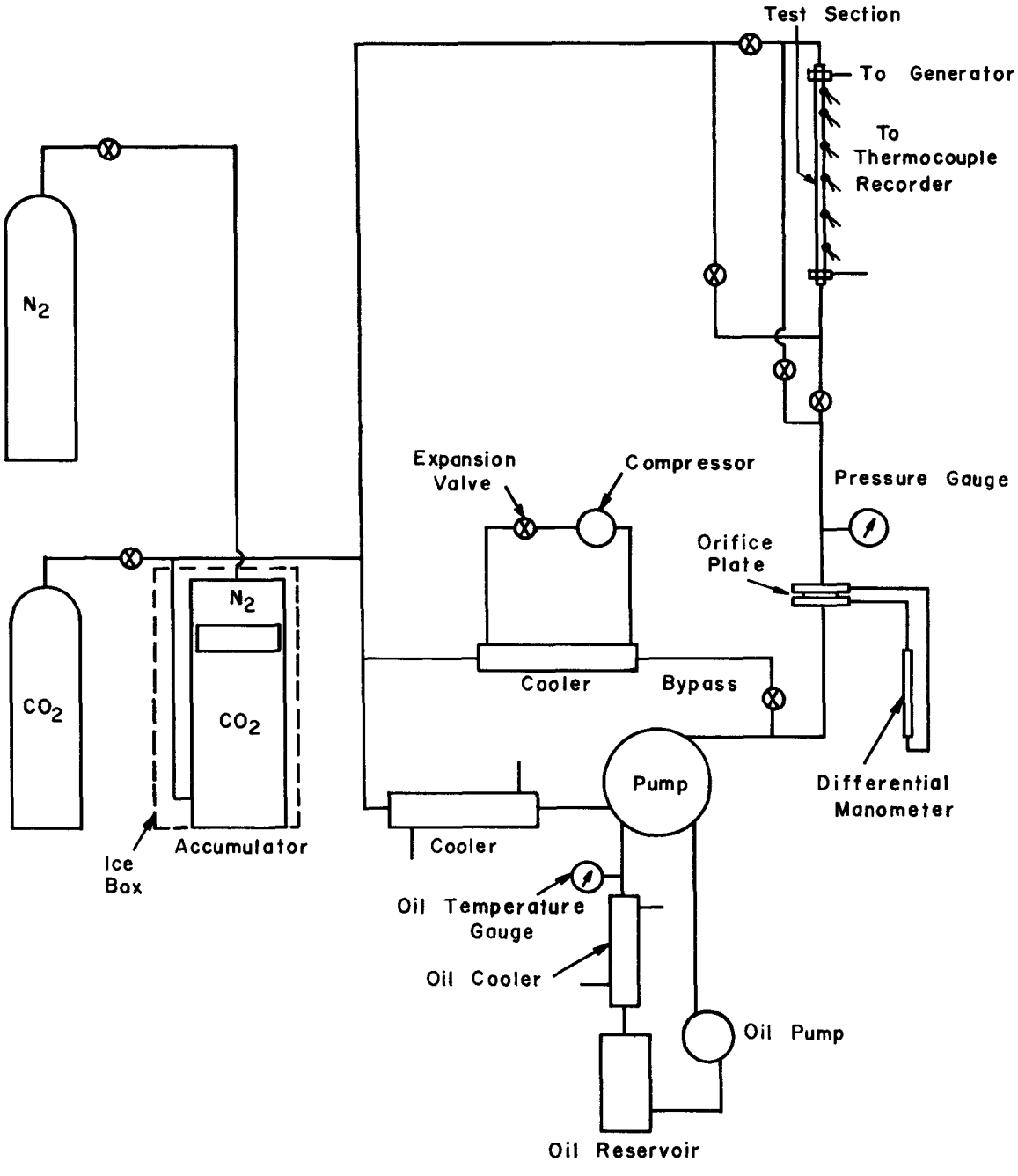

FIG.23: SCHEMATIC DRAWING OF EXPERIMENTAL LOOP

which was loaded with high pressure nitrogen gas. The accumulator has a capacity of 7.5 gallons and is rated for 3000 psi. The nitrogen was obtained from a commercial welding equipment supplier. The nitrogen and carbon dioxide sides of the accumulator are separated by a piston with Teflon O-rings for sealing. The accumulator was kept in an ice bath so that the carbon dioxide could be stored as a liquid at 800 psi. The carbon dioxide used was obtained from the Liquid Carbonic Division of General Dynamics and was 99.9 percent pure, with a very low moisture content. High pressure hoses were used to charge the nitrogen and carbon dioxide into the accumulator.

A Westinghouse Model 30 centrifugal pump was used to circulate the carbon dioxide within the loop. The pump was used to provide only the flow pressure drop in the loop and the possibility of large pressure oscillations was thus minimized. The pump, which is constructed of stainless steel, is designed to operate at up to 2000 psi. and is rated for 30 GPM at 45 psi. It is provided with a thermal protection device which cuts off operation at 120 ^{o}F. The windings are cooled by transformer oil circulated through the pump casing by means of a gear pump. The cooling oil was kept clean with the help of a Fram Filcron filter and was cooled in an oil-to-water BCF heat exchanger. A cold water line was available for use in the heat exchanger. A bypass line was used in the loop because of the large flow capacity of the pump. The bypass line flow rate was controlled by means of a gate valve.

Two heat exchangers were provided in the main system. One was a once-through heat exchanger which used cold water flow counter current

to the carbon dioxide. This was located in the main line. Another heat exchanger was located in the bypass line. This consisted of a refrigeration loop with the cold refrigerant flowing counter current though a stainless steel tube inside the carbon dioxide line. The refrigeration unit consisted of a Copeland motor-compressor unit rated for 3/4 ton at 0 ^{o}F and a Sporlan CFE-1-1/2-Z expansion valve. Freon 12 was used as the refrigerant. The refrigeration unit was added to the system to obtain greater cooling capacity. At a later stage, liquid nitrogen was blown through the main heat exchanger instead of water to obtain greater inlet subcooling. Liquid nitrogen was obtained from the Cryogenics Laboratory at M.I.T. in 180-liter containers fitted for liquid withdrawal.

The carbon dioxide was pumped through an orifice plate and via the plumbing upstream of the test section through the test section. It then returned via the return line, merged with the cold liquid from the bypass line,and then flowed to the cooler and back to the pump. The orifice plate had a 1/8-inch sharp edged orifice and was located between 1-inch pipe sections. The orifice flange assembly is rated for 3000 psi. and has flange pressure taps. The pressure drop across the orifice was measured with a 60-inch Merriam differential manometer rated for an internal pressure of 2000 psi and mercury as the manometric fluid. For smaller flow rates, this was later replaced by a bellows type of differential pressure gage made by the Barton Instrument Co., which reads pressure differences up to 50 inches of water. The orifice was calibrated for water, in the same Reynolds number range as was used with carbon dioxide, by direct measurement. The system pressure upstream

of the test section was measured with a Heise Bourdon gage, calibrated from 0 - 2000 psig. in intervals of 2 psi. The plumbing was arranged so that the flow could be either up or down through the vertical test section. Hoke ball valves were used for flow control. An exhaust valve was located between the test section and the cooler to enable the removal of carbon dioxide from the loop. The plumbing enabled the test section to be isolated and removed from the loop without evacuating the system. The low pressure cooling water supply was brought in through a 1-inch copper line. Jamesbury ball valves were used to regulate the cooling water supply. The coolers and piping upstream of the test section were insulated with fiberglas insulation.

Electrical power was supplied to the test section by a General Electric Motor Generator DC unit rated at 15 KW and 1000 amps. The voltage could be varied from 0-24 volts. A calibrated shunt was installed to enable current measurement. Power was transmitted to the test section through four power cables rated for a total of 1200 amps. current capacity. The power cables were connected to the electrodes which clamped on the test section at the top and bottom. The top electrode was fixed at the beginning, but was later replaced by a "floating" electrode attached to a flexible braided copper connector. Each electrode consisted of two aluminum parts bolted together to clamp the test section or heater between them. A slit cylindrical sleeve was used to provide good contact between the electrode and the test section. The rest of the plumbing was electrically insulated from the power supply by using couplings at the ends of the test section, which were separated by mica sheets.

Power for the compressor and the gear pump was taken from an overhead 110-volt AC line. The main pump required a 440-volt, 3-phase supply. A switch was provided in the system to ensure that the generator could not be switched on when the pump was not on, in order to prevent overheating of the test section.

6.3 Description of the Test Sections

In all, four different test sections were employed in the carbon dioxide tests. All were used in a vertical position. The first three sections consisted of stainless steel tubes of circular cross section. The fourth was used for visual observation and had an annular geometry.

The first test section used was a 3/8-inch by .065-inch wall tube of 304 seamless stainless steel tubing. This test section, with an inner diameter of 0.245 inch and a heated length of 60 inches (L/D = 245) was used for the bulk of the early experiments. A further unheated length of 12 inches (L/D $\sim$ 50) was provided at each end of the section. One-inch fittings were provided at the ends of the section and helped to mix the exiting fluid. Power was supplied through electrodes 60 inches apart between their inner faces. Since DC heating was employed, thermocouples had to be mounted on the tube wall with thin mica insulators in between. No special precautions were taken to insulate the test section thermally, except the use of fiberglas insulation around the test section. Two flanges were welded on to the ends of the test section. To facilitate removal and changing of test sections, the flanges were bolted to the corresponding flanges welded on in the system, thus providing metal-to-metal seals.

The second test section was a 1/8-inch inside diameter tube, used to provide a larger L/D ratio. This was a seamless 304 stainless steel

tube with a heated length of 60 inches. This section was also instrumented with thermocouples and insulated with fiberglas insulation. This was used in conjunction with large inlet subcooling.

A test section with a twisted tape inside was also used. A sheared strip of Inconel (0.0135-inch thick) was used to fabricate the twisted tape. The strip was twisted by suspending a weight of 80 pounds from the end of the strip, the other end of which was held in a clamp at the top. The weight was then turned to produce the required tape twist. The tape used had a twist of one complete turn in four inside diameters of the tube. A layer of Teflon paint was baked onto the tape for insulation. A tube of 1/4-inch inner diameter was used in connection with the twisted tape. The clearance between the tape and the tube was of the order of two mils. The tape was pulled into place and fitted snugly within the tube. The twisted tape covered the entire heated length of the tube. The outside of the tube was instrumented with thermocouples like the other sections.

The fourth test section used consisted of an annular section with a central heater in the form of a 3/16-inch stainless steel rod. A high pressure manometer was used for this purpose to enable visual observation through the glass window. The outside of the test section consisted of a rectangular column which was enclosed in stainless steel on three sides and had a glass window 60 inches long on the fourth side. The manometer had a pressure capability of 2000 psi. The glass window consists of a 1/2-inch thick Herculite glass plate, held between the stainless steel back plate and flanges in the front and sealed with long rubber O-rings.

The inside channel is a rectangular volume confined by stainless steel on three sides and glass on the fourth. Since the channel was rectangular (1/4-inch wide by 5/16-inch deep), only qualitative observations could be made with this test section. No thermocouples were provided on the heater rod in this case. The stainless steel heater was silver soldered to copper rods near the end fittings in order to prevent overheating of the heater in the sections not in contact with the fluid. The heater tube passed through two conax fittings at the entrance and exit of the manometer tube. The conax fittings were equipped with ceramic insulators to prevent contact between the heater and the stainless steel manometer. A view of this test section and the exit fittings is shown in Figure 24. The conax fittings were mounted in mixing chambers at the inlet and outlet. These mixing chambers also held conax fittings for thermocouples that measured the inlet and outlet temperatures in the fluid. Rubber O-rings were used for sealing. An attempt had been made previously to use a length of high strength glass tube outside a stainless steel tube which served as a heater and was instrumented with thermocouples. However, the glass tube proved to be incapable of sustaining the pressure and was abandoned.

6.4 Instrumentation, Measurements, and Capabilities

Instrumentation was provided to monitor the fluid inlet and outlet temperatures and the outside wall temperatures along the length of the heated section. All fluid and wall temperatures were measured by means of 30-gage, copper-constantan thermocouples from Leeds and Northrup duplex wire. Calibration checks were made on two of the thermocouples against a mercury thermometer of 1/2-degree accuracy in a water bath.

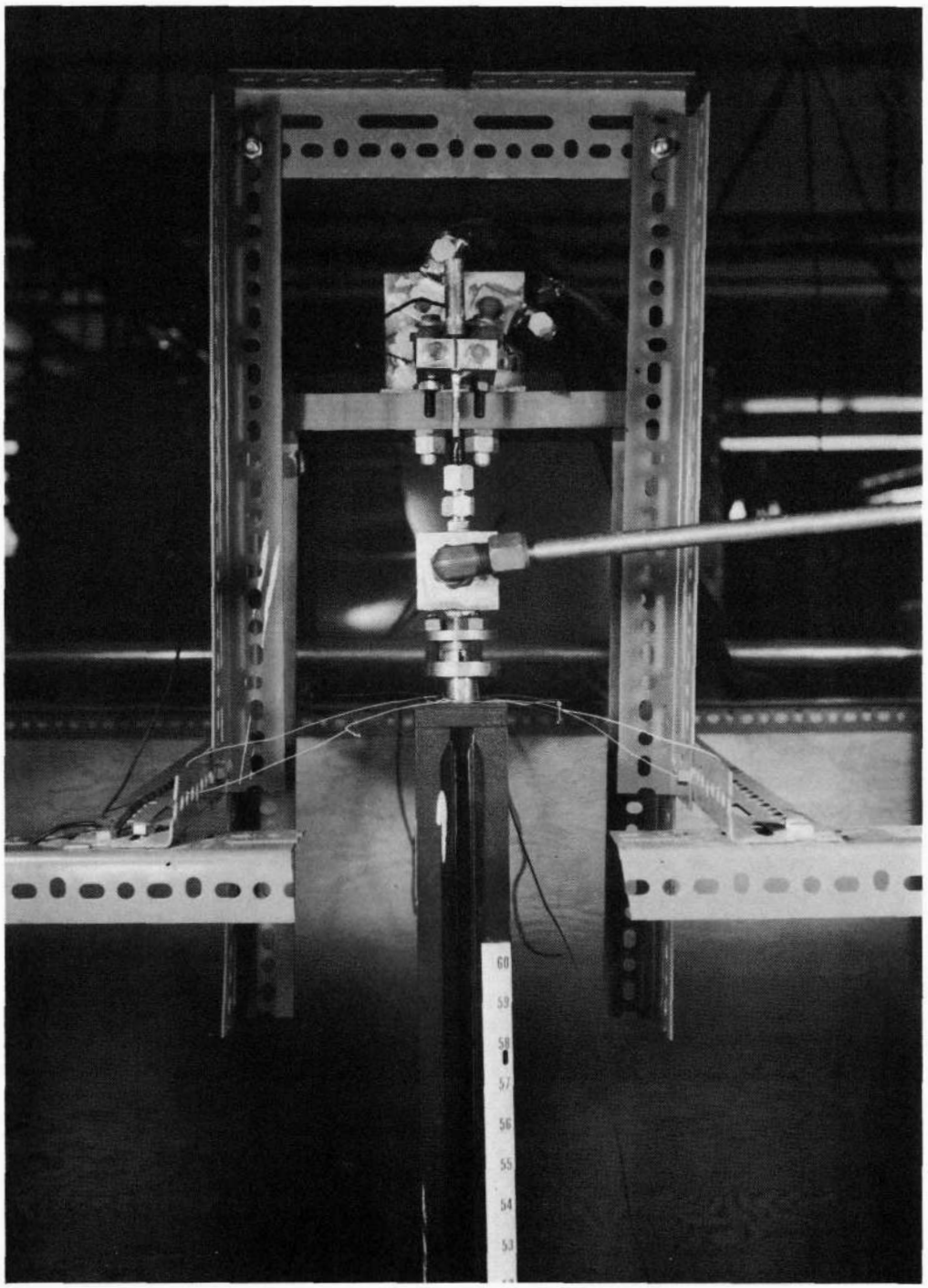

FIG. 24: VIEW OF GLASS TEST SECTION & FITTINGS

No corrections were found to be necessary. Sixteen thermocouples were installed on the tube wall and two in the fluid. Because of DC heating, mica insulation was used between the tube wall and the thermocouples, which were held against the tube with Scotch Electrical tape. Spot-welded thermocouples were tried, and an attempt was made to calibrate them for the voltage gradient along the tube by reversing the polarity of the DC supply. This was not successful due to the large differences in the wall temperature that were often present along the wall. The thermocouples that measure the inlet and outlet temperatures were directly immersed in the fluid at the end fittings. The thermocouples were introduced through conax fittings with teflon sealants.

The cold junctions of the thermocouples were immersed in a common ice bath, and the millivolt output was read on a Honeywell Brown potentiometer, which incorporates a switching circuit and prints the output of sixteen thermocouples in succession. Because of the limitation on the number of thermocouples to sixteen, only fourteen of the sixteen thermocouples were used at a time. If the region of interest was near either the entrance of exit of the test section, one of the extra thermocouples was used in place of another thermocouple away from the region of interest. The wall thermocouples were spaced from 3 to 6 inches apart along the heated length of the tube, with the ones in the middle of the tube being closer together. The recorder had a range of 0-10 mV. Later, the range was altered to -5 to 20 mV, which was useful in reading the low inlet temperatures. An accuracy of 2 ^{o}F can be assumed for the temperature measurements.

The system pressure immediately upstream of the test section was read on a 10-inch Bourdon gage, calibrated from 0 - 2000 psig. in intervals of 2 psi. The gage had a specified accuracy of 1/10 percent of full-scale reading. The error in measurement of the inlet pressure is thus less than 2 psi. The outlet pressure was not measured, but the pressure drop in the test section was calculated to be of the order of 1 psi. or less for the larger diameter section and 5 psi. for the smaller diameter section.

The flow rate was measured by noting the pressure drop across a previously calibrated orifice in inches of mercury in a 60-inch differential manometer. Later, this was replaced by a differential pressure gage for smaller flow rates. The flow rate can be measured within 2 percent.

The heat input was measured by reading the voltage drop across the test section and the current through it. A Simpson voltmeter was used to measure the voltage drop (0-25 V, accuracy of 2 percent of full-scale reading). The current was measured by measuring the voltage drop across a calibrated shunt (50 mV/1000 Amps) in series with the test section. A Simpson milli-voltmeter, 0 to 50 mV range (accuracy 1 percent of full-scale reading) was used for this purpose. Heat loss checks were made on the setup, and the heat losses were found to be very small. An accuracy of 2 percent can be assumed for the heat flux values.

Heat balance checks were also run on the loop at a pressure of 1200 psi and by arranging the flow and heat flux so that the inlet and outlet temperatures were not in the critical range. These were better than 5 percent. Near the critical region, heat balance checks were poor

when either inlet or outlet temperature was close to the pseudocritical temperature. Errors as high as 25-30 percent were possible. This is because dH/dT is very large in this region, and hence a small error in measuring the temperature can throw the enthalpy balance off by a large margin.

The capabilities of the loop in terms of the flow rates heat fluxes and inlet temperatures are:

1. 1/4-inch section

   Maximum flow rate: 2×10^6 lbs/ft^2-hr

   Maximum heat flux: 120,000 BTU/ft^2-hr

   Minimum inlet temperature: 34 ^oF

2. 1/8-inch section

   Maximum flow rate: 3.5×10^6 lbs/ft^2-hr

   Maximum heat flux: 150,000 BTU/ft^2-hr

   Minimum inlet temperature: 0 ^oF.

6.5 Experimental Procedure

When a new test section was installed into the loop or when operating after an extended break, precautions were taken to bleed the air in the loop. The valve to the carbon dioxide was opened, the pressure on the nitrogen side of the accumulator was relieved, and the carbon dioxide was allowed to fill the loop and pressurize the accumulator. At the same time, air and carbon dioxide were bled through an exhaust valve. The air in the pump was bled through a bleed valve provided in the pump. Precautions were also taken to force out any air that might have been trapped in the manometer tube. After a reasonable period of time, the bleed valves were shut off, and the carbon dioxide allowed to pressurize the system.

At this time, the oil heat exchanger, the system heat exchanger, and the refrigeration unit were activated, and the oil pump was switched on. The system valves were arranged for either upflow or downflow. When the pressure was about 600 psig. so that the carbon dioxide was sufficiently dense, the main pump was started. After the system had been brought to the highest pressure possible using the carbon dioxide bottles at room temperature (about 800 psi), the valve to the carbon dioxide supply was shut off, and the cylinder was disconnected. The high pressure nitrogen cylinder was connected to the nitrogen end of the accumulator, and the pressure applied until the desired supercritical pressure was reached. The generator was then started, and the heat flux on the test section adjusted to the required value. The flow rate was controlled with the Hoke valves in the frontpanel. The bypass valve was usually kept fully open. In order to reach steady state at a particular flow rate, it was necessary to manipulate the system pressure, which increases as the enthalpy of the fluid in the system increases due to heat addition; the flow control valves, since changes in the exit state of the fluid can change the pressure drop and thus the pump flow rate; and the heat exchanger cooling capacity, adjusted with the refrigerant flow valve and the cooling water valve. The flow rate cannot be read off directly from the pressure drop since it also depends on the density of the fluid and, therefore, the temperature of the fluid at the orifice. Due to these difficulties, no attempt was made to fix the flow rate accurately during the experiments. Once the heat exchangers had been adjusted to maintain constant inlet and outlet temperatures, the flow rate was fixed approximately. The system pressure at the test section inlet was adjusted

by either bleeding off some nitrogen from the accumulator, if the pressure was higher than the desired pressure, or increased by using some more high pressure nitrogen.

The experimental procedure consisted in fixing the heat flux and the pressure and varying the flow rate from a small value to a large value. Steady-state measurements were possible except at the highest heat fluxes used, when adequate cooling was not available for the larger diameter test section. The measurements made in each case were the inlet pressure, the pressure drop across the orifice, the voltage drop across the test section, and the millivolt drop across the shunt, and the temperatures along the wall and the bulk temperature at inlet and outlet, which were recorded on the recorder chart.

Data were taken under the following set of conditions: Two pressures were used, 1100 and 1150 psia, and data were taken in upflow and downflow. The inlet temperature was varied from 0 ^{o}F to supercritical. With the visual section no data were taken; only qualitative observations were made.

6.6 Data Reduction Procedures

Fortran 4 computer programs were written to reduce the data and present it in useful form. The IBM 1130 in the Mechanical Engineering Department at M.I.T. and the IBM 360 at the M.I.T. Computation Center were used for this purpose. Figure 25 shows a sample printout. The heat flux and the flow rate are based on the inner diameter of the tube. The outer wall temperatures are corrected to give the inner wall temperatures, assuming that the outer wall is completely insulated, and

PRESSURE	Q	G	TIN	TOUT	TCAL	TB	TWALL	H	ENTH	RATIO	
1100.0	136728.0000	3261227.00	1.0	89.0	90.0	16.2	139.8	1106.0	25.9	1.46	
						29.7	164.8	1012.0	32.2	1.73	
						37.2	185.8	919.9	36.5	2.01	
						42.7	189.8	929.5	39.7	2.06	
						48.2	197.8	913.8	42.8	2.17	
						53.5	205.8	897.6	46.0	2.29	
						58.7	210.8	898.8	49.2	2.39	
						63.6	216.8	892.4	52.4	2.50	
						67.0	220.8	889.3	55.5	2.61	U
						70.3	214.8	946.7	58.7	2.56	
						73.8	209.8	1005.2	61.9	2.52	
						77.3	189.8	1215.5	65.1	2.19	
						81.3	191.8	1237.5	69.3	2.30	
						86.5	191.8	1298.8	76.7	2.70	

PRESSURE	Q	G	TIN	TOUT	TCAL	TB	TWALL	H	ENTH	RATIO	
1100.0	136728.0000	2486088.00	13.0	99.0	101.5	36.7	154.8	1158.1	36.2	1.28	
						54.3	203.8	914.5	46.5	1.82	
						64.7	212.8	923.5	53.4	1.97	
						70.0	224.8	883.3	58.5	2.20	
						75.7	232.8	870.5	63.6	2.40	U
						80.8	222.8	963.0	68.8	2.35	
						84.4	217.8	1025.4	73.9	2.48	
						87.7	201.8	1198.2	79.0	2.61	
						89.1	191.8	1332.0	84.2	2.77	
						89.4	201.8	1217.0	89.3	2.98	
						89.7	208.8	1148.5	94.5	3.09	
						90.1	224.8	1015.0	99.6	3.40	
						90.8	249.8	860.2	106.4	3.58	
						93.7	253.8	854.2	118.4	2.99	

PRESSURE	Q	G	TIN	TOUT	TCAL	TB	TWALL	H	ENTH	RATIO	
1100.0	136728.0000	1954847.00	41.0	191.0	189.9	65.9	339.8	499.2	54.4	3.05	
						80.0	346.8	512.4	67.8	3.59	U
						86.6	285.8	686.4	76.8	3.40	
						89.1	274.8	736.3	83.6	4.15	
						89.5	257.8	812.4	90.3	3.67	
						89.9	232.8	956.8	97.0	3.03	
						90.5	244.8	886.4	103.7	3.01	
						91.4	257.8	821.9	110.5	2.94	
						93.1	277.8	740.4	117.2	2.95	
						96.6	292.8	697.0	123.9	2.65	
						102.2	309.8	658.8	130.7	2.37	
						110.4	321.8	647.0	137.4	2.02	
						126.8	360.8	584.2	146.4	1.98	
						162.7	402.8	569.5	162.1	1.85	

FIG. 25 : DATA PRINT-OUT

there is only radial variation in temperature. TCAL represents the outlet bulk temperature calculated by a heat balance. Comparison between TCAL and TOUT, the measured outlet temperature, shows the effectiveness of the heat balance check. Unfortunately, in the smaller L/D section, in a large number of experiments, the outlet temperature was close to the critical temperature, and the heat balance checks were relatively poor. Much better checks were obtained with the smaller diameter test section. The bulk temperature TB and the bulk enthalpy ENTH are calculated assuming a linear increase in the bulk enthalpy between the inlet and the outlet. Local and average values of the important parameters were determined but are not shown in Figure 25. These include the bulk Reynolds and Prandtl numbers and the Nusselt number based on the MacAdams correlation and the bulk properties. H represents the local heat transfer coefficient obtained as the ratio of the heat flux on the inner diameter to the temperature drop between the wall and bulk temperatures at the cross section. RATIO is the ratio of the MacAdams heat transfer coefficient to the experimental heat transfer coefficient and serves as an indicator for the amount of deterioration in the heat transfer.

Slight changes were required to adapt the program to the different test sections. For the test section with the twisted tape, the mass velocity was calculated for the net area of the cross section. Lopina (57) has suggested a modified mass velocity αG instead of G to calculate the Reynolds number used to calculate the Nusselt number. α respresents a factor that gives the increase in velocity due to the tangential component of velocity. However, in order to compare the heat transfer coefficient

against the same reference as used in the other experiments, the mass velocity itself is used in the calculation of the Nusselt number.

7. EXPERIMENTAL RESULTS FOR CARBON DIOXIDE

7.1 Introduction

The results from the carbon dioxide experiments were obtained in the form of wall temperature profiles versus the length along the test section and, therefore, versus bulk enthalpy. As mentioned earlier, the data were reduced with the help of a computer to obtain the bulk temperatures and bulk enthalpy at the cross sections where thermocouples were located. The local heat transfer coefficient and the bulk Nusselt number were also calculated. The results from the 1/4-inch section, 1/8-inch section, and the swirl section are presented in that order in this section, and the effects of various system parameters on the heat transfer characteristics are also discussed. A comparison with computed results and with those of other investigators is also made in this section.

7.2 Results Obtained with 1/4-Inch Test Section

The 1/4-inch ID (0.245-inch) test section was the first one used. Because of the limitations of the water heat exchanger, inlet temperatures below 35 ^{o}F could not be used in conjunction with this test section. A difficulty also encountered with this setup was that because of the L/D ratio of 245, the exit temperature was often in the critical region, for the runs with larger subcooling. This is inconvenient for two reasons:

a. The heat balance checks are relatively poor.

b. Though the region where the temperature peaks occurred was well covered in this series of experiments, the complete S-shaped wall

temperature profile could not be obtained over the length of the tube. Piecing of wall temperature profiles with different inlet enthalpies was not successful due to entrance effects.

Experimental Range Covered with 1/4-Inch Section

Orientation of Flow: Up and down

Pressure: 1100, 1150 psi.

Mass Velocities: 640,000-2,000,000 lbs/ft^2-hr

Reynolds Number: 267,000-835,000
(based on the lower viscosity)

Inlet Temperature: 35 ^{o}F and above

7.2.1 Results in Upflow -1100 psi.

Figure 26 shows some representative wall temperature versus bulk enthalpy curves for a heat flux of 50,000 BTU/ft^2-hr. It is seen that while no deterioration in heat transfer exists for a mass velocity of 2 x 10^6 lbs/ft^2-hr, the temperature profile shows a peak as the mass velocity is decreased. For a mass velocity of 10^6 lbs/ft^2-hr, a temperature maximum is evident, and it progressively gets higher as the mass velocity is reduced further. It should be noted that the first wall temperature data point is at least twenty-five diameters from the start of the heated section so that entrance effects in the conventional sense are not large. The deterioration in heat transfer is seen to occur at a value of the bulk enthalpy that is substantially smaller than the critical enthalpy, the amount depending on the heat flux and the flow rate. It is therefore necessary for the inlet bulk temperature to be much lower than the critical temperature in order to observe the deterioration. It is thought that the chief reason this phenomenon

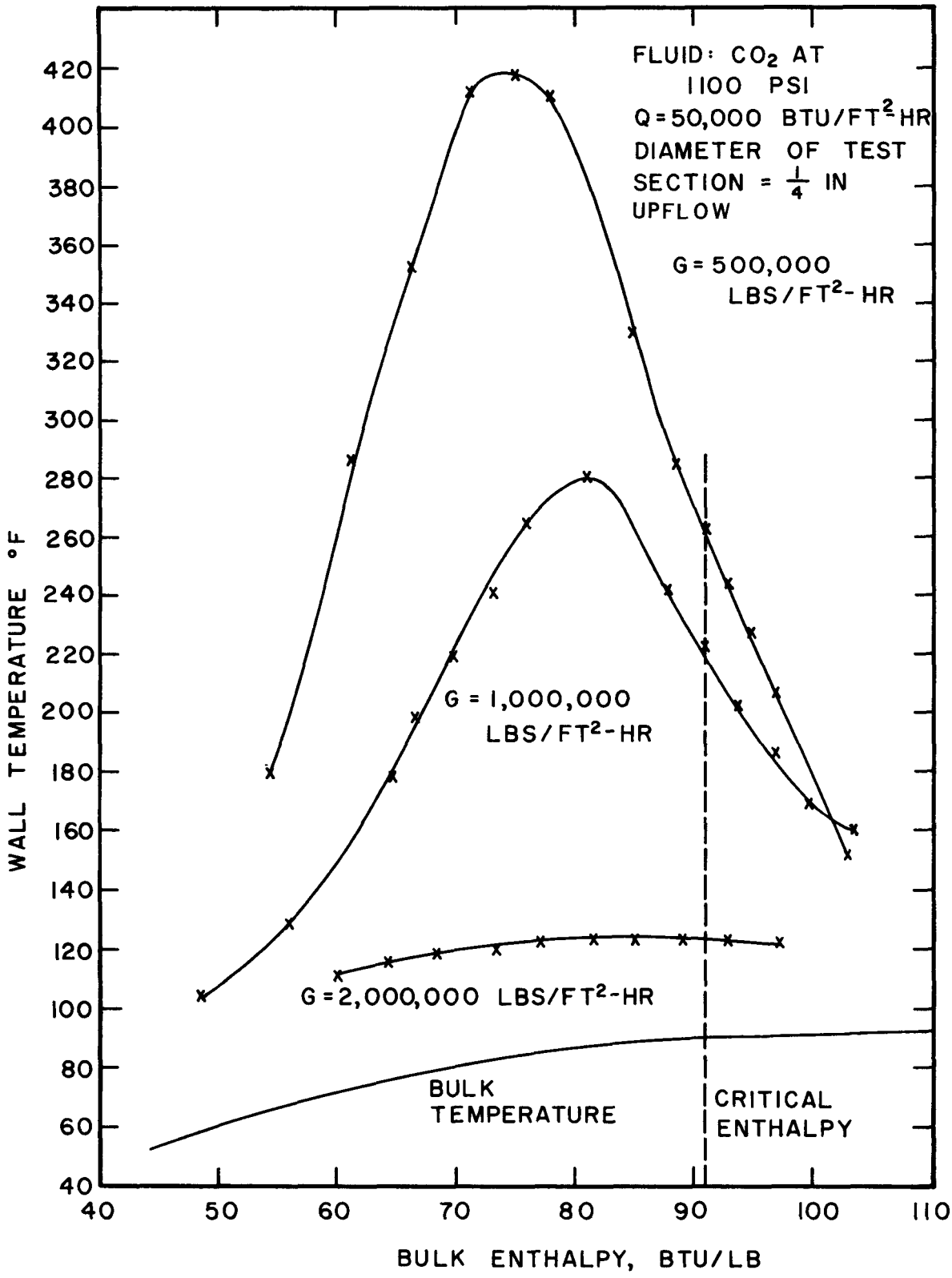

FIG. 26 EXPERIMENTAL RESULTS FOR CO_2 AT 1100 PSI

has not been observed by earlier investigators is that they did not use low enough inlet temperature. For example, the results of Koppel and Smith (27), using an inlet temperature of 70 ^{o}F, appear to show the tail end of a temperature peak.

The deterioration is found to be worse for a higher ratio of the heat flux to the mass velocity, and it occurs at a smaller value of the bulk enthalpy. In Figure 26 the heat transfer coefficient is seen to fall by a factor of about seven before it increases in the vicinity of the critical region. It has been suggested by some investigators (9, 12) that the deterioration does not occur above a certain flow rate. No evidence of any such critical mass velocity was found in the experiments. If the heat flux was raised to a sufficiently high value, the deterioration could be observed. At some of the highest heat fluxes used, enough subcooling was not available for steady-state results, and the accuracy and reproducibility of the temperature profiles cannot be assured. However, there was no doubt that very high temperatures, which were much higher than predicted by the usual correlations, were obtained at the highest mass velocities used.

By varying the inlet temperature slightly, the temperature peak could be made to move over the length of the tube. This confirms that the high temperatures obtained are due to the internal fluid mechanics in the flow and are not due to any local peculiarity in the metal tube. The effects of inlet enthalpy on the temperature peak are discussed in a later section.

Initially, lateral vibration was present in the test section, and the temperature peaks in the middle of the tube where the vibration

amplitude was the maximum were found to be much lower than near the ends of the test section. The situation was remedied by using one "floating" electrode.

Since this investigation was geared to examining the deterioration in heat transfer at high heat fluxes, the region of large mass velocities and small heat fluxes was not investigated experimentally on a systematic basis, but in some of the experiments, a large heat transfer coefficient was encountered under those conditions.

7.2.2 Results of 1150 psi. - Upflow

The experiments at 1150 psi showed a similar behaviour in the wall temperature profiles. Hot spots or temperature peaks were observed as the ratio of the heat flux to flow rate was increased. The deterioration in heat transfer was, however, noticeably smaller than at 1100 psi. under similar conditions of heat flux and flow rate. Figure 27 shows some representative wall temperature profiles at 1150 psi., and a temperature profile at 1100 psi. is also shown for comparison. At 1150 psi., it was generally found that the temperature peaks were lower and not as sharp as at 1100 psi. In general, it appears that the deterioration is the worst at the critical pressure and is not as large away from the critical pressure. This is to be expected because the variation in properties is less rapid away from the critical pressure.

7.2.3 Results in Downflow

Experiments performed with carbon dioxide flowing down through the test section have shown similar results. A sharp peak in the wall temperature occurs for large values of the heat flux. In some recent work,

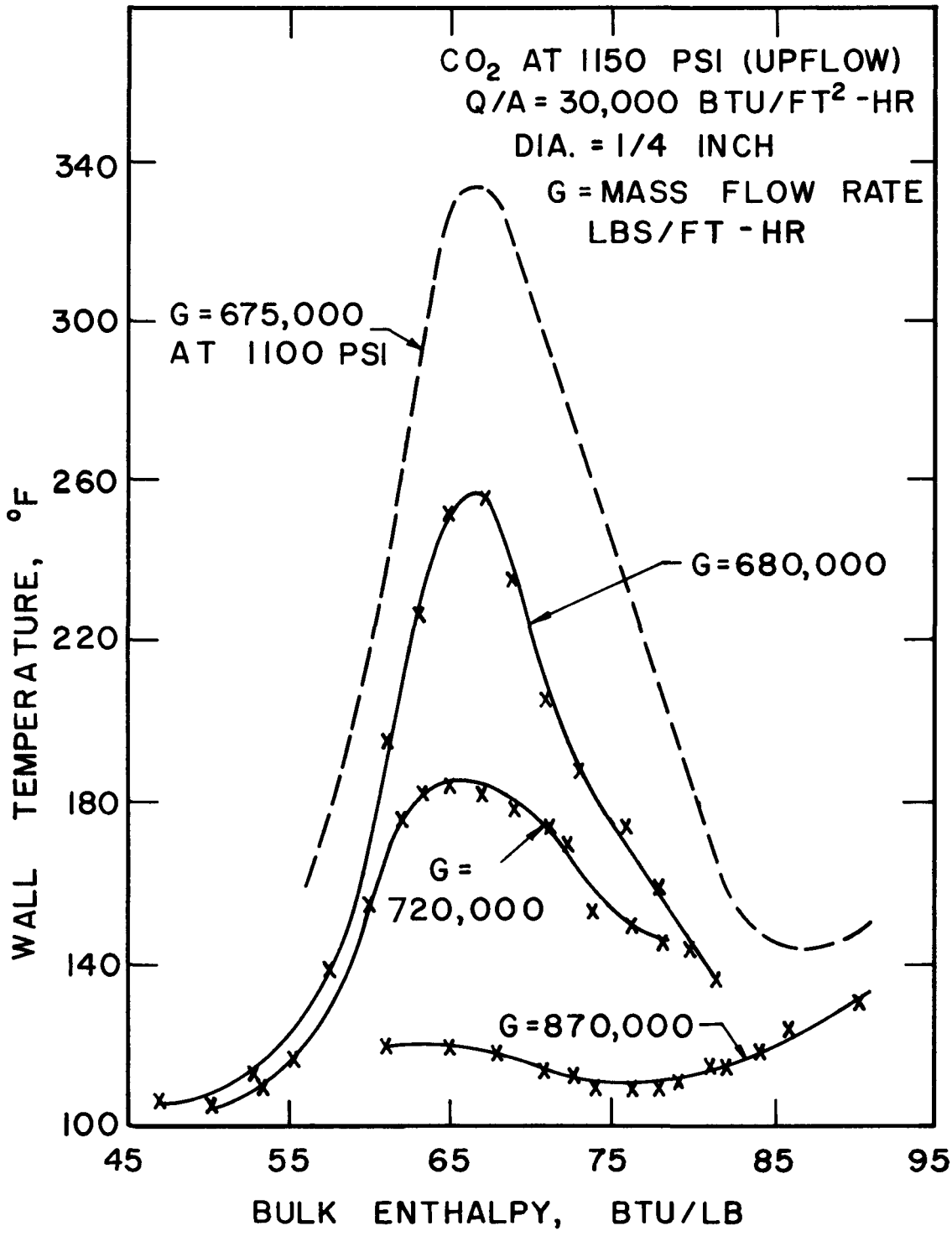

FIG. 27: EXPERIMENTAL RESULTS FOR CO_2 AT 1150 PSI

Hall (20) has reported seeing sharp peaks in upflow and one in downflow under identical conditions of heat flux and mass flow rate. His results are not necessarily contradictory to those observed in the present work because of his use of lower mass velocities and a 0.75-inch inner diameter test section.

Typical deteriorated heat transfer results in downflow are shown in Figure 28. Again, the inlet effects were found to be important. Comparison with upflow results show that, if anything, the temperature peak is somewhat sharper and higher than in upflow under similar conditions. No evidence of anything radically different was seen at the lowest mass velocities used (640,000 lbs/ft^2-hr).

7.2.4 Comparison of Experimental Wall Temperature Profiles with Theory

The analysis used for steam in Section 5 can be easily extended to carbon dioxide with the only alteration being the use of the properties of carbon dioxide at 1100 psi. instead of those of steam. Similar GD vs. bulk enthalpy plots were developed for the heat flux under consideration and cross plots made for the desired values of the mass flow rate. Figure 29 shows a comparison between experimental and calculated wall temperature profiles for carbon dioxide at 1100 psi. The experimental results are for upflow, while the calculations neglect the effect of gravity terms. The results compare in a manner similar to those for steam. The prediction of the hot spot is somewhat low at the inception of the experimental peak but high at higher heat fluxes. Again, the prediction does not do a good job in the post peak region. Due to sensitiveness of the deterioration to upstream effects, such as the entrance effects and swirl, with the restrictions of a 240 L/D test section, the

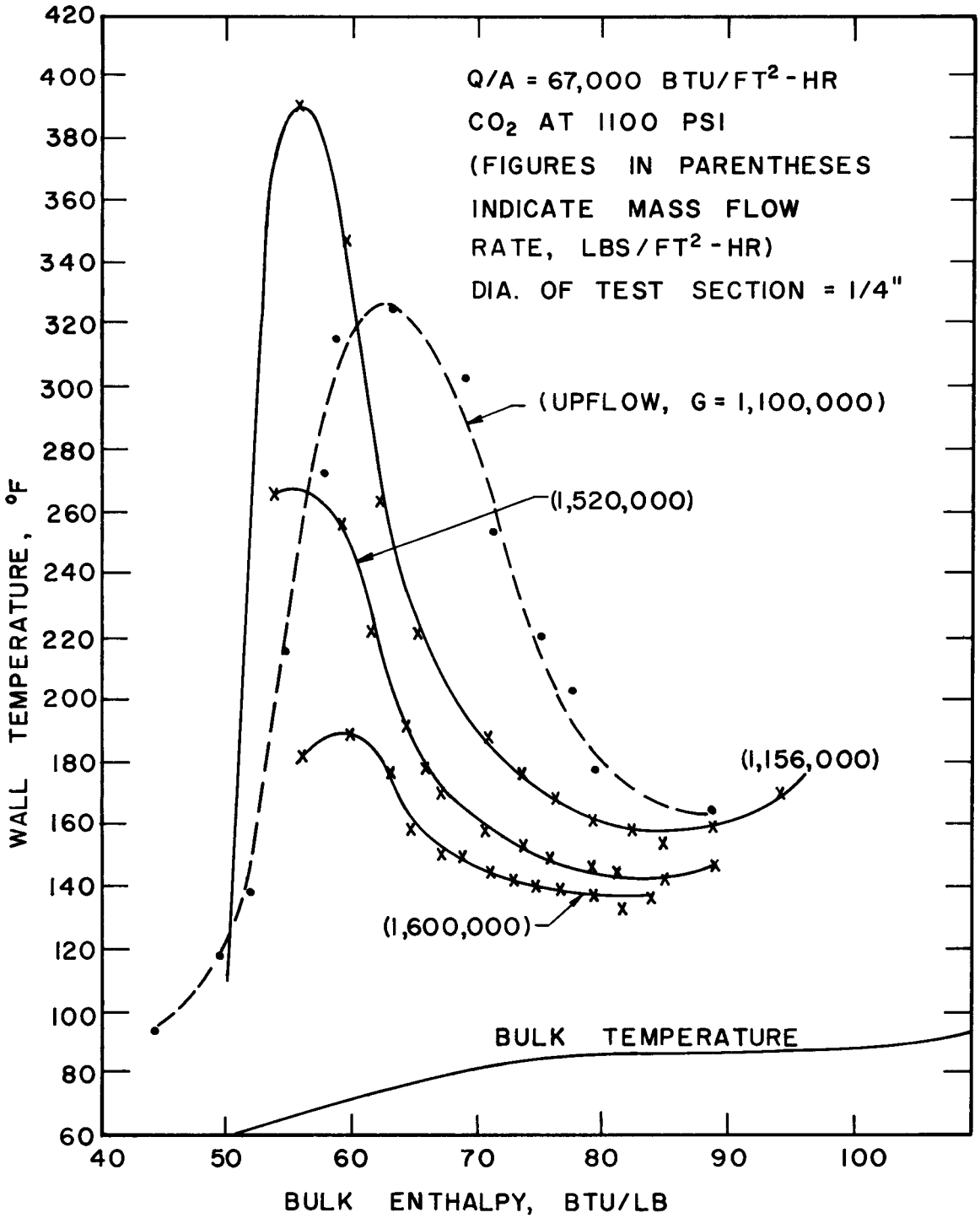

FIG. 28: EXPERIMENTAL RESULTS FOR DOWNFLOW

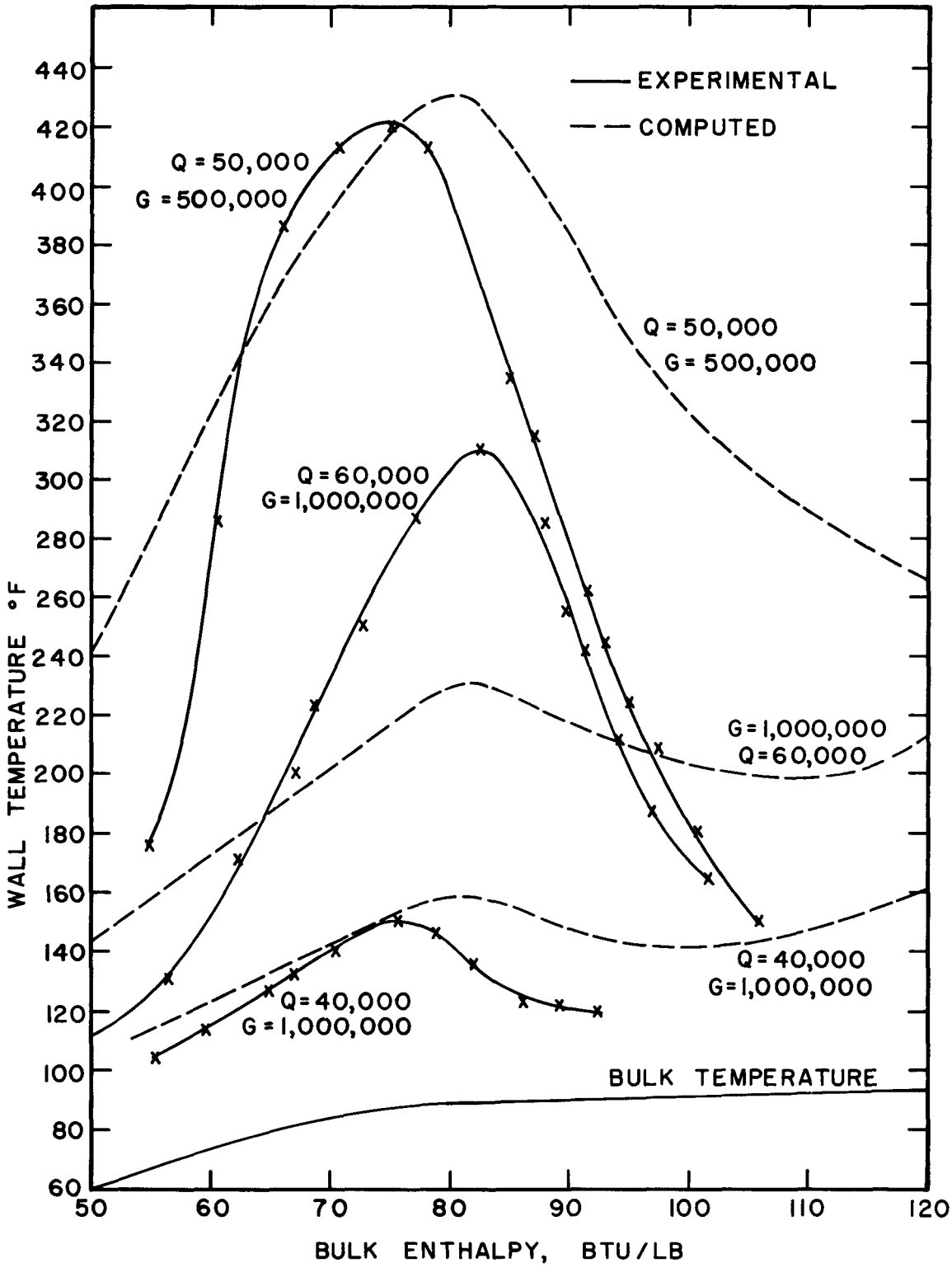

FIG. 29 COMPARISON BETWEEN COMPUTED AND EXPERIMENTAL WALL TEMPERATURE PROFILES FOR CO_2

experimental profile might be expected to be on the low side as compared to a long test section. The comparison with theory based on "fully developed" flow assumptions is surprisingly good. It should be mentioned that the experimental curves chosen for comparison were obtained from runs with adequate inlet subcooling. The data from runs without sufficient inlet subcooling are not as predictable, due to a dominance of inlet effects.

7.2.5 Presentation of Heat Transfer Results

The presentation of the heat transfer results is oriented towards showing the lowest heat transfer coefficient in each run as a function of the Reynolds number and the heat flux. No attempt has been made to correlate the local heat transfer coefficient to the local Reynolds and Prandtl numbers, since it was felt that existing correlations are adequate as long as one stays away from the deteriorated heat flux region.

Figure 30 shows the results of the runs at 1100 psi. in upflow. The ratio of the experimental Nusselt number to that calculated with a conventional MacAdams type correlation with bulk properties is plotted against the Reynolds number for different heat fluxes. The Reynolds number is calculated with the value of the viscosity at the wall temperature. Each data point represents the worst heat transfer coefficient or the smallest value of the parameter Nu/Nu_{Mac} for a particular run. The MacAdams Nusselt number is calculated at the local bulk properties. The positive slope of the constant heat flux lines indicates that the deterioration in heat transfer, represented here by the inverse of the ordinate, gets greater as the flow rate decreases and vice versa. Increasing the heat flux moves the line to the right, indicating that

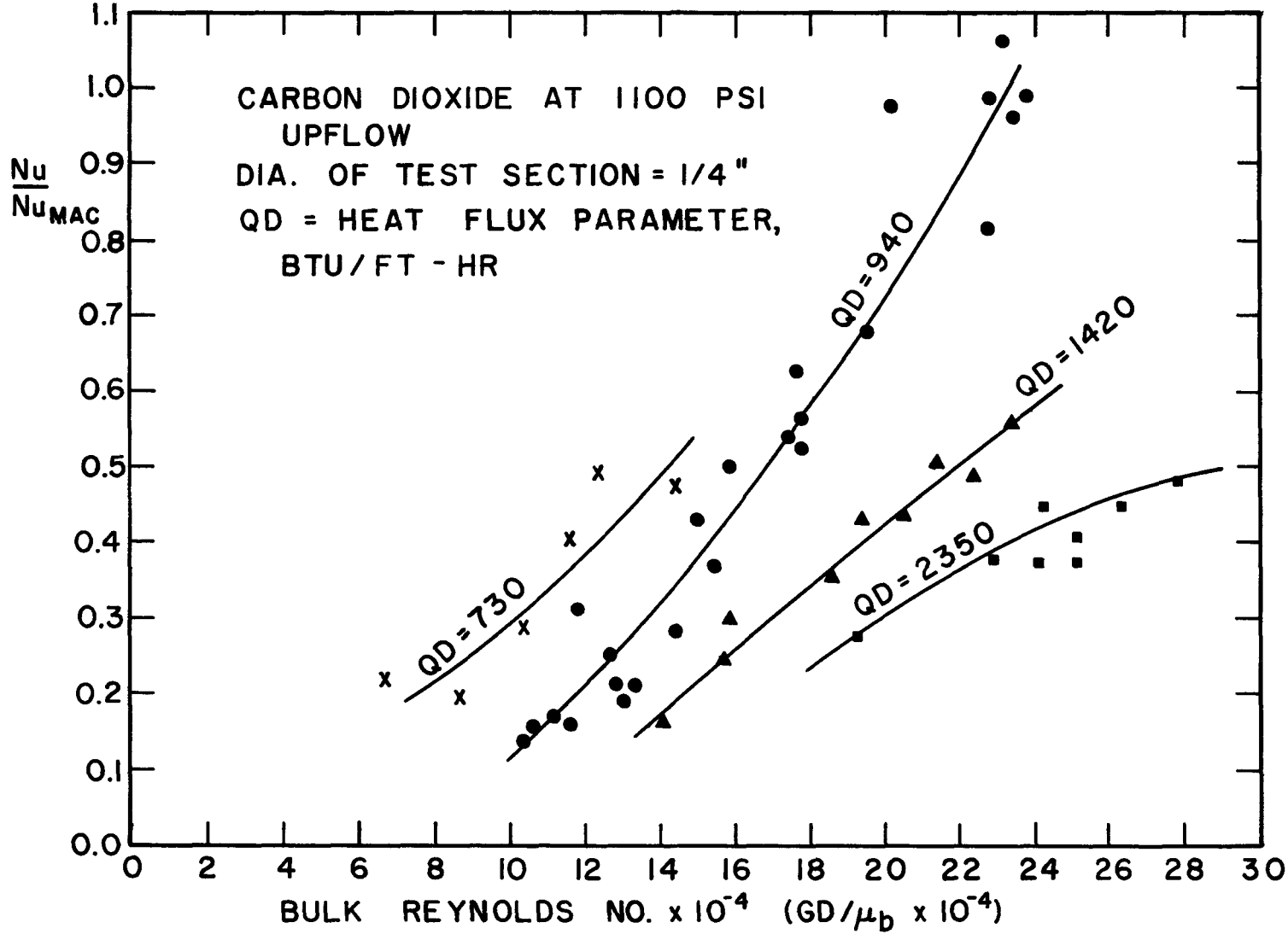

FIG. 30 : HEAT TRANSFER RESULTS FOR CO_2 AT 1100 PSI

the same degree of deterioration takes place with a larger flow rate or Reynolds number. The heat flux lines diverge at higher values of the Reynolds number. This means that at low Reynolds numbers, a small change in the Reynolds number will compensate for change in heat flux and prevent further deterioration, while at higher Reynolds numbers, a much larger change in Reynolds number is required to compensate for a comparable increase in heat flux.

This plot can be used to estimate the highest wall temperature for a particular set of operating conditions, a parameter of interest to the designer.

7.2.6 Safe vs. Unsafe Plots

The data in Figure 30 can be cross plotted in the form of heat flux vs. mass velocity corresponding to a certain constant Nu/Nu_{Mac} ratio. Such a plot might be termed a safe vs. unsafe plot in terms of the mass velocity and the "allowable" heat flux, where the allowable heat flux is such that the ratio of Nu/Nu_{Mac} is not less than the prescribed value. The safe vs. unsafe plot for steam was defined similarly for a Nu/Nu_{Mac} ratio of 0.5. If the same criterion is used again, corresponding safe vs. unsafe plots can be drawn for carbon dioxide.

Figure 31 is the safe vs. unsafe plot for carbon dioxide at 1100 psi. in upflow. A fairly clear demarcation can be made on this basis between the safe and unsafe regions. The region above the curve in Figure 31 is unsafe, and the region below it, safe.

Figure 32 is the corresponding plot for carbon dioxide at 1150 psi. in upflow. The limits of "safe operation" are extended in this case to

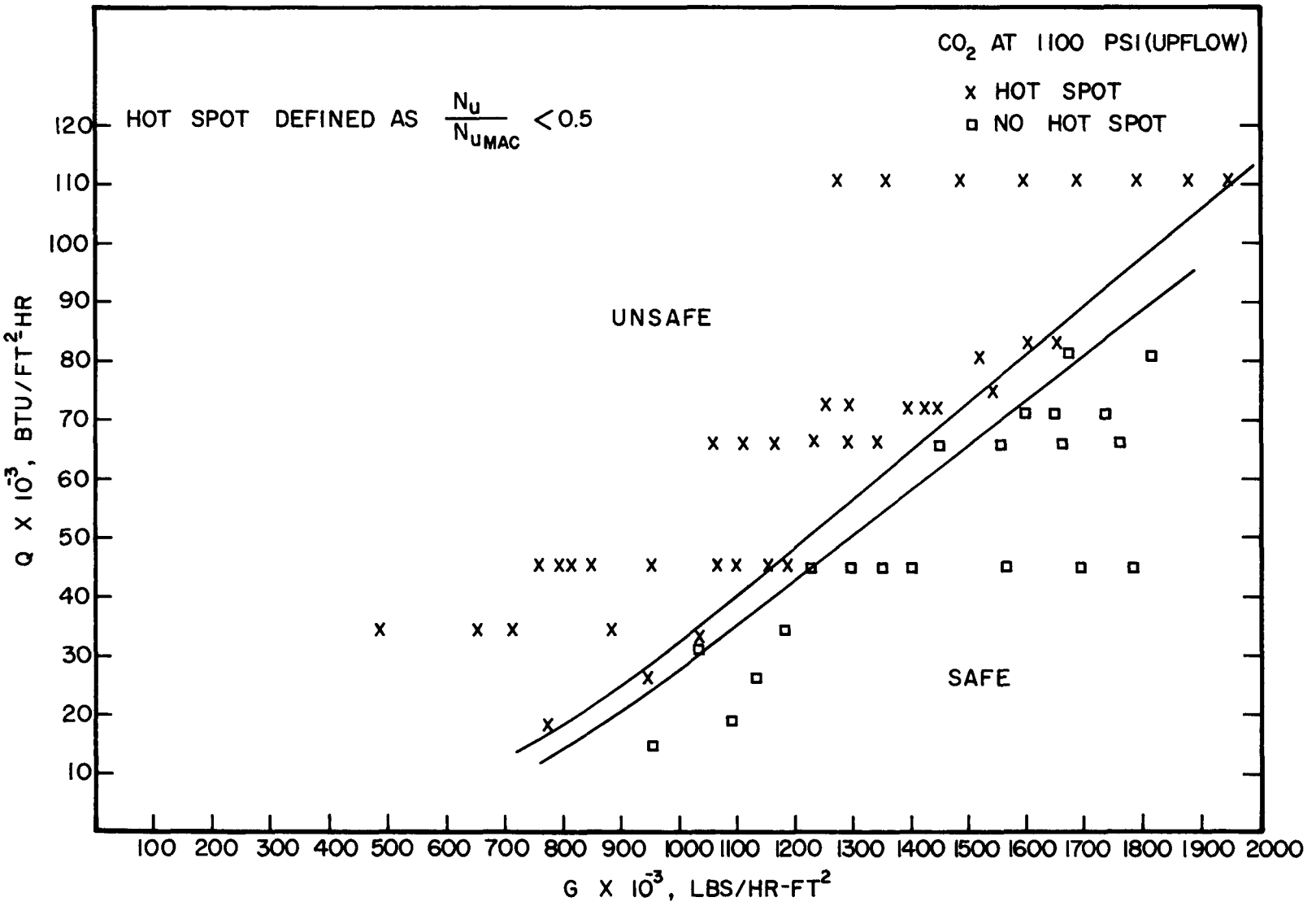

FIG. 31 : EXPERIMENTAL SAFE VS. UNSAFE PLOT FOR CO_2 AT 1100 PSI

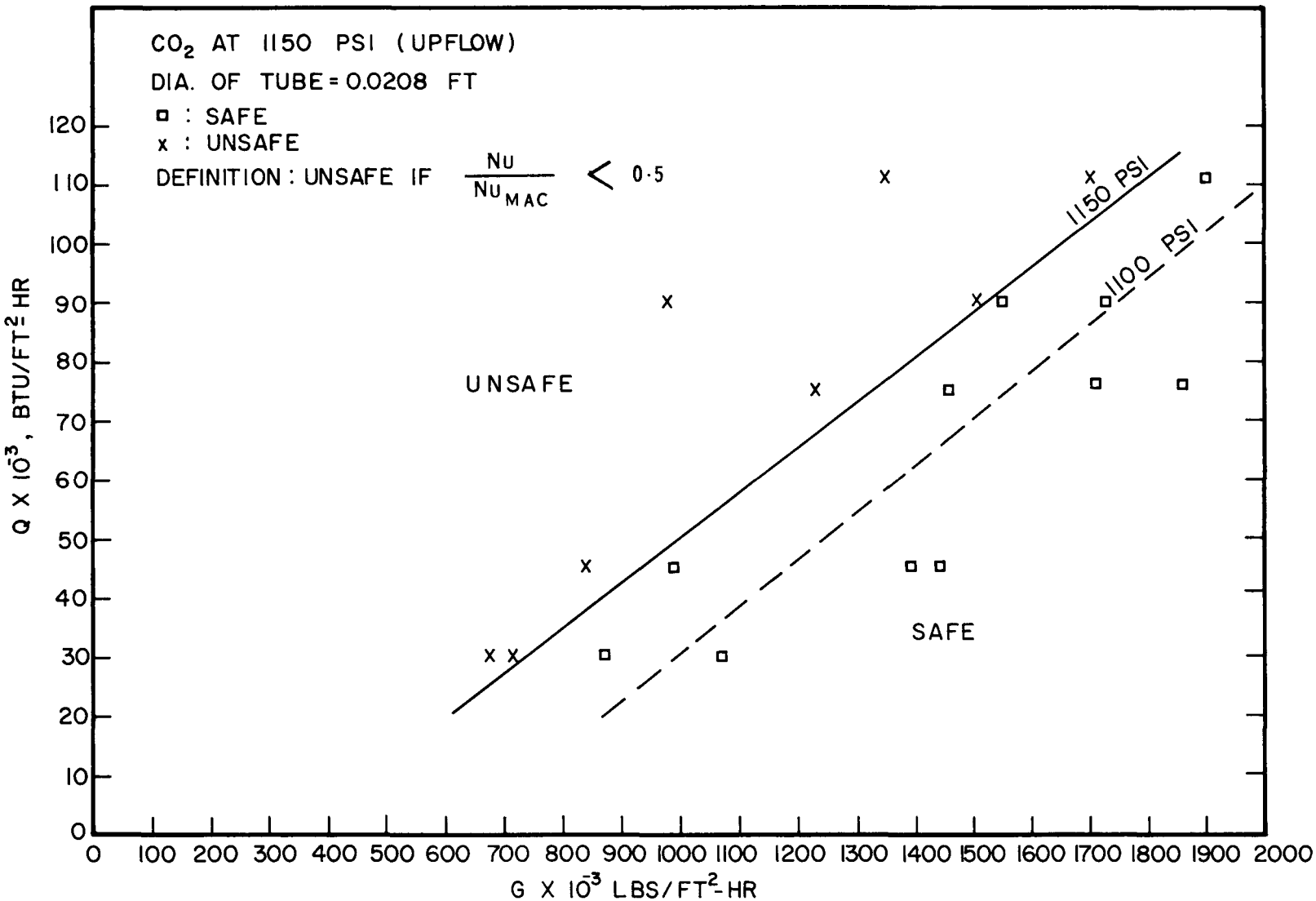

FIG. 32 : EXPERIMENTAL SAFE VS. UNSAFE PLOT FOR CO_2 AT 1150 PSI

a higher heat flux for a particular flow rate, as can be seen by comparison with the limit for 1100 psi.

A similar plot was also made for downflow. This is shown in Figure 33. A comparison is also made with the corresponding upflow plot. The two curves have a different slope with an intersection near the low velocity end. It appears that at low mass velocities, deterioration occurs in the heat transfer rate at higher heat fluxes in downflow than in upflow, but that the situation reverses at higher mass flow rates. However, at the high mass velocity end it seems unlikely that there should be much difference between up and down flow. Probably the reason for the discrepancy is that at the highest heat fluxes used in upflow, adequate inlet subcooling was not available, with the result that some of the data at the high end may be in error to the extent that some temperature peaks were suppressed. The two lines in Figures 31 and 33 show a region which separates the safe and unsafe regions. Since this region is fairly narrow, it has been replaced by a central line in the subsequent plots.

A comparison of these plots with the computed plots will be made in a later section.

7.3 Results Obtained with the 1/8-Inch I.D. Test Section

The 1/8-inch test section was used to replace the 1/4-inch section because of a need for an increased L/D ratio, with the existing setup. With the larger L/D ratio, it was possible to use even greater subcooling and still obtain exit bulk temperatures well above the pseudocritical temperature. This increased the reproducibility of the results due to a decrease in the importance of entrance effects and also enabled the observation of the entire S-shaped wall temperature profile in the

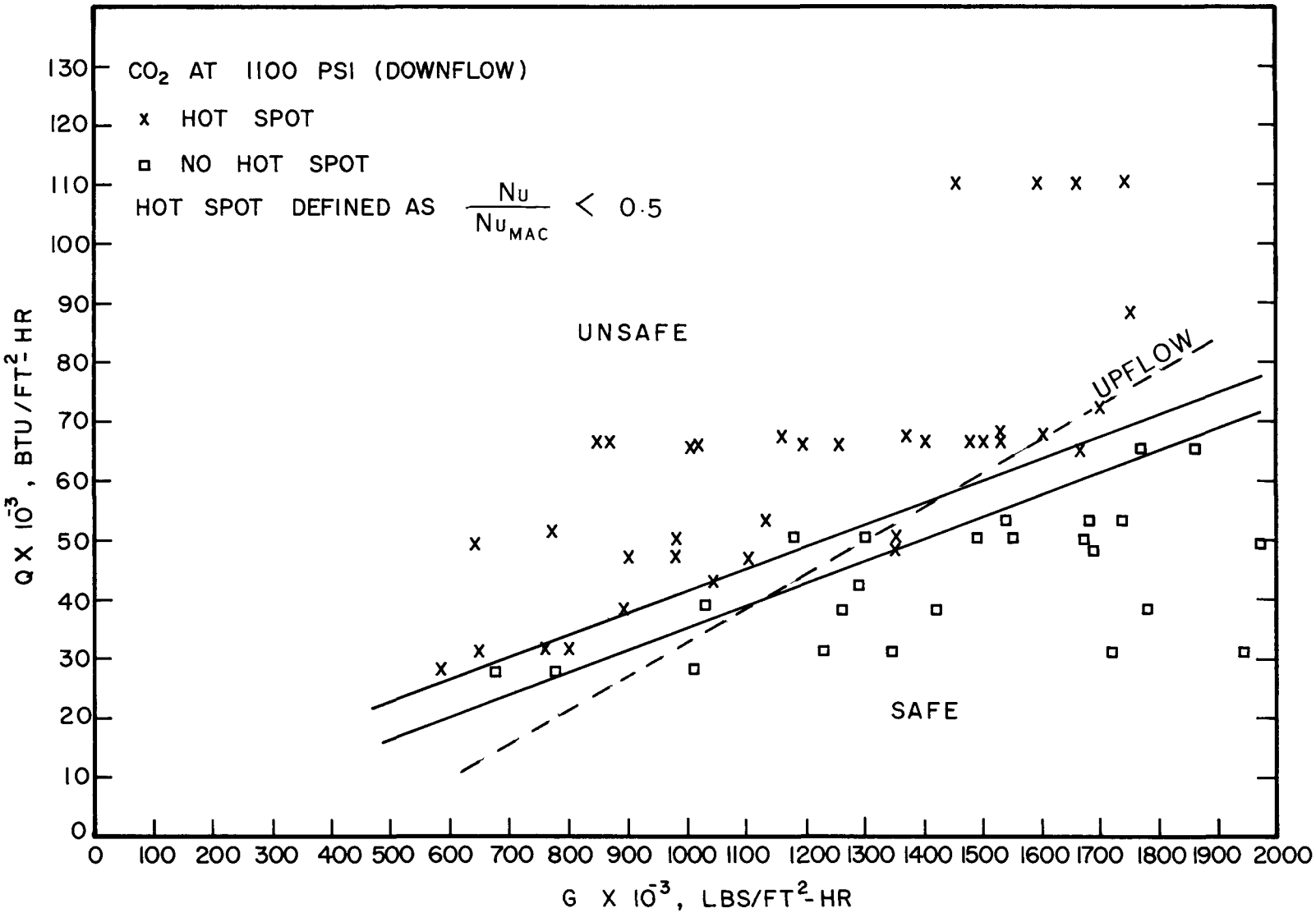

FIG. 33 EXPERIMENTAL SAFE VS. UNSAFE PLOT FOR DOWNFLOW

pre- and post-critical enthalpy regions. Good heat balance checks were also obtained with this test section. Liquid nitrogen, obtained from the Cryogenics Laboratory at M.I.T., was used to replace the water heat exchanger in the system. The nitrogen was blown counter current to the flow of carbon dioxide. Carbon dioxide bulk temperatures as low as 0 ^{o}F were obtained in this way.

The small diameter test section with a relatively thick wall does have the disadvantage that axial conduction along the metal tube wall is increased. Due to this, the temperature peaks were generally not quite as sharp as with the larger test section, especially at high heat flux to mass velocity ratios. However, the results did not prove to be significantly different in character from those of the larger tube and were particularly useful in regions where the deterioration was not too great.

Experimental Range Covered with 1/8-Inch Section

Orientation of Flow: Up and down

Pressure: 1100 psi.

Mass Velocities: 1,200,000-3,000,000 lbs/ft^2-hr

Heat Fluxes: 50,000-144,000 BTU/ft^2-hr

Reynolds Numbers: 250,000-600,000
(based on lower viscosity)

Inlet Temperature: 0 ^{o}F and above

7.3.1 Upflow Results

Figure 34 shows some of the results obtained with the 1/8-inch test section. The first wall temperature measuring thermocouple was located at a distance of 50 diameters from the beginning of the heated section.

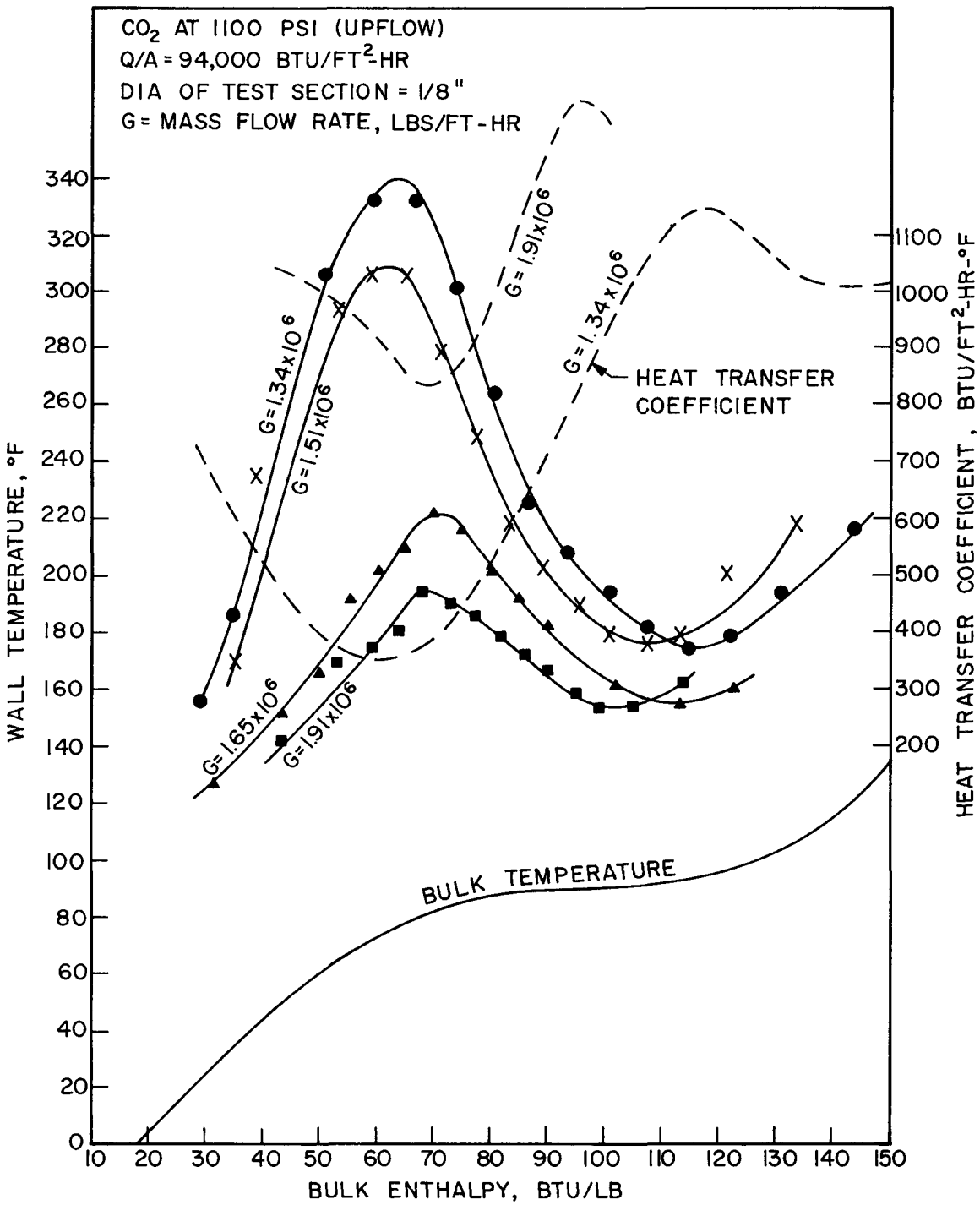

FIG. 34: EXPERIMENTAL WALL TEMPERATURE PROFILES WITH 1/8" TEST SECTION (UPFLOW)

For a heat flux of 94000 BTU/ft^2-hr, a temperature peak begins to form when the mass velocity is 1.91 x 10^6 lbs/ft^2-hr. When the velocity is decreased further, the peak becomes more prominent. For a mass velocity of 1.34 x 10^6 lbs/ft^2-hr, the wall temperature is as high as 340 ^oF, more than 160 ^oF higher than in the critical region. The heat transfer coefficient is also shown in the figure for the largest and smallest mass velocities. This is smaller by a factor of three in the deteriorated region as compared to the critical enthalpy region. The temperature peaks were mostly found in the bulk enthalpy range of 60-70 BTU/lb., with the majority in the region of 65 BTU/lb, corresponding to a bulk temperature of about 75 F. Beyond the temperature peak, the heat transfer improves in the critical enthalpy region. The minimum in the wall temperature corresponds to the maximum heat transfer coefficent which is usually located in the bulk enthalpy range from 90 to 110 BTU/lb. Beyond this point the wall temperature increases monotonically as the fluid is almost entirely beyond the critical region.

7.3.2 Comparison with Theory

Wall temperature profiles were calculated in the same way as for the larger diameter test section. Figure 35 shows a GD vs. bulk enthalpy plot for carbon dioxide at 1100 psi. and for QD = 1475 BTU/ft-hr , analogous to Figures 6-9 for steam. This corresponds to a heat flux of 144,000 BTU/ft^2-hr for the 1/8-inch section. The wall temperature profile for a particular flow rate is cross plotted from this plot in the usual manner. Figure 36 shows a comparison between the computed and experimental curves for a heat flux of 144,000 BTU/ft^2-hr. The computed peaks in temperature occur at a larger value of the bulk enthalpy, but

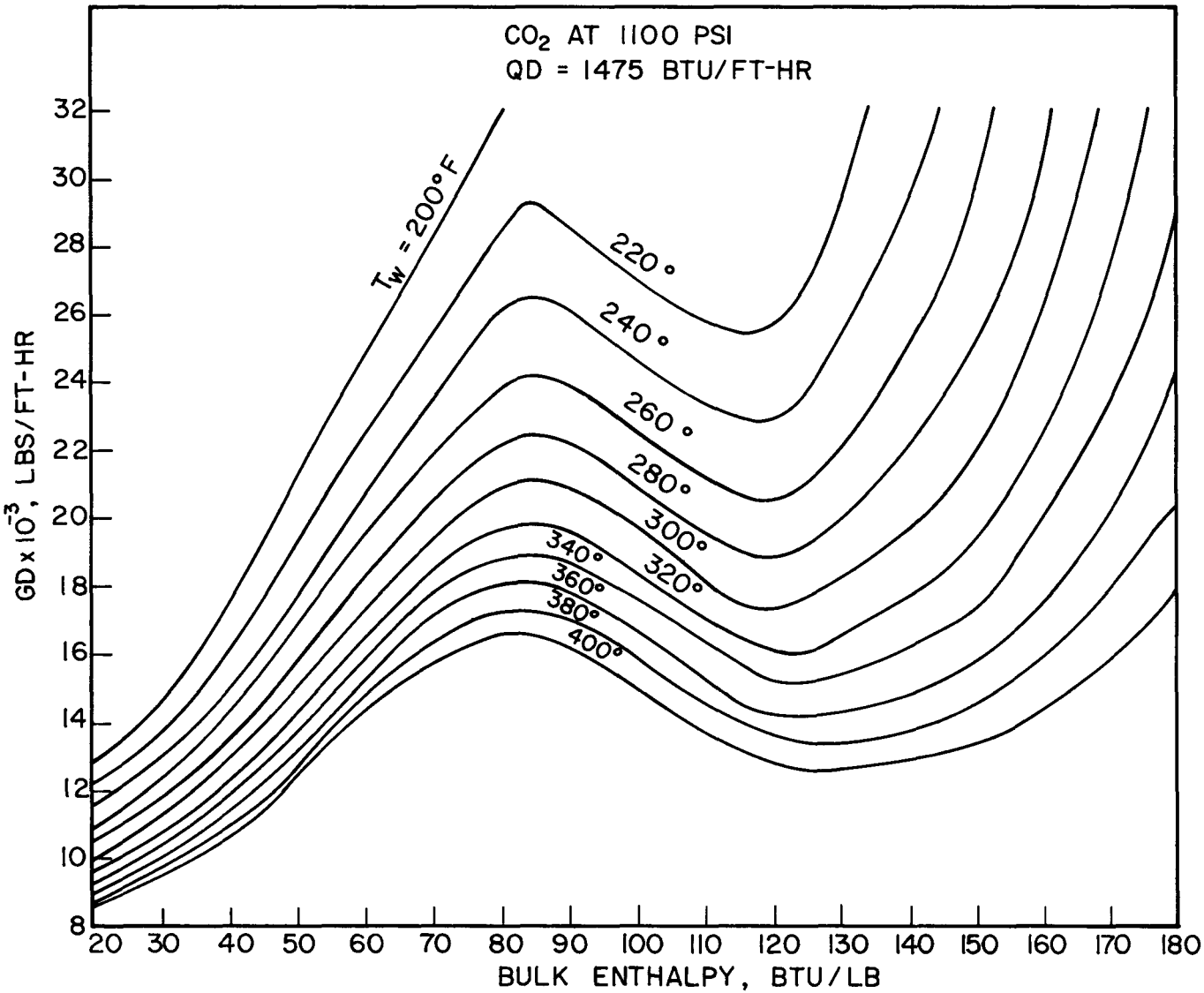

FIG. 35 COMPUTED GD VS. BULK ENTHALPY PLOT FOR CO_2 AT 1100 PSI

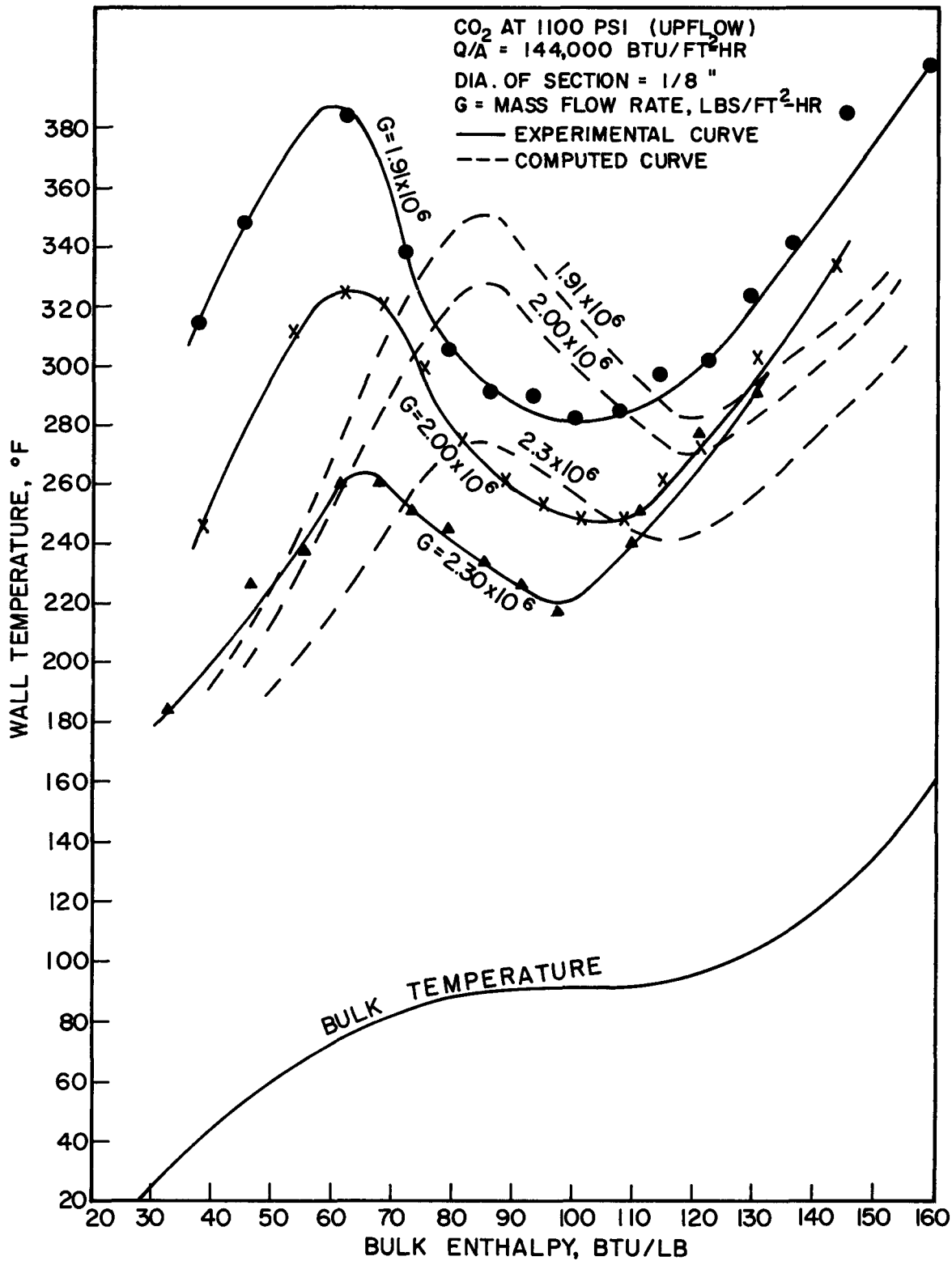

FIG. 36 : COMPARISON BETWEEN COMPUTED AND EXPERIMENTAL WALL TEMPERATURE PROFILES

the general features of the peaks and the peak temperatures are predicted very well. The possible reasons for the better agreement between theory and experiment in this case than for the larger section are that inlet effects have been minimized, and the large velocities and small diameter both considerably reduce any possible free convection effects.

7.3.3 Experimental Downflow Results

Figure 37 shows some typical wall temperature profiles taken in downflow with the 1/8-inch test section. The S-shaped temperature profile is again evident, with the temperature peak getting higher and sharper as the mass velocity is lowered progressively from 2.5×10^6 to 1.86×10^6 lb/ft^2-hr for the heat flux of 144,000 BTU/ft^2-hr. The dotted lines show the wall temperature profiles in upflow. As should be expected at the mass velocities used, there is very little difference between the upflow and downflow results. The amount and nature of the deterioration in heat transfer is similar and takes place in the same enthalpy region as does the subsequent improvement in heat transfer.

7.3.4 Safe vs. Unsafe Plot

With the same definition for an unsafe run as before, i.e.,

$$Nu/Nu_{Mac} < 0.5$$

where $Nu_{Mac} = 0.023\ (Re)^{0.8}\ (Pr)^{0.4}$

with Re, Pr based on the bulk properties,

and $Nu = hD/k_b$,

a safe vs. unsafe plot was constructed for the 1/8-inch section. This is shown in Figure 38. A similar plot for downflow was not drawn due to a lack of sufficient experimental data, but the similarity of the wall

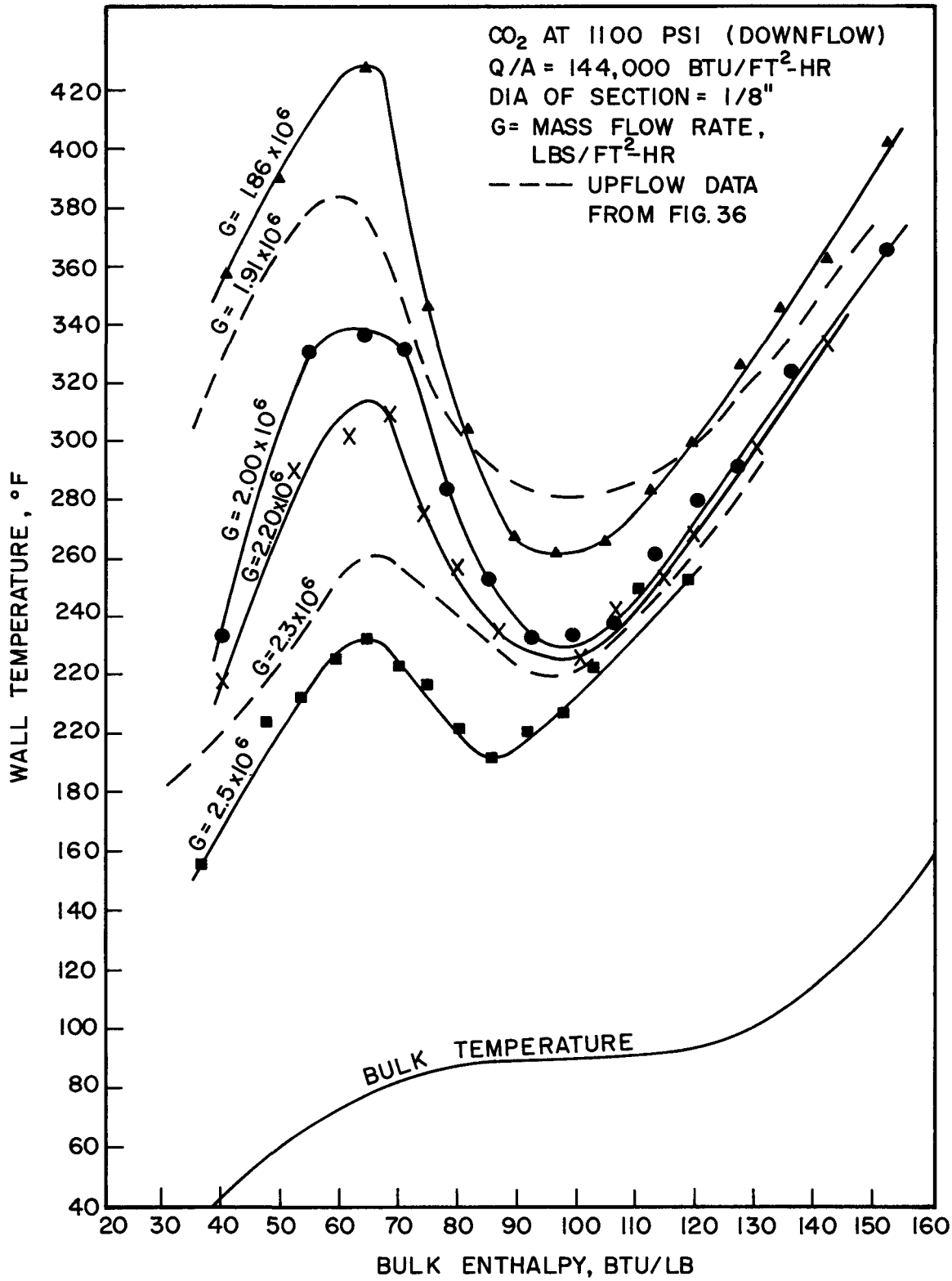

FIG. 37: WALL TEMPERATURE PROFILES FOR 1/8" TEST SECTION IN DOWNFLOW

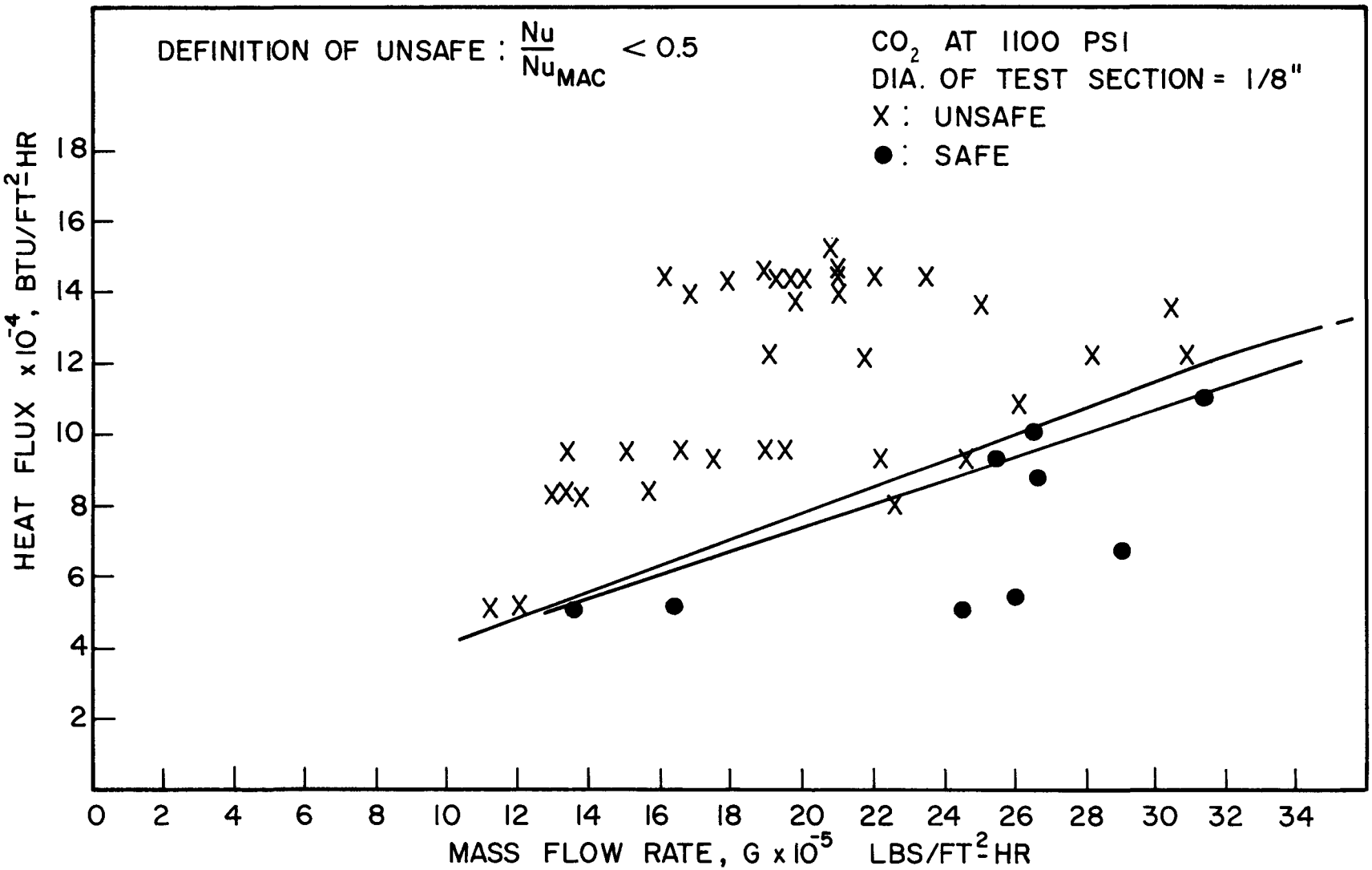

FIG. 38 : EXPERIMENTAL SAFE VS. UNSAFE PLOT FOR 1/8" TEST SECTION

temperature profiles in upflow and downflow indicates that this would very closely follow the upflow plot. Figure 38 shows that the safe vs. unsafe plot for the 1/8-inch test section has a relatively small slope when compared with Figure 31. A more detailed comparison with the 1/4-inch test section plot is made in the next section.

7.4 Comparison between Experimental and Theoretical Safe vs. Unsafe Plots

A theoretical safe vs. unsafe plot was computed for carbon dioxide in the same way as for steam. GD vs. bulk enthalpy plots were calculated for several heat fluxes along with the Nu/Nu_{Mac} ratios along the different curves. The largest flow rate for which this ratio fell below 0.5 in the enthalpy region of interest was then designated the critical flow rate for the heat flux in question. These corresponding pairs of GD and QD were then plotted on the safe vs. unsafe curve. Figure 39 shows a comparison between the computed curve, the experimental curves for upflow and downflow for the 1/4-inch test section, and the experimental curve for the 1/8-inch section.

A comparison shows that the computed curve is conservative with respect to all the experimental curves. The 1/8-inch test section plot is the closest to the computed curve, as expected, because the external factors such as inlet effects and free convection, which are not included in the theory, are held to a minimum. The downflow plot for the 1/4-inch tube has a slope similar to the computed curve than the upflow curve. The disparity between the computed curve and the 1/4-inch section curves at high mass velocities and heat fluxes is due to some extent to the lack of sufficient inlet subcooling. At the low end, the difference in the upflow

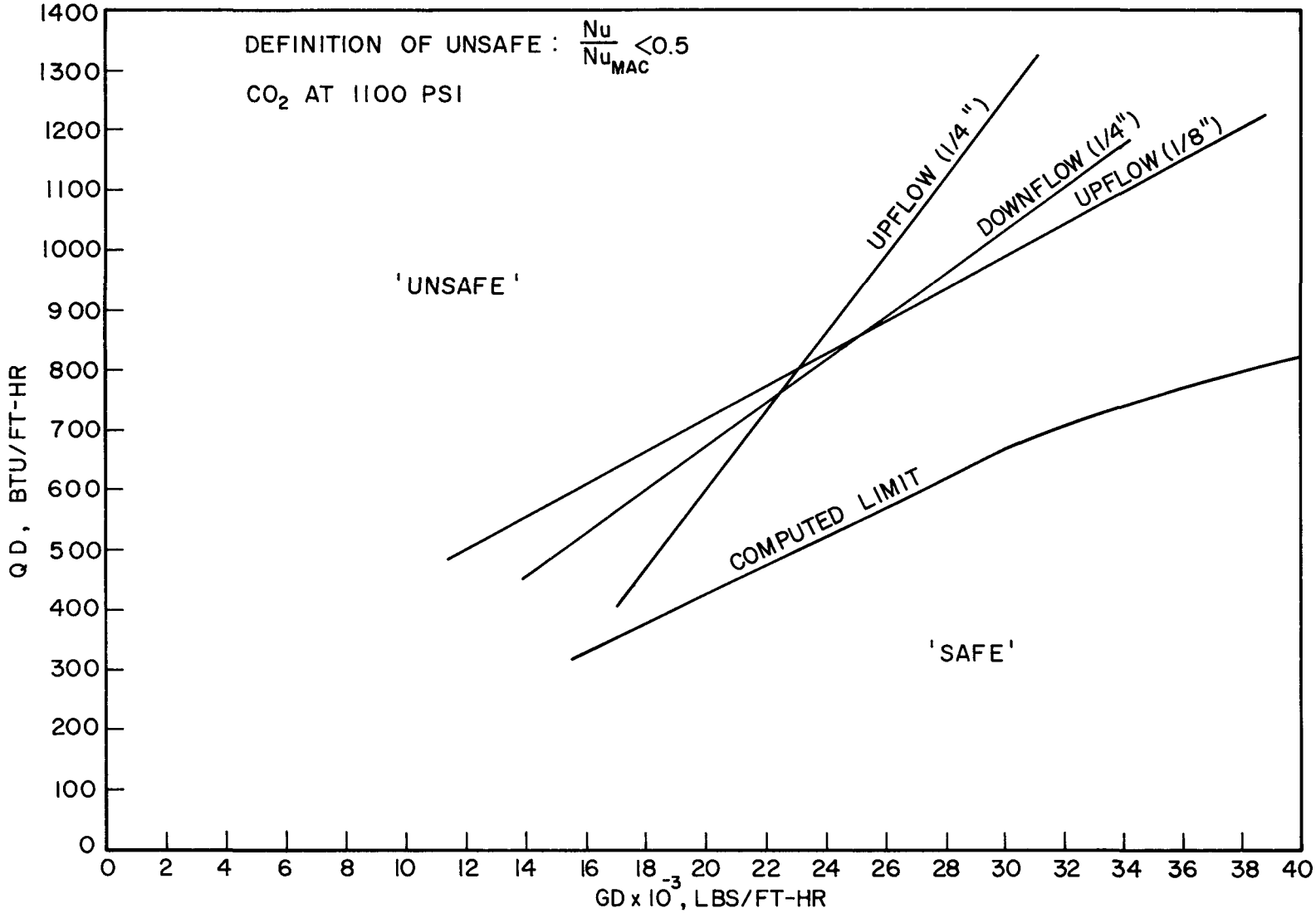

FIG. 39 : COMPARISON OF EXPERIMENTAL AND COMPUTED SAFE VS. UNSAFE PLOTS

and downflow curves is partly due to the effects of free convection which are beginning to be noticeable.

7.5 Results Obtained with Swirl Test Section

Since upstream effects that tend to disrupt the boundary layer near the wall have been seen to reduce the deterioration in heat transfer to supercritical pressure carbon dioxide, it was expected that swirl induced within the test section would greatly improve the heat transfer. For this purpose, a snug fitting twisted tape of Inconel was used inside the 1/4-inch test section to generate swirl. The twist used was one turn of 360° in four diameters. Tests were performed in both up and down flow at 1100 psi. The tape induces centrifugal forces in the fluid and helps to replace the light fluid near the wall with the cooler and heavier fluid in the core of the flow.

7.5.1 Improvement in Heat Transfer and Wall Temperature Profiles

As expected, the heat transfer rates were significantly improved by the introduction of the twisted tape. However, the deterioration in heat transfer was not completely eliminated. It occurred to some extent at higher heat fluxes in both upflow and downflow.

Figure 40 shows some wall temperature profiles with this test section for a heat flux of 46,500 BTU/ft^2-hr. As the mass flow rate is reduced, deterioration is seen to occur at a mass velocity of 840,000 lbs/ft^2-hr. For comparison, a wall temperature profile for a mass flow rate of 10^6 lbs/ft^2-hr, and the same heat flux in a 1/4-inch tube without swirl is included. This is shown by the dotted line in the figure. It is seen that for an equivalent mass velocity, the swirl completely eliminates the peak in wall temperature.

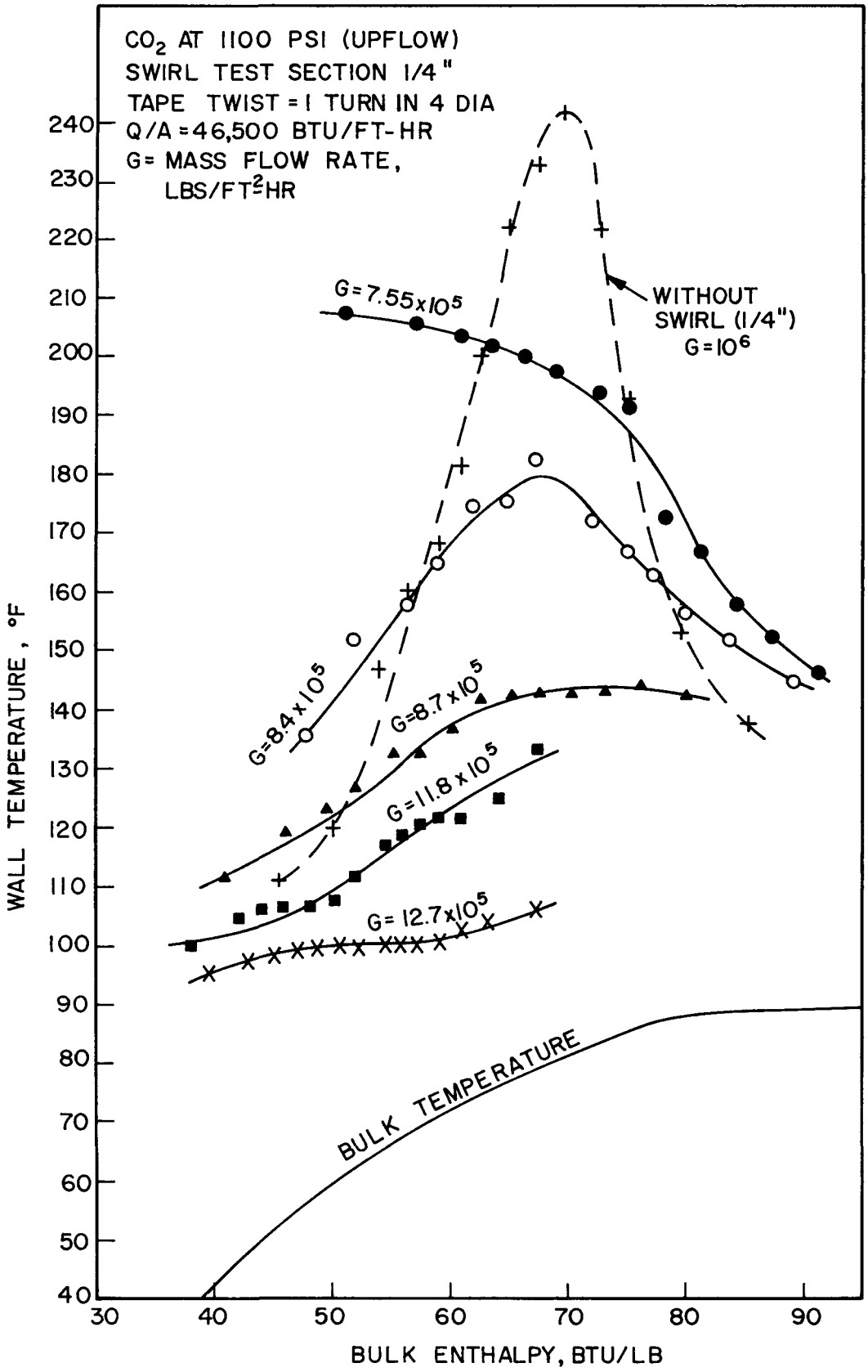

FIG. 40 : WALL TEMPERATURE PROFILES FOR SWIRL TEST SECTION

An examination of the wall temperature profiles in swirl flow reveals the following features as compared to flow without swirl:

1. The peaks in wall temperature, when they do occur, occur at a much larger value of the heat flux for a similar mass velocity.
2. These peaks are not sharp but spread out over a large bulk enthalpy range.
3. There is also noticeable improvement in the post peak enthalpy region, where the bulk enthalpy is close to and above the critical enthalpy.
4. In many runs for large heat flux to mass velocity ratios, the deterioration appeared in the form of a monotonic decrease in the wall temperature, with the highest temperature at the entrance, rather than as a sharp temperature peak. This may be due to the peak shifting to the entrance region at the beginning of the twisted tape.

Lopina (57) has suggested a method of correlating the heat transfer in swirl flow. The essential feature of this method consists in relating the improvement in heat transfer due to swirl to the centrifugal convection effect. Thus for fluids without strong variations in properties, the overall local Nusselt number is related to the flow conditions by the relation:

$$\frac{hD_h}{K} = F\{.023(\alpha Re_h)^{0.8} Pr^{0.4} + 0.193[(\frac{Re_h}{y})^2 (\frac{D_h}{D_i}) \beta\Delta T_f Pr]^{1/3}\}. \quad (7.1)$$

Here, h = local heat transfer coefficient

D_h = hydraulic diameter: 4x(Flow Area)/(Wetted Perimeter)

$D_h/D_i = (1-4\ \delta_f/\pi D_i)/(1+2/\pi\ (1 - \delta_f/D_i))$

where δ_f = thickness of tape

D_i = inner diameter of tube

F = a factor used to account for the fin effect of the tape

α = ratio of resultant velocity to the axial velocity

$= \frac{1}{2y} (4y^2 + \pi^2)^{1/2}$

y = tape twist, in terms of inside diameters /180° of tape twist

Re_h = Reynolds number based on hydraulic diameter

$= \frac{GD_h}{\mu}$

Pr = Prandtl number = $C_p \mu/k$

β = volumetric coefficient of thermal expansion

ΔT_f = difference of wall and bulk temperatures.

This correlation represents the linear addition of the Nusselt numbers in forced convection and free convection where the acceleration due to gravity, occurring in the Grashof number is replaced by the centrifugal acceleration. The Nusselt number for forced convection is obtained from the MacAdams' correlation, corrected to include the effects of the hydraulic diameter and a modified velocity, which is the resultant of the axial and tangential components. The correlation used for the "centrifugal" convection is that recommended by Fishenden and Saunders (57) for heat transfer with turbulent convection from a vertical plate; i.e.,

$$Nu = 0.114 \, (Gr.Pr)^{1/3}.$$

Here, the Grashof number Gr has been defined as

$$Gr = \frac{4.94}{y^2} Re_h^{\,2} \frac{D_h}{D_i} \beta \Delta T_f$$

where the acceleration due to gravity g has been replaced by the centrifugal acceleration a given by

$$a = \frac{1}{2D_i} \left(\frac{V_a \pi}{y}\right)^2 .$$

This correlation was found to give very good results in the case of swirl flows in air and low pressure water. It is not expected that a linear addition of Nusselt numbers will yield good results over a large range of operating conditions in supercritical carbon dioxide where the properties vary by large amounts, depending on the temperature. A difficulty also arises in the choice of the reference temperature to calculate the properties used in the Grashof and Prandtl numbers. However, an attempt was made to predict the heat transfer in swirl flow along these lines, since it appears to be the most direct method of approach. This yields approximate estimates of the improvement in the heat transfer coefficient. For this purpose, Lopina's equation (7.1) was modified to the form:

$$hD_h/k_w = \frac{h_{FC} D_h}{k_w} + C\left[\left(\frac{Re_h}{y}\right)^2 \left(\frac{D_h}{D_i}\right) \frac{\Delta\rho}{\rho_b} \frac{C_{p_{av}} \mu_w}{k_w}\right]^{1/3} \qquad (7.2)$$

where h_{FC} = forced convection heat transfer coefficient calculated by the analytical methods previously described;

C = constant to be evaluated empirically;

$\Delta\rho$ = difference in the densities at the bulk and wall temperatures

$C_{p_{av}}$ = average value of the specific heat, given by the ratio of the drop in enthalpy between wall and bulk temperatures divided by the difference of the wall and bulk temperatures.

A procedure of this type necessitates iteration as the wall temperature is not known to start off with. For this purpose, a wall temperature is assumed, and the viscosity, density, and conductivity and enthalpy at this temperature are found. The terms on the right-hand side of equation (7.2) are then evaluated. h_{FC} is calculated from the GD versus bulk enthalpy plot for the particular heat flux, and the term in the parenthesis is evaluated. This gives a first estimate of the heat transfer coefficient which is used to calculate the wall temperature. If this does not agree with the initial assumption for the wall temperature, the process is repeated until good agreement is obtained between successive trials. This procedure was not altogether successful in that different values of the constant C were required under different conditions of heat flux and flow rate. At very low heat fluxes the value of 0.193 suggested by Lopina was satisfactory. However, the best value to correlate the heat transfer at the incipience of deterioration in the heat transfer was found to be 0.115. It is suggested that this value be used as a first estimate to obtain an idea of the heat transfer coefficient in the presence of swirl. Figure 41 shows the correlation between the experimental and predicted values of the heat transfer coefficient in the range of bulk enthalpy corresponding to the deteriorated region (60-70 BTU/lb.), based on equation (7.2) with C = 0.115. The data points correspond to three heat fluxes (46,000, 72,000, and 118,000 BTU/ft^2-hr) and represent conditions ranging from no deterioration, for which the predicted heat transfer coefficient is low, to severe deterioration, for which the predicted heat transfer coefficient is on the high side.

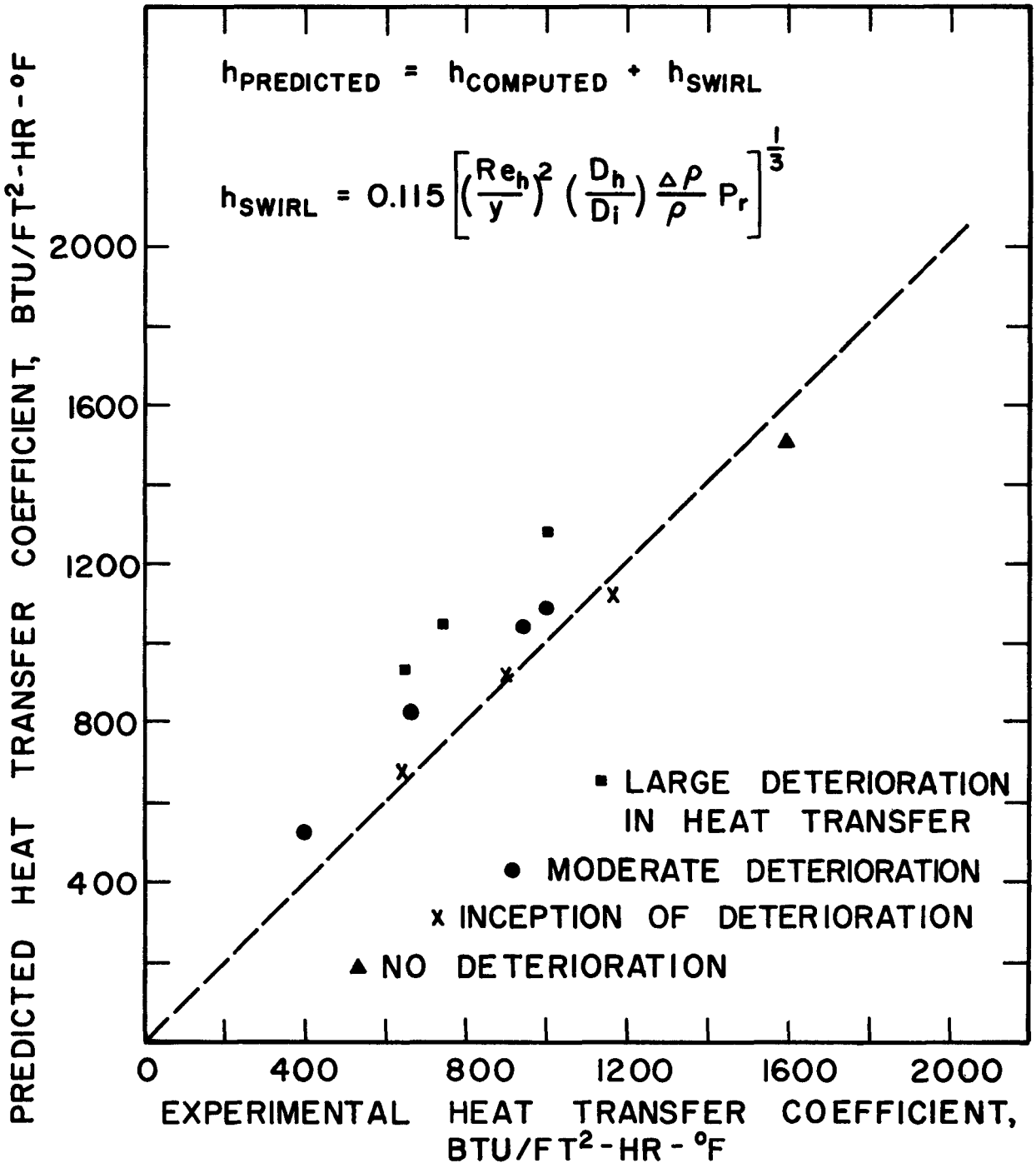

FIG. 41: CORRELATION OF SWIRL HEAT TRANSFER

7.5.2 Safe versus Unsafe Plot for Swirl Flow

A safe vs. unsafe plot based on a similar criterion as for forced convection serves to show the extent of improvement in heat transfer obtained by using the swirl generating tape. As before, the definition of an unsafe heat flux is that $Nu/Nu_{Mac} < 0.5$. The Nusselt number and the Reynolds number in this case are based on the hydraulic diameter of the tube rather than its inside diameter. Figure 42 shows the safe vs. unsafe plot obtained experimentally for the swirl test section. A comparison with the corresponding curve for the 1/4-inch test section without swirl shows that the allowable heat flux is increased by a factor of two. With more tightly twisted tape, the improvement would be expected to be even greater.

In a number of practical applications, the steam tubes are heated over a small portion of the circumference and not along the whole periphery. In this event, swirl would be of much greater use as a means of replacing the fluid near the heated portion of the wall by the cooler fluid away from it, and a correspondingly larger improvement would be expected in the heat transfer rate. The introduction of a swirl tape would mean an increased pressure drop within the section, but twisted tape would be required only in a small enthalpy range along the heated length, and the overall pressure drop would not be increased by a large factor for a long boiler tube.

7.6 Visual Test Section

A visual test section was used to examine qualitatively the flow of carbon dioxide at high subcritical and supercritical pressures. In order

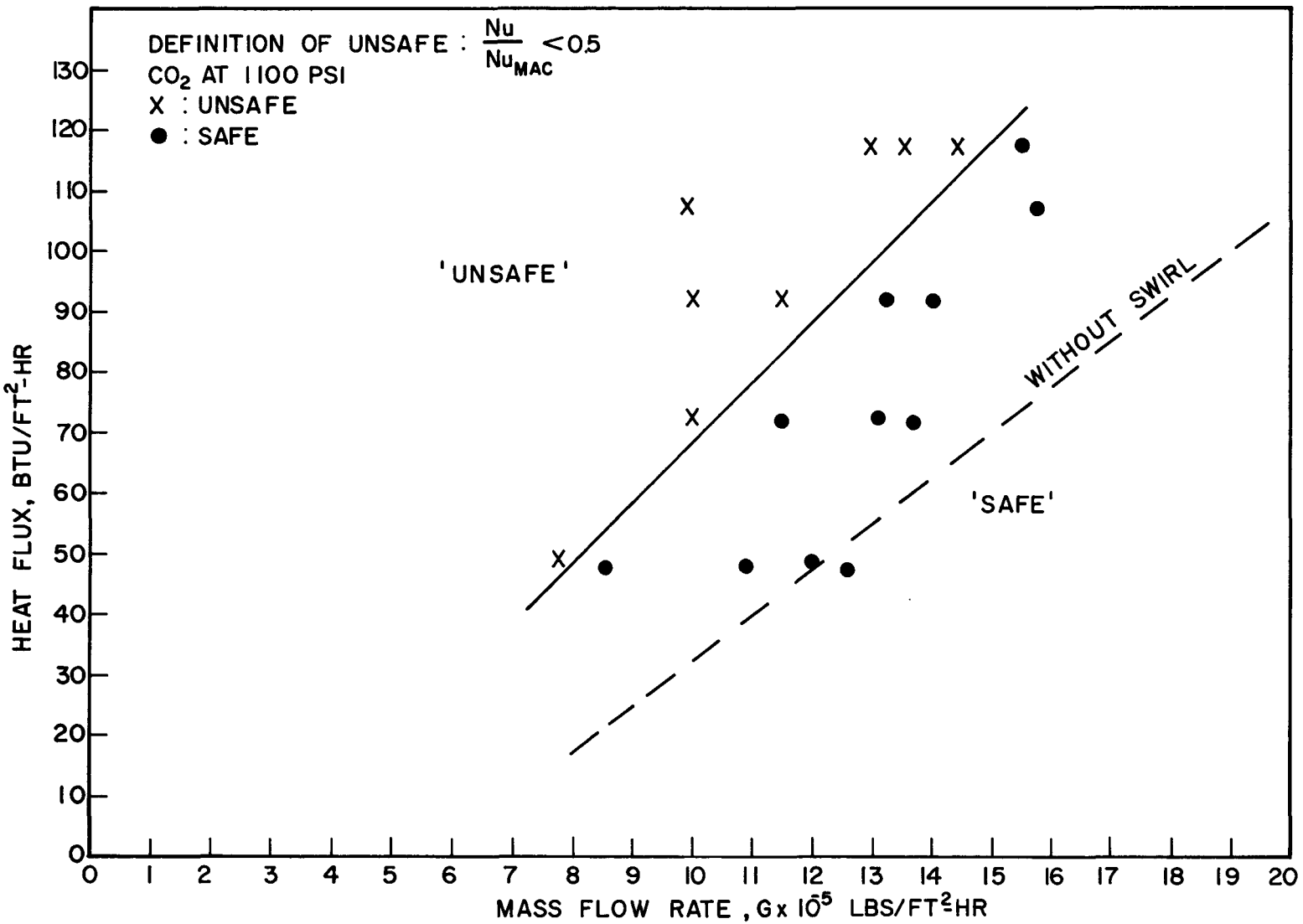

FIG. 42: SAFE VS. UNSAFE PLOT FOR SWIRL FLOW

to make use of readily available equipment, an annular test section was used consisting of a central stainless steel heater inside a high pressure manometer. Only reflected lighting could be used which precluded taking meaningful photographs.

The flow at supercritical pressures appeared at first sight very much like boiling at high subcritical pressures. At low heat fluxes, small amounts of "vapor" coming off the heater could be distinguished. This appeared to come off in wisps rather than as bubbles. The amount of "vapor" slowly increased along the length of the heated section. As the critical enthalpy was reached, the fluid was practically filled with "vapor" and became opaque so that the heater inside could not be seen.

At higher heat fluxes, no significant differences were observed. No temperature measurements were made along the heater wall. However, under conditions of heat flux, mass velocity, and inlet temperature for which there was a pronounced deterioration in heat transfer for the previous test section, the only difference visible in the flow pattern was that the rate of "vapor" production increased fairly sharply in a small part of the heated length. Calculations based on the inlet and outlet temperatures and the heat flux and mass flow rate showed that this was the enthalpy region where the deterioration occurred in the other test section.

No significant differences were observed in downflow. This is not surprising because of the small hydraulic diameter of the test section used (.119 inch).

7.7 Discussion of Results

The results on the carbon dioxide loop establish that deterioration in heat transfer can occur in carbon dioxide as in other fluids like water,

hydrogen, etc., in the critical region. The temperature peaks are fairly sharp and occur in a region where the bulk enthalpy is below the critical enthalpy and the wall temperature above the pseudocritical temperature. The bulk enthalpy region where the peaks occur was found to be relatively small, generally between 60 and 70 BTU/lb corresponding to bulk temperatures between 70 and 80 ^{o}F for carbon dioxide at 1100 psi. These temperature peaks were found in both up and down flow under the conditions of operation.

The effects of the various experimental parameters on the nature and amount of deterioration will now be discussed.

1. The Heat Flux and Flow Rate

   The ratio of heat flux to flow rate has to be sufficiently high in order to get a deterioration in heat transfer. As seen from the wall temperature curves in Figure 26 or 34, the higher this ratio, the greater is the deterioration. Generally, the wall temperature peaks occur at a smaller value of the bulk enthalpy as the ratio is increased.

2. Inlet Enthalpy

   The amount of deterioration is strongly influenced by the inlet enthalpy, especially if the inlet enthalpy is not appreciably less than the enthalpy at which the deterioration occurs. The greatest deterioration occurs when the inlet enthalpy is low. Figure 43 shows the effect of inlet temperature on the wall temperature profile. As seen from the figure, the wall temperature may be reduced substantially when the inlet temperature is increased from 52 to 80 ^{o}F. When the fluid enters above a certain enthalpy,

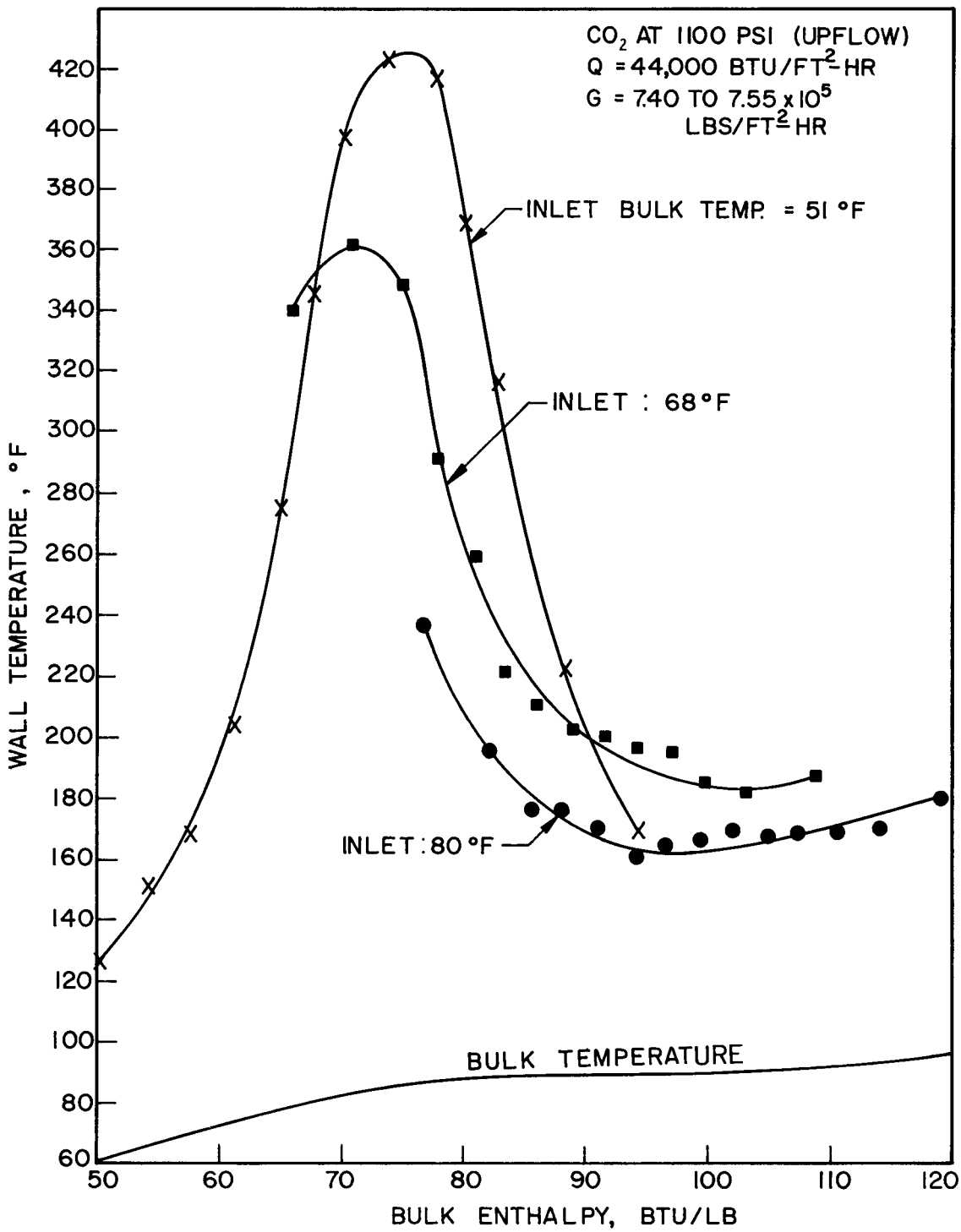

FIG. 43: EFFECT OF INLET ENTHALPY ON WALL TEMPERATURE PROFILE

the deterioration in heat transfer is very small even though the inlet enthalpy is below the critical enthalpy. This is tied in with the entrance effect which has considerable influence when the critical temperature is in the fluid film next to the wall in the entrance region. This effect would presumably be of little importance when the wall temperature in the entrance region is below the pseudocritical temperature.

3. Upstream Conditions

Swirl, vibration, or flow instabilities tend to reduce the amount of deterioration. The effects of tape generated swirl have shown that the allowable heat flux can be substantially raised (Figure 42). Swirl inherent in the flow due to upstream disturbances can also reduce the deterioration. This is because of the tendency of such disturbances to disrupt the low density boundary layer and replace it by the fluid from the central flow. The effects of lateral vibration in the test section had a similar effect. This is illustrated in Figure 44 which shows that the wall temperature is greatly reduced in the presence of vibration. The effect is the greatest in the middle of the tube where the vibration amplitude is greatest. This was the case in the run shown in Figure 44.

4. Pressure

The deterioration is the greatest near the critical pressure and is less at higher pressures. Figure 27 and 32 show that the deterioration at 1150 psi. is not as sharp as at 1100 psi. and also that the allowable heat flux at 1150 psi. is greater than at 1100 psi. under identical conditions of flow rate.

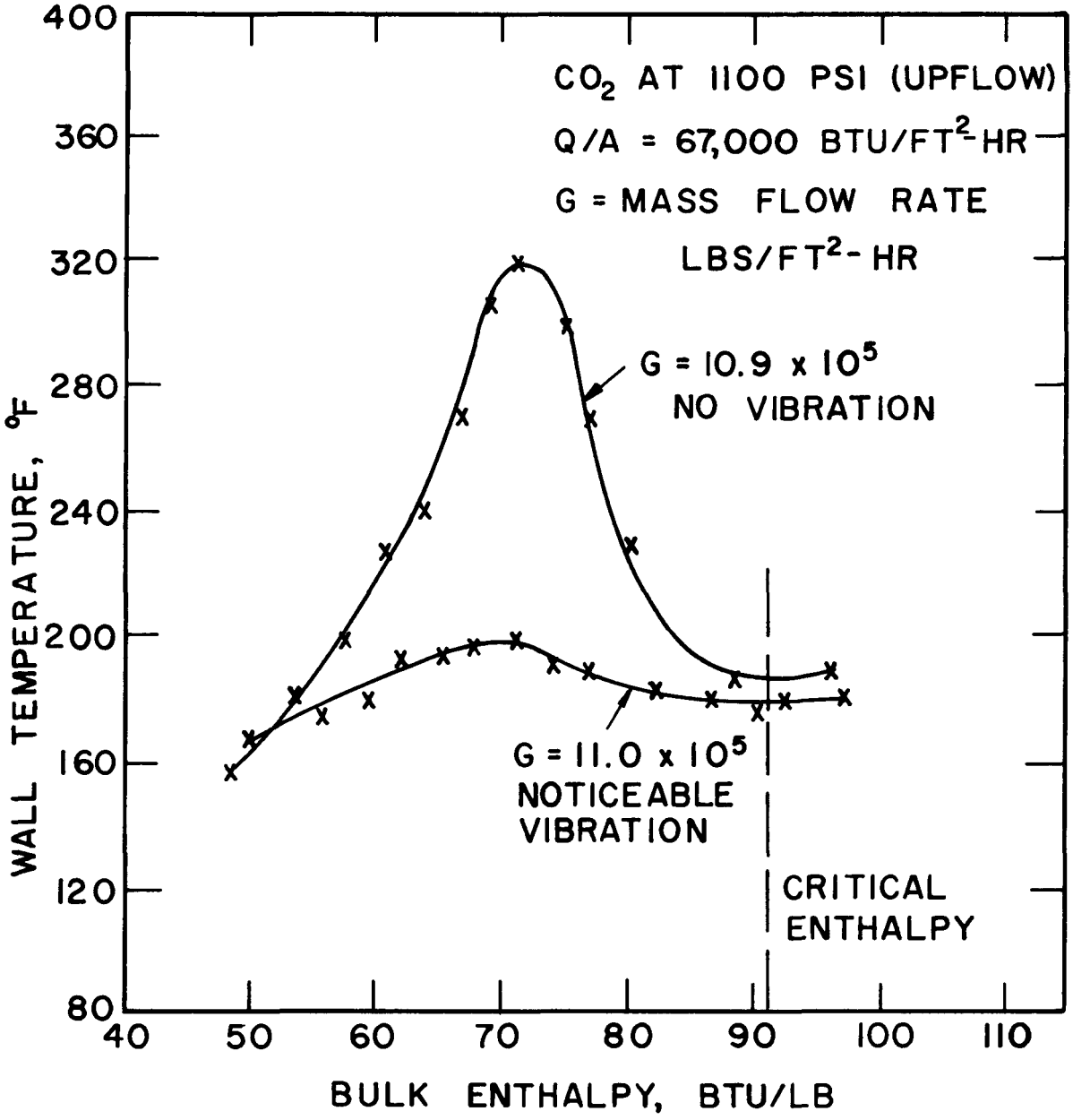

FIG. 44 : EXPERIMENTAL RESULTS SHOWING THE EFFECTS OF VIBRATION

5. Effect of Orientation

Hot spots were observed in both up and down flow, and in general, no significant differences were seen within the limits of the operating conditions. Figure 33 does show that at low mass velocities, the allowable heat fluxes were higher for downflow than for upflow. Though a horizontal test section was not tested, deterioration is expected to occur in that orientation, but probably reduced in sharpness and degree due to the influence of convective effects on the boundary layer.

6. Test Section Diameter

The slope of the experimental safe vs. unsafe plots as well as the computed plot indicates that greater deterioration may be expected for larger diameter tubes. This is also to be expected from the computed safe vs. unsafe plot. However, the situation is complicated by the presence of strong natural convection effects in the larger diameter tubes for larger GR/Re^2. A comparison of the 1/4-inch and 1/8-inch section plots in Figure 39 shows that there is some discrepancy in the low velocity region which is partly due to this effect.

7.8 Comparison of Results with those of Other Investigators for Carbon Dioxide

It was briefly mentioned earlier that most of the earlier investigators have not observed deterioration in heat transfer to carbon dioxide in the form of temperature peaks, whereas one investigator reports sharp peaks in upflow and none in downflow. A more detailed comparison between those results and the present work is made in this section with a view

to explaining the apparent contradictions. In Table 4 the results and operating conditions of Koppel and Smith (27), Tanaka (24), Hall (20), Krasnoschekov et al (61), and the present work (Shiralkar) are compared.

Koppel and Smith used a wide range of heat fluxes and mass velocities with inlet temperatures of 60°F and above. The test section used was horizontal and small in diameter (0.194 inch). Though no deterioration in heat transfer was reported as such, a number of anomalous results are shown. With some of the lower inlet temperatures used, there is often a sharp fall in the wall temperature with length. For example, for one run at a heat flux of 71,200 BTU/ft^2-hr and an inlet temperature of 70°F and a mass flow rate of 722,000 lbs/ft^2-hr., a sharp drop in wall temperature was observed from 180 to 140°F, which was atrributed to entrance effects. In the light of the present investigation, this would appear to be the tail end of a temperature peak, modified by entrance effects. The use of the horizontal test section would also tend to reduce the amount of deterioration.

Tanaka et al have confined their experiments to very small heat fluxes and inlet temperatures above 80 °F. Under these conditions it would not be possible to observe deterioration in heat transfer.

The results of Hall are especially interesting because they illustrate the effects of natural convection in large tubes or large values of $\frac{Gr}{Re^2}$. A comparison with the results of Shiralkar shows that the Gr was much higher in these experiments and the mass flow rates smaller than those used by Shiralkar. Both these conditions serve to increase the dominance of buoyancy effects. A comparison of the nature of the

TABLE 4

Comparison of Experimental and Theoretical Results for CO_2

No.	Source	Pressure psi	Tube Dia. Inches	G Lbs/Ft^2-Hr	Q/A BTU/Ft^2-Hr	Orientation of Flow	Min. Inlet Temp., ^oF	Enthalpy at Peak BTU/Lb	Nature of Peak	$Re = GD/\mu_w$	$Gr = \frac{\Delta\rho}{\rho_b}\left(\frac{\rho_b}{\mu_w}\right)^2 R^3 g$	$\frac{Gr}{Re^2}$ (Max.)
1	Shiralkar	1100	0.25	640,000-2,000,000	16,000-117,000	Upflow	35^oF	60-75	Sharp	267,000-835,000	$2.3x10^8$	$3.2x10^{-3}$
2	Shiralkar	1100	0.25	640,000-2,000,000	28,000-110,000	Downflow	35^oF	55-68	Sharp	267,000-835,000	$2.3x10^8$	$3.2x10^{-3}$
3	Shiralkar	1100	0.125	$1.2x10^6$-$2.6x10^6$	50,000-144,000	Upflow	0^oF	60-70	Not as Sharp as (1),(2)	250,000 540,000	$0.28x10^8$	$4.5x10^{-4}$
4	Shiralkar	1100	0.125	$1.3x10^6$-$3x10^6$	50,000 144,000	Downflow	0^oF	60-69	Similar to (3)	260,000-625,000	$0.28x10^8$	$4.4x10^{-4}$
5	Hall	?	0.75	468,000	16,000	Upflow	53^oF	50	Sharp	586,000	$61.4x10^8$	$1.73x10^{-2}$
6	Hall	?	0.75	468,000	17,500	Upflow	53^oF	49	Very Sharp	586,000	$61.4x10^8$	$1.73x10^{-2}$
7	Hall	?	0.75	468,000	17,500	Downflow	53^oF	-	No Peak	586,000	$61.4x10^8$	$1.73x10^{-2}$
8	Koppel and Smith	1071-1100	0.194	93,000-930,000	20,000-200,000	Hotizontal	70^oF	-	No Peak Sharp Drop in Temp. at Inlet	30,000-300,000	-	-
9	Tanaka et al	1130	0.4	300,000-675,000	5,000-17,800	Upflow	83^oF	-	No Peak	200,000-450,000	$9.4x10^8$	$2.3x10^{-2}$
10	Krasnoschekov et al	1130-1470	0.16	375,000-1,875,000	825,000 and below	Horizontal	70^oF	-	No Peak Low Heat Trans. Coeffi-ients	100,000-500,000	-	-
11	Calculations	1100	0.25, 0.125	1,000,000	60,000	No Gravity Terms	-	77-80	Not as Sharp as Experi-ment in (1),(2)	415,000	-	-

peaks is also revealing. The peaks in Hall's results are much sharper; i.e., they occur over a much smaller enthalpy range, and they were not found in downflow. They also occur at a substantially smaller value of the bulk enthalpy. This adds weight to the deductions made by comparing the results for steam as obtained by various investigators. The influence of natural convection thus tends to produce sharper peaks in upflow, which occur at a smaller value of the bulk enthalpy. Here again, it can be seen that the inlet enthalpy can be important. Tanaka et al, though working under nearly the same conditions of small Reynolds numbers and large Grashof numbers, did not report any comparable behaviour in their results.

In a recent investigation by Krasnoschekov and Protopopov, the heat transfer to carbon dioxide at very high temperature drops was measured. Heat fluxes as high as 825,000 BTU/ft^2-hr were used at pressures of 1130 and 1420 psia. A horizontal test section 4.08 mm (0.16 inch) and with L/D = 51 was used for the purpose. The Reynolds number range used was 10^5 to 5 x 10^5. The lowest inlet temperature used was 70 ^oF, and consequently, no sharp peaks were seen in the pre-critical enthalpy range. However, it was found that the heat transfer coefficient became increasingly poor at high heat fluxes. Values as low as 1/10th of the expected heat transfer coefficient, as calculated by correlations for supercritical pressure heat transfer at low heat fluxes, were encountered. They suggest a multiplication factor of $(\frac{\rho_w}{\rho_L})^{0.3}$ $(\frac{C_{p_{av}}}{C_{p_b}})^n$ in order to adapt the low heat flux correlation to their results, where n varies from 0.4 to 0.7 under different conditions.

These results lead one to the conclusion that the operating conditions governing the nature and extent of deterioration at a particular supercritical pressure are:

1. Heat flux parameter
2. Flow rate or Reynolds number
3. A free convection parameter, e.g. Gr/Re^2
4. Inlet temperature

It is seen from Table 4 that the parameter Gr/Re^2 is an order of magnitude higher in Hall's results than the highest value for the conditions of Shiralkar. A critical value of about 10^{-2} can be attached to Gr/Re^2 where the free convection effects become important.

Figure 45 shows a three-dimensional plot of the operating conditions of the investigators mentioned in this section and shows that these were quite different from each other. In particular, the region of investigation in the present work is seen to be in the portion where the heat fluxes were high and the importance of buoyancy effects very small. The influence of the inlet temperature is not shown in this map. A comparison in Table 4 shows, however, that Shiralkar used the widest range of inlet temperatures and the greatest degree of subcooling. Hall used a fairly low inlet temperature in the small sample of his results seen by this author ($50^{o}F$). Koppel and Smith and Tanaka et al, as well as Krasnoschekov, generally used inlet temperatures too high to allow observation of the temperature peaks.

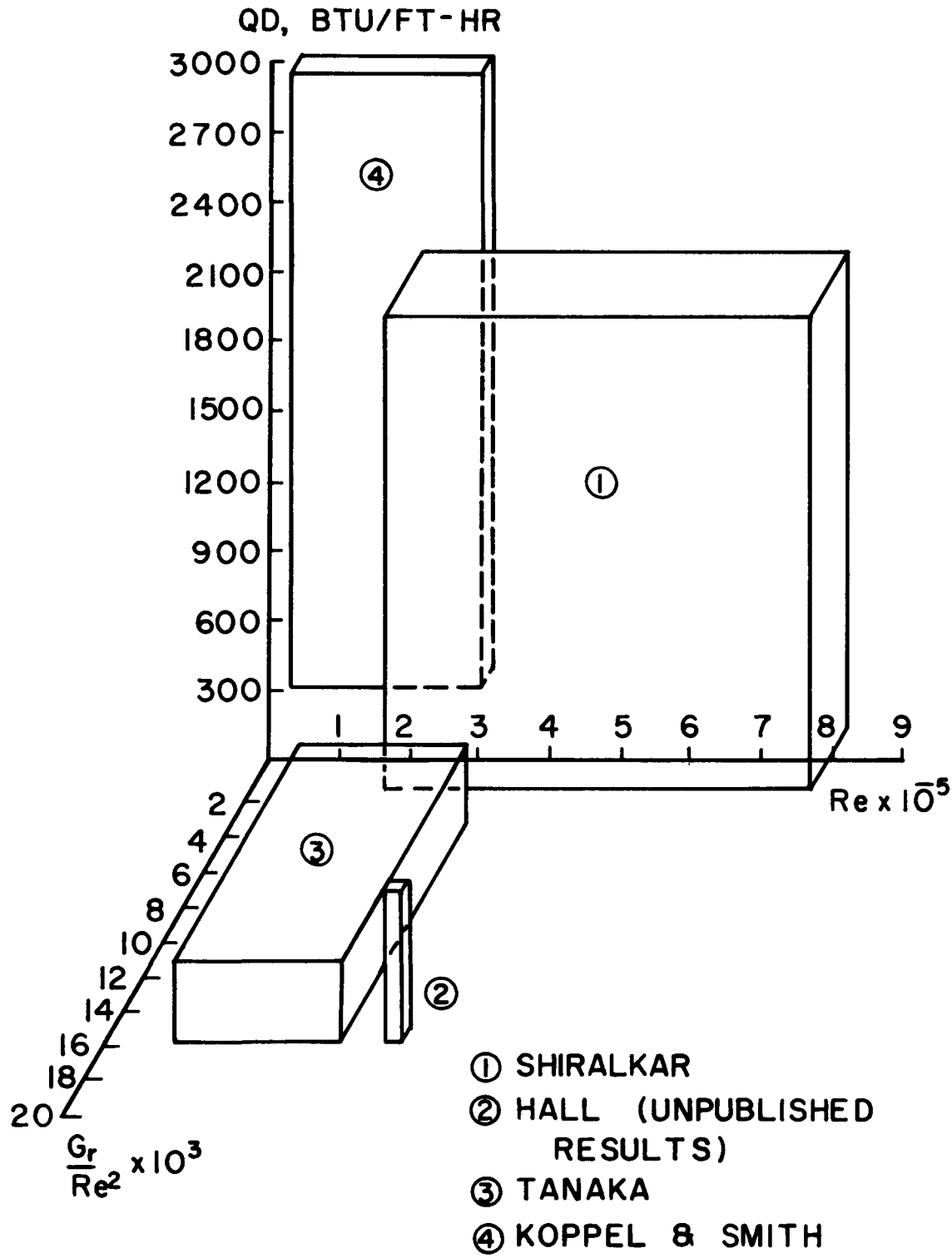

FIG. 45 : MAP SHOWING REGIONS OF OPERATION

8. SUMMARY AND CONCLUSIONS

1. The Nusselt numbers for the heat transfer to a fluid at supercritical pressure differ sharply in different regions, the boundaries of which are governed by the mass velocity, a heat flux parameter, and a parameter governing the relative importance of free convection to the forced convection. Depending on the region of operation, varying degrees of improved and deteriorated heat transfer rates are possible.
2. In the region where free convection effects are not important (i.e., the region covered by the experiments in this investigation), deteriorated heat transfer can occur when the heat flux is sufficiently high and the bulk temperature is below the pseudocritical temperature. The deteriorated region is confined to a relatively small range of bulk enthalpies, depending on the fluid and the pressure.
3. The deterioration occurs because the effects of the low density and conductivity near the wall are not yet compensated by increased velocities in the core of the flow.
4. The occurrence of the deteriorated region can be predicted reasonably well, but the heat transfer in the critical bulk enthalpy region beyond the peak in wall temperature cannot, because of inadequacies in the expressions used for the eddy diffusivity.
5. The location and extent of the deterioration is sensitive to the details of the system geometry and the inlet subcooling.

6. Deterioration in heat transfer can occur in both upflow and downflow when the free convection effects are not predominant.
7. The introduction of a swirl generating twisted tape within the test section substantially improves the heat transfer. However, if the heat flux is increased to a larger value, deterioration can occur again. This is not as sharp as the deterioration in the absence of twisted tape.
8. Deterioration in heat transfer to carbon dioxide was not observed by earlier investigators because the inlet temperatures were not low enough in their experiments. The different observations made by different investigators in other fluids can be explained in terms of influence of natural convection, orientation, and entrance effects.

9. FUTURE WORK

The problem of heat transfer to fluids at supercritical pressure when free convection is the dominant influence is an area that needs further investigation. Probably the most promising approach to the problem would be based on direct visual observation of the flow at low mass velocities and in large diameter tubes. This has not yet been done by any of the earlier investigators. It seems likely that significantly different flow patterns will be encountered, e.g., reversal of flow, etc. A study made with improved transmitted lighting as compared to the reflected lighting used with the present visual test section would no doubt prove more profitable.

A theoretical approach would probably be influenced by the nature of the visual observations. It is clear that if a formal integration procedure is to be used, better estimates of the eddy diffusivities of heat and momentum are necessary. Some information (57) is already available for this purpose. A "history" effect might have to be incorporated into the calculations to remove the anomalies of zero diffusivities at the points where the shear stress vanishes. It is expected, however, that a theoretical approach will have to be modified to include an analysis of flow instabilities that are possible under these circumstances.

REFERENCES

1. Styrikovich, M. A., Margulova, T. Kh., and Miropolskiy, Z. L., "Problems in the Development of Designs of Supercritical Boilers," Teploenergetika 14 (6), pp. 4-7, 1967.

2. Dickinson, N. L. and Welch, C. P., "Heat Transfer to Supercritical Water," Transactions ASME 80, pp. 746-752, 1958.

3. Dubrovina, E. N. and Skripov, V. P., "Convection and Heat Transfer Near the Critical Point of Carbon Dioxide," Zhurnal Prikladnoi Mekhaniki i Tekhnicheskoi Fiziki, 1, pp. 115-119, 1965.

4. Knapp, K. K. and Sabersky, R. H., "Free Convection Heat Transfer to Carbon Dioxide near the Critical Point," Int. Journ. Heat Mass Transfer 19, pp. 41-51, 1966.

5. Larson, J. R. and Schoenhals, R. J., "Turbulent Free Convection in Near Critical Water," ASME paper 65-HT-57, 1965.

6. Petukov, B. S., Krasnoschekov, E. A., and Protopopov, V. S., "An Investigation of Heat Transfer to Fluids Flowing in Pipes under Super-Critical Conditions," Int. Dev. in Heat Transfer, Part 3, ASME pp. 569-579, 1961.

7. Cornelius, A. J., "An Investigation of Instabilities Encountered during Heat Transfer to a Supercritical Fluid," Argonne National Lab. report ANL-7032, 1965.

8. Cornelius, A. J. and Parker, J. D., "Heat Transfer Instabilities Near the Thermodynamic Critical Point," Proceedings of the 1965 Heat Transfer and Fluid Mechanics Institute, Stanford University Press, pp. 317-330, 1965.

9. Shitsman, M. E., "Impairment of the Heat Transmission at Supercritical Pressures," High Temperature, 1, No. 2, pp. 237-244, 1963. (translated from Teplofizika Vysokikh Temperatur)

10. Schmidt, K. R., "Thermodynamic Investigation of Highly Loaded Boiler Heating Surfaces," AEC-tr-4033. (Argonne National Lab. translation from Mitteilungen der Vereinigung der Grosskesselbesitzer 63, p. 391, 1959).

11. Miropolskiy, Z. L., Picus, V. J., and Shitsman, M. E., "Regimes of Deteriorated Heat Transfer at Forced Flow of Fluid in Curvilinear Channels," 3rd Annual Heat Transfer Conference, A.I.Ch.E. pp. 95-105, 1966.

12. Vikrev, Yu, V. and Lokshin, V. A., "An Experimental Study of Temperature Conditions in Horizontal Steam Generator Tubes at Supercritical Pressures," Teploenergetika, 11, pp. 79-82, 1964.

13. Swenson, H. S., Carver, J. R., and Kakarala, C. R., "Heat Transfer to Supercritical Water in Smooth Bore Tubes," Jour. of Heat Transfer, Trans. ASME, 87, pp. 477-483, 1965.

14. Powell, W. B., "Heat Transfer to Fluids in the Region of the Critical Temperature," Jet Propulsion 27, pp. 776-783, 1957.

15. Szetela, E. J., "Heat Transfer to Supercritical Hydrogen," American Rocket Society Journal 32, No. 8, pp. 1289-1292.

16. Hendricks, R. C., Graham, R. W., Hsu, Y. Y., and Friedman, R., "Experimental Heat Transfer Results for Cryogenic Hydrogen Flowing in Tubes at Subcritical and Supercritical Pressures to 800 psia.," NASA Technical Note, NASA TN-D-3095, 1966.

17. McCarthy, J. R., Seader, J. E., and Trebes, D. M., "Heat Transfer to Supercritical Nitrogen Tetroxide at High Heat Fluxes and In Axially Curved Flow Passages," ASME paper 67-HT-69, 1967.

18. Hsu, D. and Zoschak, R. J., "An Experimental Investigation of the Stability of Heat Transfer to Supercritical Water Flowing Upwards in Vertical Tubes," Foster Wheeler Corp. Research Report RN-163/54-665604, 1968.

19. Shitsman, M. E., "The Effect of Natural Convection on Temperature Conditions in Horizontal Tubes at Supercritical Pressures," Teploenergetika 13, (7), pp. 52-56, 1966.

20. Hall, W. B., Personal Communication.

21. Miropolskiy, Z. L., Personal Communication with Prof. Griffith.

22. Bringer, R. P. and Smith, J. M., "Heat Transfer in the Critical Region," A.I.Ch.E. Journal 3, pp. 49-55, 1957.

23. Wood, R. D. and Smith, J. M., "Heat Transfer in the Critical Region-Temperature and Velocity Profiles in Turbulent Flow," A.I.Ch.E. Journal, 10, (2), pp. 180-186, 1964.

24. Tanaka, H., Nishiwaki, N., and Hirata, M., "Turbulent Heat Transfer to Supercritical Carbon Dioxide," Semi-International Symposium, J.S.M.E., Tokyo, September, 1967.

25. Hall, W. B., Jackson, J. D., and Khan, S. A., "An Investigation of Forced Convection Heat Transfer to Supercritical Pressure Carbon Dioxide," 3rd Annual Conference on Heat Transfer, I.Mech.E. Section, pp. 257-266, 1966.

26. Sabersky, R. H. and Hauptmann, E. G., "Forced Convection Heat Transfer to Carbon Dioxide Near the Critical Point," Int. Jour. Heat Mass Transfer, 10, pp. 1499-1508, 1967.

27. Koppel, L. B. and Smith, J. M., "Turbulent Heat Transfer in the Critical Region," Int. Dev. in Heat Transfer, Part 3, ASME, pp. 579-585, 1961.

28. Deissler, R. G., "Heat Transfer and Fluid Friction for Fully Developed Turbulent Flow of Air and Supercritical Water with Variable Fluid Properties," Trans. ASME, 76, pp. 73-85, 1954.

29. Shitsman, M. E., "Heat Transfer to Water, Oxygen, and Carbon Dioxide in the Vicinity of the Critical Point," Teploenergetika, 1, p. 68-72, 1959.

30. Hess, H. L. and Kunz, H. R., "A Study of Forced Convection Heat Transfer to Supercritical Hydrogen," Jour. of Heat Transfer, Trans. ASME 87, pp. 41-48, 1965.

31. Novak, E. S., Grosh, R. E., and Liley, P. E., "A Survey of P-V-T Data for Water in the Critical Region," Jour. of Heat Transfer, Trans. ASME 83, C, pp. 1-11, 1961.

32. Novak, E. S. and Grosh, R. J., "An Investigation of Certain Thermodynamic and Transport Properties of Water Vapor in the Critical Region," ANL-6064, 1959.

33. Michels, A., Bijl, A., and Michels, C., "Isotherms of CO_2," Proc. Royal Society, London, A160, p. 376, 1937.

34. Michels, A., Blaise, B., and Michels, M., "Isotherms of CO_2 in the Neighborhood of the Critical Point and Round the Coexistence Line," Proc. Royal Society, London, A160, p. 358, 1937.

35. Michels, A. Botzen, A., and Schurmann, W., "The Viscosity of CO_2 Between 0 - 75°C and up to 200 Atmospheres," Physica 23, p. 95, 1957.

36. Michels, A. and Michels, M., "Isotherms of CO_2 Between 0 - 150 °C and 1 - 250 Atmospheres," Proc. Royal Soc., London, A153, p. 201, 1935.

37. Michels, A., et al., "The Joule-Thomson Coefficient and the Specific Heat at Constant Pressure of CO_2," Physica 14, p. 218, 1948.

38. Clark, A. L., "The Critical State of Pure Fluids," Chemical Review 23, p. 1, 1938.

39. Keesom, W. H., "Density of Carbon Dioxide," International Critical Tables, 3, p. 12, 1928.

40. Tzederberg, N. V. and Morosova, N. A., "Heat Conductivity of Carbon Dioxide at Pressures of 1 - 200 kg/cm^2 and Temperatures upto 1200 °C," Teploenergetika, 1, p. 75, 1960.

41. Starling, K. E., Eakin, B. E., Dolan, J. P., and Ellington, R. T., "Critical Region Viscosity Behaviour of Ethane, Propane, and n-Butane," Prog. Int. Res. in Thermodynamic and Transport Prop. ASME, Academic Press, 1962.

42. Sengers, J. V. and Michels, A., "The Thermal Conductivity of Carbon Dioxide in the Critical Region," Prog. Int. Res. in Thermodynamic and Transport Prop., ASME, Academic Press, 1962.

43. Khan, S. A., "Forced Convection Heat Transfer to Fluids Near the Critical Point," Ph.D. Thesis, Victoria University of Manchester, 1965.

44. Kutateladze, S. S. and Leont'ev, A. I., "Turbulent Boundary Layers in Compressible Gases," Academic Press, 1964.

45. Hsu, Y. Y. and Smith, J. M., "The Effect of Density Variations on the Heat Transfer in the Critical Region," Trans. ASME, 83, pp. 176-183, 1961.

46. Townsend, A. A., "Equilibrium Layers and Wall Turbulence," Jour. of Fluid Mechanics, 11, pp. 97-120, 1961.

47. Deissler, R. G., "Analytical and Experimental Investigation of Adiabatic Turbulent Flow in Smooth Tubes," NACA TN-2138, 1950.

48. Van Driest, E. R., "On Turbulent Flow Near a Wall," Journal Aeronaut. Sci., 23, p. 1007, 1956.

49. Sleicher, C. A., Jr., "Turbulent Flows of Newtonian Systems," Modern Chemical Engineering, Vol. 1, Physical Operations, Reinhold Publ. Corp., pp. 45-89.

50. Reichardt, H., "Volstandige Darstellung der Turbulenten Geschwindigkeitverteilung in glatten Leitungen," Z. angew. Math. Mech. 31, 208-219, 1951.

51. Spalding, D. B., "A Single Formula for the 'Law of the Wall'," Jour. Appl. Mech., Trans. ASME 28 E, p. 455, 1961.

52. Rohsenow, W. M. and Choi, H. Y., "Heat, Mass and Momentum Transfer," Prentice-Hall Pub. Co., p. 190.

53. Goldmann, K., "Heat Transfer to Supercritical Water and Other Fluids with Temperature Dependent Properties," Chem. Engr. Prog. Symp. Series, Nuclear Engrg., Part 1, 50, (11), 1954.

54. Hall, W. B., "The Effect of Buoyancy Forces on Forced Convection Heat Transfer in a Vertical Pipe," Research Report N. E. 1, U. of Manchester, Dept. of Nuclear Engg., 1968.

55. Lynn, Scott, "Center Line Value of the Eddy Viscosity," A.I.Ch.E. Journal, 5, pp. 566-567, 1959.

56. Bourne, D. E., "Eddy Diffusivities in Forced and Free Convection Boundary Layers," J. Aero/Space Sci., 26, (7), pp. 459-460, 1959.

57. Lopina, R. F. and Bergles, A. E., "Heat Transfer and Pressure Drop in Tape Generated Swirl Flow," E.P.L. Report No. DSR 70281-47, Dept. of Mech. Engg., Mass. Inst. of Tech., 1967.

58. Buleev, N. I., El'tsova, L. D., and Biyukova, G. P., "Calculation of the Temperature Field in a Turbulent Fluid Flow in the Thermal Entry Section of a Circular Tube," High Temperature, 4, (4), pp. 510-521, 1966.

59. Deissler, R. G., "Analysis of Turbulent Heat Transfer and Flow in the Entrance Region of Smooth Passages," NACA TN-3016, 1953.

60. Melik-Pashaev, N. I., "Calculation of Convective Heat Transfer at Supercritical Pressure," High Temperature 4, (6), pp. 789-798, 1966.

61. Krasnoschekov, E. A. and Protopopov, V. S., "Experimental Study of Heat Exchange in Carbon Dioxide in the Supercritical Range at High Temperature Drops," High Temperature, 4, (3), pp. 375-382, 1966.

APPENDIX 1

Recommended Procedure for Calculating the Heat Transfer Coefficient to Supercritical Pressure Fluids

This section summarizes the results obtained in this report in the form of a step-wise procedure for estimating the heat transfer coefficient to supercritical pressure fluids (particularly, steam and carbon dioxide) when the flow rate, heat flux, and boiler tube size are known.

1. Calculate the Reynolds number and approximate Grashof number for the flow as

$$Re = \frac{GD}{\mu_w} \quad , \quad Gr = \frac{\Delta\rho}{\rho_b} \left(\frac{\rho_b}{\mu_w}\right)^2 gR^3 \quad .$$

First estimates of μ_w and ρ_b can be made by using the supercritical temperature viscosity, which does not change rapidly and an approximate value of the bulk density. Since the region of interest, where the Grashof number is the largest, is such that the bulk temperature is below critical and the wall temperature above the critical temperature, a suitable value of the bulk density in the below-critical enthalpy region should be chosen, e.g., at 695-700 ^{o}F for steam at 3300 psi., 77-80 ^{o}F for carbon dioxide at 1100 psi. The value of $\Delta\rho$ can be obtained by drawing parallel tangents to the low and high sides of the density vs. temperature curve and measuring the difference.

2. Calculate $\frac{Gr}{Re^2}$ to get an estimate of the influence of natural convection. If this is not too large, e.g., smaller than 4×10^{-3} for steam and 10^{-2} for carbon dioxide, the following procedure can be used with a high degree of confidence. If $\frac{Gr}{Re^2}$ is large, the heat transfer coefficient may be expected to be lower than the calculated one, especially in upflow. A more general criterion, applicable to more fluids may be that $Gr \times Pr/Re^2$ should be less than a critical value, where the Prandtl number is of the form

$$Pr = \frac{\Delta H}{\Delta T} \frac{\Delta \mu}{\Delta K}$$

ΔH = Enthalpy increase in the critical region in a temperature interval ΔT

$\Delta \mu$, ΔK = Viscosity and thermal conductivity drops in the same region.

However, it is difficult to generalize from the data on just two fluids.

3. Locate the operating conditions in terms of the mass velocity, tube diameter, and heat flux on the relevant safe vs. unsafe plot, e.g., Figure 19 for steam; Figure 39 for carbon dioxide. If the region of operation lies in the "safe" region, go to step 4; if it lies in the unsafe region, go to step 5.

4. For "safe" operating conditions a number of correlations for the Nusselt number are adequate and can be used with confidence. Perhaps the correlation for steam that covers the largest operating range is the one due to Swenson et al (page 27) which is

$$\frac{hD}{K_w} = 0.00459\left[\frac{GD}{\mu_w}\right]^{0.923} \left[\frac{(H_w - H_b)}{(T_w - T_b)} \frac{\mu_w}{K_w}\right]^{0.631} \left(\frac{\rho_w}{\rho_b}\right)^{0.231} .$$

In order to use this, a wall temperature has to be assumed in order to evaluate the properties at the wall temperature. With this, the Nusselt number, and thus the heat transfer coefficient, are calculated. This leads to a better estimate of the wall temperature. The iteration is continued until a satisfactory agreement between successive estimates is reached.

This correlation has also been found to be successful for carbon dioxide at low heat fluxes.

5. When deterioration takes place in the heat transfer, none of the previous correlations will lead to satisfactory agreement with experiment. For this purpose, the GD vs. bulk enthalpy plots for the particular heat flux (e.g., Figures 6-9 for steam; Figure 35 for carbon dioxide) can be used either to generate the complete wall temperature profile along the tube or to read off the maximum wall temperature obtained under the circumstances. The procedure in using the plots has been described in the report in conjunction with Figures 6-9 and consists in cross-plotting the wall temperature vs. bulk enthalpy for the flow rate in question. The maximum temperature corresponds to the maximum in the GD vs. bulk enthalpy plot. These results can then be translated to heat transfer coefficients by dividing the heat flux by the wall to bulk temperature difference.

APPENDIX 2

Computer Programs Used for Analysis

The Fortran 4 computer programs used can be divided into two main groups: two-dimensional and one-dimensional solutions. Each of these groups were further sub-divided into two categories: solutions with and without gravity terms. Several different forms of eddy diffusivity were used in conjunction with different programs and a number of relaxation and forward difference procedures were tried.

A sample program is shown in this section. This is the simplest program used and employs an explicit first-order forward difference procedure and has the advantage of requiring the least amount of computer time without too great a loss in accuracy. The program shown is for a one-dimensional solution without gravity terms. Goldmann's formulation for the eddy diffusivity is used.

Notation used:

CBULK	Conductivity at bulk enthalpy
COND	Local thermal conductivity
DBULK	Density at bulk enthalpy
DELTW	Increment in wall temperature
DENS	Local Density
DTDY	$\frac{dT}{dY}$
DUDY	$\frac{dU}{dY}$
DUPLUS	Increment in UPLUS

DY	Increment in Y
DYPLUS	Increment in YPLUS
ENTH	Local enthalpy
EPS	Eddy Diffusivity
FLOW	Mass flow rate x Diameter of Tube
HBULK	Bulk enthalpy
HEAT	Heat flux
HNUM	MacAdams Nusselt number = $.023(Re_b)^{0.8}(Pr_b)^{0.4}$
HNU2	Nusselt number = hD/k_b
I	Incremental variable
J	Incremental variable
L	Dummy variable
RAD	Radius of tube
RATIO	HNUM/HNU2
RCOND	Tabulated value of conductivity (tabulated versus temperature)
RDENS	Tabulated value of density
RENTH	Tabulated value of enthalpy
RSPHT	Tabulated value of specific heat
RT	Tabulated value of temperature
RVISC	Tabulated value of viscosity
SBULK	Specific heat at bulk enthalpy
SPHT	Local specific heat
TAU	Wall shear stress
TBULK	Bulk temperature

TFIN	Highest wall temperature for run
TPR	Local temperature
TRANSITION	Radial distance at which Y=YLIM
U	Local axial velocity
UPLUS	$\int_0^U \frac{dU}{\sqrt{\tau_o/\rho}}$
VBULK	Viscosity at bulk enthalpy
VISC	Viscosity
X	Dummy variable
Y	Non-dimensionalized distance from wall= y/R
YLIM	Y at YPLUS= 28/RAD
YPLUS	$\int_0^Y \frac{\sqrt{\tau_o/\rho}}{\mu/\rho} dY$

The data required for the program consists of:

1. Eighty tabulated values of temperature and the properties corresponding to these temperatures, i.e., density, viscosity, thermal conductivity, specific heat, and enthalpy at the pressure in question.
2. Eighty values of Y, the dimensionless distance from the wall, ranging from 0 to 1.
3. Fifty-six values of the wall shear stress in the region of interest.

The formats for these are contained in statements 200, 100, and 1000.

Apart from this data, the inputs for a particular run are:

a. The heat flux, HEAT in BTU/ft^2-hr.
b. The initial or lowest wall temperature, TPR(1) in ^oF.
c. The increases in wall temperature for each successive solution, DELTW in ^oF.

d. The highest wall temperature, TFIN in ^{o}F.

e. The radius of the tube, RAD in ft.

Statement 500 indicates the format for these inputs.

The outputs for each set of inputs consist of:

a. The radial temperatures, TPR(1) to TPR(80), in ^{o}F.

b. The local axial velocities along the radius, U(1) to U(80), in ft/hr.

c. The mass flow rate parameter, FLOW in lbs/ft-hr.

d. The bulk enthalpy, HBULK in BTU/lb.

e. The transition from the wall layer to the core of the flow, TRANSITION.

f. The ratio of the local bulk MacAdams Nusselt number to the computed Nusselt number, RATIO.

The main equations used in symbolic form are:

$$\frac{dT}{dY}(I) = \frac{-Q_o/A \times R \times (1 - Y(I))}{k(I) + \rho(I)\, C_p(I)\varepsilon(I)}$$

$$\frac{dU}{dY}(I) = \frac{\tau_o R(1 - Y(I))}{\mu(I) + \rho(I)\varepsilon(I)}$$

$$dY = Y(I + 1) - Y(I)$$

$$T(I + 1) = T(I) + \frac{dT}{dY}(I) \times dY$$

$$U(I + 1) = U(I) + \frac{dU}{dY}(I) \times dY$$

The eddy diffusivity is evaluated by

$$\varepsilon(I) = 0.01536\ RU^{+}(I)Y^{+}(I)\ \frac{\mu(I)}{\rho(I)}\ (1 - e^{-.01536\ RU^{+}(I)Y^{+}(I)},$$

$$\text{for } Y^{+}(I) < 28/R).$$

For $Y^+(I) > 28/R$, the quadratic equation for $\frac{dU}{dY}(I)$ is solved first, and ε is obtained later; i.e.,

$$\frac{dU}{dY}(I) = \frac{[\,-1 + \sqrt{1 + .5184\, Y^+(I)^2 R^2 (1 - Y(I))}\,]}{.2592\, RY^+(I)^2 \mu(I)/\tau_o}$$

$$\varepsilon(I) = 0.1296\, \frac{RY^+(I)^2 \mu(I)^2}{\rho(I)\, \tau_o} \times \frac{dU}{dY}(I).$$

Y^+ and U^+ are calculated by the following method:

$$DY^+(I) = \frac{\tau_o \rho(I)}{\mu(I)}$$

$$DU^+(I) = \frac{\rho(I)}{\tau_o}$$

$$Y^+(I) = Y^+(I - 1) + \frac{[DY^+(I) + DY^+(I - 1)]}{2} \times dY$$

$$U^+(I) = U^+(I - 1) + \frac{[DU^+(I) + DU^+(I - 1)]}{2} \times [U(I) - U(I - 1)].$$

Subroutines

Two subroutines were written up to evaluate properties at given values of temperatures and enthalpies. These are called PROP(I,T) and PROP2(Y), respectively. The properties are obtained by linear interpolation between tabular values. For temperatures and enthalpies which lie outside the tabular range, algebraic expressions are provided for small regions on either side of the tabular limits.

```
C      ONE DIMENSIONAL  RUN WITHOUT GRAVITY TERMS
C      CARBON DIOXIDE AT 1100 PSI.
C      GOLDMANN'S FORMULATION FOR EDDY DIFFUSIVITY
C      HEAT=144000 BTU/FT2-HR, RAD=.125 INCHES
       DIMENSION TPR(80),Y(80),U(80),DENS(80),VISC(80),COND(80),ENTH(80),
      1SPHT(80),EPS(80),DTDY(80),DUDY(80),RDENS(80),RVISC(80),RCOND(80),
      2RSPHT(80),RENTH(80),RT(80),YPLUS(80),UPLUS(80),DYPLUS(80),DUPLUS(8
      30),TAU(56)
       COMMON DENS,VISC,COND,SPHT,ENTH,RDENS,RVISC,RCOND,RSPHT,RENTH,RT,
      1TBULK,SBULK,VBULK,CBULK
       READ(5,200) (RT(I),I=1,80),(RDENS(I),I=1,80),(RVISC(I),I=1,80),(RC
      1OND(I),I=1,80),(RSPHT(I),I=1,80),(RENTH(I),I=1,80)
200    FORMAT(10F7.2)
100    READ(5,1) (Y(I),I=1,80)
1      FORMAT(10F7.2)
       READ(5,500) HEAT,TPR(1),TFIN,RAD,DELTW
500    FORMAT(5F12.2)
       READ(5,1000) (TAU(J),J=1,56)
1000   FORMAT(10E7.2)
3      J=1
       TPR(1)=TPR(1)+DELTW
8      L=0
       EPS(1)=0.
       U(1)=0.
       YPLUS(1)=0.
       UPLUS(1)=0.
       X=PROP(1,TPR(1))
       DTDY(1)=-HEAT*RAD/COND(1)
       DUDY(1)=TAU(J)*RAD/VISC(1)
       DY=Y(2)-Y(1)
       U(2)=DUDY(1)*DY
       TPR(2)=TPR(1)+DTDY(1)*DY
       DYPLUS(1)=SQRT(TAU(J)*DENS(1))/VISC(1)
       DUPLUS(1)=SQRT(DENS(1)/TAU(J))
       DO 4 I=2,79
       X=PROP(I,TPR(I))
       DYPLUS(I)=SQRT(TAU(J)*DENS(I))/VISC(I)
       DUPLUS(I)=SQRT(DENS(I)/TAU(J))
       DY=Y(I)-Y(I-1)
       YPLUS(I)=YPLUS(I-1)+DY*DYPLUS(I)-DY/2.*(DYPLUS(I)-DYPLUS(I-1))
       DU=U(I)-U(I-1)
       UPLUS(I)=UPLUS(I-1)+DU*DUPLUS(I)-DU/2.*(DUPLUS(I)-DUPLUS(I-1))
       X=YPLUS(I)
       IF(X-28./RAD)5,5,6
5      EPS(I)=.01536*RAD*UPLUS(I)*X*VISC(I)/DENS(I)*(1.-EXP(-.01536*RAD*U
      1PLUS(I)*X))
       DUDY(I)=(1.-Y(I))*TAU(J)*RAD/(VISC(I)+DENS(I)*EPS(I))
       GO TO 7
6      IF(L-1)371,372,372
371    YLIM=Y(I)
       L=1
372    DUDY(I)=(-1.+SQRT(1.+.5184*X*X*RAD*RAD*(1.-Y(I))))/(.2592*RAD*X*X*
      1VISC(I)/TAU(J))
       EPS(I)=ABS(.1296*RAD*X*X*VISC(I)/DENS(I)*VISC(I)/TAU(J)*DUDY(I))
7      DTDY(I)=-(1.-Y(I))*HEAT*RAD/(COND(I)+DENS(I)*SPHT(I)*EPS(I))
       DY=Y(I+1)-Y(I)
       U(I+1)=U(I)+DUDY(I)*DY
       TPR(I+1)=TPR(I)+DTDY(I)*DY
4      CONTINUE
       X=PROP(80,TPR(80))
       DEL16=0.
       DEL17=0.
       DO 10 I=2,80
```

```
      DY=Y(I)-Y(I-1)
      P=(1.-Y(I))*DENS(I)*U(I)
      Q=(1.-Y(I-1))*DENS(I-1)*U(I-1)
      DEL16=DEL16+.5*(P+Q)*DY
10    DEL17=DEL17+.5*(P*ENTH(I)+Q*ENTH(I-1))*DY
      HBULK=DEL17/DEL16
      FLOW=4.*DEL16*RAD
      X=PROP2(HBULK)
      HNUM=.023*((SBULK*VBULK/CBULK)**0.4)*((FLOW/VBULK)**.8)
      HNU2=2.*HEAT*RAD/((TPR(1)-TBULK)*CBULK)
      RATIO=HNUM/HNU2
      WRITE(6,997)
997   FORMAT(1H1,50X,8HTWALL = ,F6.1/48X,21H**********************)
      WRITE(6,999)
999   FORMAT(///8X,4HFLOW,11X,5HHBULK,12X,3HTAU,10X,10HTRANSITION,9X,
     15HRATIO)
      WRITE(6,998) FLOW,HBULK,TAU(J),YLIM,RATIO
998   FORMAT(6E16.6)
      WRITE(6,990)
990   FORMAT(//3X,12HTEMPERATURES)
      WRITE(6,31) TPR(1),TPR(3),TPR(5),TPR(7),TPR(9),TPR(11),TPR(13),
     1TPR(15),TPR(17),TPR(19),TPR(21),TPR(28),TPR(33),TPR(38),TPR(41),
     2TPR(40),TPR(47),TPR(49),TPR(51),TPR(57),TPR(62),TPR(70),TPR(72),
     3TPR(74),TPR(76),TPR(78),TPR(80)
31    FORMAT(//8(2X,E13.6))
      WRITE(6,32)
32    FORMAT(//3X,4HU...)
      WRITE(6,31) U(1),U(3),U(5),U(7),U(9),U(11),U(13),U(15),U(17),U(19)
     1,U(21),U(28),U(33),U(38),U(41),U(43),U(47),U(49),U(51),U(57),U(62)
     2,U(70),U(72),U(74),U(76),U(78),U(80)
      J=J+1
      IF(FLOW-30000.)904,904,803
904   IF(J-56)8,8,803
803   IF(TPR(1)-TFIN)3,804,804
804   STOP
      END
```

```
      FUNCTION PROP(I,T)
      DIMENSION DENS(80),VISC(80),COND(80),ENTH(80),RDENS(40),RVISC(40),
     1RSPHT(40),RENTH(40),RT(40),RCOND(40),SPHT(80)
      COMMON DENS,VISC,COND,SPHT,ENTH,RDENS,RVISC,RCOND,RSPHT,RENTH,RT,
     1TBULK,SBULK,VBULK,CBULK,DBULK
      IF(T-550.)40,8,8
8     IF(T-1050.)1,1,20
1     J=0
2     J=J+1
      IF(T-RT(J))3,10,2
3     RA=(T-RT(J-1))/(RT(J)-RT(J-1))
      RB=1.-RA
      GO TO 4
10    RA=1.
      RB=0.
4     DENS(I)=RB*RDENS(J-1)+RA*RDENS(J)
      VISC(I)=RB*RVISC(J-1)+RA*RVISC(J)
      COND(I)=RB*RCOND(J-1)+RA*RCOND(J)
      SPHT(I)=RB*RSPHT(J-1)+RA*RSPHT(J)
      ENTH(I)=RB*RENTH(J-1)+RA*RENTH(J)
      PROP=0.
      RETURN
20    ENTH(I)=1467.6+.75*(T-1050.)
      SPHT(I)=1.04-.006*(T-1050.)
      COND(I)=.047
      VISC(I)=.075
      DENS(I)=4.26-.0068*(T-1050.)+4.0E-5*((T-1050.)**2.)
      PROP=0.
      RETURN
40    DENS(I)=47.60+.0567*(550.-T)-6.6E-5*((550.-T)**2.)
      ENTH(I)=545.3-(550.-T)*1.16
      VISC(I)=.245+(550.-T)*.0003
      COND(I)=.350
      SPHT(I)=1.25
      PROP=0.
      RETURN
      END
```

```
      FUNCTION PROP2(Y)
      DIMENSION Z(400),RVISC(40),RDENS(40),RSPHT(40),RENTH(40),RT(40),
     1RCOND(40)
      COMMON Z,RDENS,RVISC,RCOND,RSPHT,RENTH,RT,TBULK,SBULK,VBULK,CBULK,
     1DBULK
      IF(Y-545.3)40,8,8
8     IF(Y-1467.6)1,1,20
1     J=0
2     J=J+1
      IF(Y-RENTH(J))3,10,2
3     RA=(Y-RENTH(J-1))/(RENTH(J)-RENTH(J-1))
      RB=1.-RA
      GO TO 4
10    RA=1.
      RB=0.
4     VBULK=RB*RVISC(J-1)+RA*RVISC(J)
      CBULK=RB*RCOND(J-1)+RA*RCOND(J)
      SBULK=RB*RSPHT(J-1)+RA*RSPHT(J)
      TBULK=RB*RT(J-1)+RA*RT(J)
      DBULK=RB*RDENS(J-1)+RA*RDENS(J)
      PROP2=0.
      RETURN
20    TBULK=(Y-1467.6)/.75+1050.
      SBULK=1.04-.006*(TBULK-1050.)
      DBULK=4.26-.0068*(TBULK-1050.)+4.0E-5*((TBULK-1050.)**2.)
      CBULK=.050
      VBULK=.075
      PROP2=0.
      RETURN
40    CBULK=.350
      VBULK=.245+.003*(545.3-Y)/1.25
      TBULK=550.-(545.3-Y)/1.16
      SBULK=1.25
      DBULK=47.60+.0567*(550.-TBULK)-6.6E-5*((550.-TBULK)**2.)
      PROP2=0.
      RETURN
      END
```

DATA USED FOR CARBON DIOXIDE PROGRAM

DISTANCE FROM WALL

0.	.0005	.0010	.0015	.0020	.0025	.0030	.0035	.0040	.0045
.0050	.0055	.0060	.0065	.0070	.0075	.0080	.0085	.0090	.0095
.010	.011	.012	.013	.014	.016	.018	.020	.022	.024
.026	.028	.030	.032	.034	.036	.038	.040	.042	.045
.050	.055	.060	.065	.070	.075	.080	.085	.090	.095
.10	.11	.12	.14	.16	.18	.20	.22	.24	.26
.28	.30	.32	.34	.36	.38	.40	.42	.45	.50
.55	.60	.65	.70	.75	.80	.85	.90	.95	1.

PROPERTIES OF CARBON DIOXIDE AT 1100 PSI

20.	30.	40.	50.	60.	61.	62.	63.	64.	65.
66.	67.	68.	69.	70.	71.	72.	73.	74.	75.
76.	77.	78.	79.	80.	81.	82.	83.	84.	85.
86.	87.	88.	89.	90.	91.	92.	93.	94.	95.
96.	97.	98.	99.	100.	101.	102.	103.	104.	105.
106.	107.	108.	109.	110.	111.	112.	113.	114.	115.
116.	117.	118.	119.	120.	121.	122.	124.	126.	128.
130.	140.	150.	160.	170.	180.	190.	200.	210.	220.
57.9	56.3	54.9	54.2	53.9	53.5	53.3	53.2	53.0	52.7
52.5	52.1	51.9	51.5	51.2	50.8	50.4	50.0	49.5	49.0
48.6	48.2	47.6	47.1	46.6	45.9	45.4	44.5	43.7	43.1
41.8	40.6	38.9	35.9	28.2	22.8	20.7	19.1	18.1	17.5
17.0	16.5	16.2	16.0	15.7	15.5	15.3	15.1	14.9	14.6
14.3	14.1	14.0	13.7	13.5	13.4	13.3	13.1	13.0	12.9
12.8	12.7	12.6	12.5	12.4	12.4	12.3	12.1	11.9	11.7
11.5	10.9	10.3	9.9	9.5	9.0	8.5	8.0	7.8	7.7
.337	.307	.277	.247	.217	.214	.211	.208	.205	.202
.199	.196	.193	.189	.185	.181	.178	.174	.170	.167
.164	.159	.156	.153	.149	.146	.142	.139	.135	.132
.128	.125	.121	.115	.101	.083	.070	.065	.0625	.0595
.0577	.0565	.0555	.0540	.0532	.0528	.0522	.0515	.0512	.0510
.0505	.0498	.0495	.0495	.0494	.0494	.0493	.0493	.0493	.0493
.0493	.0492	.0492	.0491	.0490	.0490	.0489	.0489	.0488	.0488
.0488	.0486	.0483	.0481	.0478	.0476	.0474	.0472	.0472	.0470
.0540	.0530	.0520	.0510	.0510	.0509	.0509	.0508	.0508	.0508
.0508	.0507	.0506	.0504	.0500	.0496	.0492	.0488	.0483	.0479
.0475	.0469	.0462	.0456	.0449	.0443	.0437	.0430	.0424	.0420
.0415	.0398	.0378	.0341	.0280	.0238	.0227	.0214	.0203	.0196
.0190	.0185	.0181	.0179	.0177	.0175	.0173	.0171	.0170	.0169
.0169	.0168	.0167	.0166	.0165	.0165	.0164	.0164	.0163	.0163
.0162	.0162	.0162	.0161	.0161	.0161	.0161	.0160	.0160	.0160
.0159	.0157	.0157	.0157	.0157	.0157	.0157	.0157	.0157	.0157
.48	.55	.61	.65	.70	.705	.71	.72	.72	.73
.74	.75	.76	.77	.80	.82	.84	.86	.88	.90
.93	.96	.99	1.02	1.07	1.12	1.20	1.28	1.40	1.54
1.75	2.05	2.85	4.50	4.50	3.20	2.55	2.20	2.00	1.80
1.62	1.50	1.39	1.30	1.20	1.12	1.05	1.00	.95	.90
.85	.80	.75	.72	.69	.67	.64	.62	.61	.60
.58	.56	.54	.53	.52	.52	.52	.52	.52	.51
.50	.48	.43	.42	.40	.40	.40	.38	.35	.33
27.6	32.4	38.1	43.9	50.0	50.5	51.2	51.9	52.7	53.6
54.5	55.5	56.5	57.7	58.5	59.1	60.0	61.2	62.1	63.0
63.9	64.8	65.7	66.5	67.9	69.0	70.0	71.5	73.2	74.8
75.9	77.5	79.8	82.0	99.0	108.	114.	117.	119.	121.
123.	124.5	126.	127.	128.3	129.2	130.5	131.2	132.	133.
133.9	134.8	135.5	136.1	137.	137.9	138.5	139.	139.5	140.
141.	141.5	142.	142.5	143.	143.5	144.	145.	146.	147.
148.	153.	157.	161.	165.	169.	173.	176.	179.	182.

SHEAR STRESS VALUES

2.5E6	3.0E6	3.5E6	4.0E6	4.5E6	5.0E6	5.5E6	6.0E6	6.5E6	7.0E6
8.0E6	9.0E6	1.0E7	1.1E7	1.2E7	1.4E7	1.6E7	1.8E7	2.0E7	2.2E7
2.4E7	2.6E7	2.8E7	3.0E7	3.5E7	4.0E7	4.5E7	5.0E7	5.5E7	6.0E7
7.0E7	8.0E7	9.0E7	1.0E8	1.2E8	1.4E8	1.6E8	1.8E8	2.0E8	2.5E8
3.0E8	3.5E8	4.0E8	4.5E8	5.0E8	5.5E8	6.0E8	6.5E8	7.0E8	8.0E8
9.0E8	1.0E9	1.2E9	1.5E9	2.0E9	2.5E9				

INPUTS

144000.	340.	440.	.00521	20.

ERRATA

Page	Line	
14	Bottom	should be 'Page 166'
20	Column Heading	'Temp. Peak' instead of 'Temp. Perc.'
37	6	omit 'wall'
47	4	'$\sqrt{\tau_o/\rho_w}$' instead of 'τ_o/ρ_w'
48	8	'$\sqrt{\tau_o/\rho}$' instead of 'τ_o/ρ'
52	5	'ℓ' missing on L.H.S. of equation
78	4	omit 'mass'
87	10	add 'of the mass velocity' after 'high values'
123	1	'none' instead of 'one'